

REPUBLIQUE DU CAMEROUN

Paix – Travail – Patrie

UNIVERSITE DE YAOUNDE I
FACULTE DES SCIENCES
DEPARTEMENT DE PHYSIQUE

CENTRE DE RECHERCHE ET DE
FORMATION DOCTORALE EN
SCIENCES, TECHNOLOGIE ET
GEOSCIENCES
LABORATOIRE DE MECANIQUE,
MATERIAUX ET STRUCTURE



REPUBLIC OF CAMEROUN

Peace – Work – Fatherland

UNIVERSITY OF YAOUNDE I
FACULTY OF SCIENCE
DEPARTMENT OF PHYSICS

POSTGRADUATE SCHOOL
OF SCIENCE TECHNOLOGY
AND GEOSCIENCES
LABORATORY OF MECHANICS,
MATERIALS AND STRUCTURE

**ON THE MAGNETO-RHEOLOGICAL DAMPER
CONTROL OF TIMOSHENKO BEAM SUBJECTED
TO EARTHQUAKE ACTION**

This dissertation is submitted to the postgraduate school of the
University of Yaoundé 1 in partial fulfilment of the requirements for the
award of the degree of Doctorat/PhD in Physics

Par : **NDEMANOU Buris Peggy**
Msc in Physics

Sous la direction de
NANA NBENDJO Blaise Reméo
Associate Professor
WOAFO Paul
Professor

Année Académique : 2018





DÉPARTEMENT DE PHYSIQUE
DEPARTMENT OF PHYSICS

ATTESTATION DE CORRECTION DE LA THÈSE DE
DOCTORAT/Ph.D

Nous, Professeur **SIEWE SIEWE Martin** et Professeur **KOFANE Timoléon Crépin**, respectivement Examinateur et Président du jury de la Thèse de Doctorat/Ph.D de Monsieur **NDEMANOU Buris Peggy**, Matricule **07W600**, préparée sous la direction du Professeur **NANA NBENDJO Blaise Romeo** et supervisé par le Professeur **WOAFO Paul**, intitulée : « **ON THE MAGNETO-RHEOLOGICAL DAMPER CONTROL OF TIMOSHENKO BEAM SUBJECTED TO EARTHQUAKE ACTION** », soutenue le **Mercredi, 25 Juillet 2018**, en vue de l'obtention du grade de Docteur/Ph.D en Physique, Spécialité **Mécanique, Matériaux et Structures**, Option **Mécanique Fondamentale et Systèmes Complexes**, attestons que toutes les corrections demandées par le jury de soutenance ont été effectuées.

En foi de quoi, la présente attestation lui est délivrée pour servir et valoir ce que de droit.

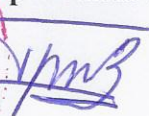
Fait à Yaoundé le **04 SEPT. 2018**

Examinateur


Prof. SIEWE SIEWE Martin



Le Chef de Département de Physique


Prof. NDJAKA Jean-Marie
Bienvenu

Le Président du jury


Prof. KOFANE Timoléon
Crépin

Dedications

I would like to dedicate this thesis to

TADJEULEMO and **NKAMDJEU** Families ...

To my father **TADJEULEMO Boniface**, for his moral supports

To my mother Mrs. **MANETEUE Elisabeth**, whose love, for her permanent assistance, advices and encouragements enabled me to achieve this work.

To my uncle Mr. **NKAMDJEU Valentin** and his wife **GEUFACK Guillaine** for generous help and their unconditional support to my studies. May you find in this work the achievement of some of your dreams and a real reason of satisfaction;

To my brothers and sisters: Mr. **NZEMTE Thibaut**, Miss. **TSOGMO Zita**, Mr. **KAMDJEU Kamille**, Miss. **MENEDONG Lydia**, Miss. **MENESOUNG Jordina**

Acknowledgments

The present PhD work was prepared in the Laboratory of Modelling and Simulation in Engineering and Biomimetics and Prototypes (LaMSEBP) of the Department of physics, Faculty of Science, University of Yaounde I (UYI) in Cameroon.

- The Almighty Father for all his marvellous and over-abundant gifts.
- I would like to express my sincere gratitude to the director of my thesis, Prof. **Blaise Roméo NANA NBENDJO**, who has initiated the topic of this work since my Master degree and has followed its evolution, through invaluable remarks and suggestions. Thanks again for his advices and criticism during my thesis works.
- I would like to express my large acknowledgement to Pr. **Paul WOAF0** for his encouragement and constructive comments. It is a great pleasure and honour to work in the research area under his expert guidance.
- I wish to express my acknowledgements to all the members of the public defence jury,
 - Prof. **Timoléon Crépin KOFANE**,
 - Prof. **Paul Woaf0**
 - Prof. **Jean-Marie Bienvenu NDJAKA**,
 - Prof. **François Beceau PELAP**,
 - Prof. **Blaise Roméo NANA NBENDJO**
 - Prof. **Martin SIEWE SIEWE**

who have accepted to discuss and appreciate the quality of results of this thesis, in spite of their numerous duties.

- I specially thank Prof. Dr. Ing. **UWE DORKA**, University of Kassel, Department of Steel and Composite Structures, Germany, for his fruitful scientific advices.
- I am grateful to Prof. **Jean-Marie Bienvenu NDJAKA**, the Head of the Department of Physics, Faculty of Science, UYI for his fruitful advices.
- I would also like to thank Prof. **Timoléon Crépin KOFANE**, for his motivation teaching especially during my first year at the University of Yaounde I.

- All the teaching staff of the Department of Physics, Faculty of Science, University of Yaoundé I, for their teachings and extension help, since my first year in this institution.
- Moreover , I would like to thank my lab elders and mates during my thesis work: Dr. **Richard KOL**, Dr. **Jimmi TALLA**, Dr. **Omer TCHEUTCHOUA**, Dr. **SIFEU TAKOUGANG**, Dr. **Herve SIMO**, Dr. **Lejuste ABOBDA**, Dr. **Serges NGUEUTEU**, Dr. **NANHA DJANAN**, Dr. **Ahoudou NDOUKOUO**, Dr. **Alain TALLA**, Dr. **Geraud GOUNE**, Mr. **Andre CHAMGOUE**, Mr. **NOTUE KADJIE**, Mr. **Eder TCHAWOU**, Mr. **Jules METSEBO**, Mr. **TEKAM OUMBE**, Mr. **Herve MBONSOU**, Mr. **Gervais MOMO**, Mr. **TOKOUE NGATCHA**, Mrs. **Rolande TSAPLA**, Mr. **Peguy NWAGOUM**, Mr. **Lionel ANAGUE**, Mr. **Cloriant MBA**, Mr. **Eric DONGMO**, Mrs **Vanessa TCHAKUI**, Mr. **Raoul THEPI**, Miss **Raissa FANKEM** for their valuable help.
- I specially like to thank my friends Dr. **Frank T. NDJOMATCHOUA**, Mr. **Antoine POMON**, Mr. **Desire DAWANG** , Mr. **Nelly FOGANG**, Mr. **Basile SA-TEU** , Miss. **Judith DONFACK** for their moral support and advices.
- All those whose names have not been mentioned here, but who have contributed in one way or another to the success of this work should hereby receive my sincere gratitude.

Contents

Dedications	i
Acknowledgments	iii
Contents	vi
Résumé	viii
Abstract	x
List of Abbreviations	xii
List of Figures	xiii
General Introduction	1
Chapter 1 Literature Review	5
1.1 Introduction	6
1.2 Generalities on beam models	6
1.2.1 Euler-Bernoulli beam model	6
1.2.2 Rayleigh beam model	7
1.2.3 Shear beam Model	7
1.2.4 Timoshenko beam model	8
1.2.5 Boundary conditions of the beam	10
1.2.6 Characteristic Equations of the beam	11
1.3 Generalities on the vibration control of mechanical structure	13
1.3.1 Concepts of control mechanisms	14
1.3.2 Dynamic modelling of MR dampers	20
1.4 Problem of the thesis	23
1.5 Conclusion	23
Chapter 2 Models of Ground Motions, analytical and numerical Formalisms	24
2.1 Introduction	25
2.2 The recorded ground motions	25
2.3 The Probabilist ground motions	28
2.3.1 White-noise	28
2.3.2 Kanai-Tajimi	29
2.3.3 Clough-Penzien	30
2.3.4 Envelope Functions	31
2.3.5 Excitation Earthquake models	33
2.3.6 Abbas and Takewaki	36

2.4	The deterministic ground motion	37
2.5	Analytical and Numerical formalisms	38
2.5.1	Method of lines	38
2.5.2	Routh-Hurwitz Stability Criterion	40
2.5.3	Fourth-order Runge-Kutta methods	41
2.5.4	Newton-Raphson Method for system of equations	42
2.5.5	Hardware and Software	43
2.5.6	Box-Muller Method	43
2.5.7	Fuzzy Logic	44
2.6	Conclusion	46
Chapter 3	Results and Discussions	47
3.1	Introduction	48
3.2	Dynamics and MR control of vibration	48
3.2.1	Derivation of the modal equation	49
3.2.2	Direct numerical simulation of the partial differential equation	51
3.2.3	Semi-active control of the cantilever Timoshenko beam	53
3.2.4	Effect of the control on the dynamics responses	55
3.2.5	Stability of semi-active structural control	57
3.3	Quenching of vibration modes on two interconnected buildings	62
3.3.1	Description of the system	62
3.3.2	Numerical results of the controlled mechanical system	65
3.4	Fuzzy MR Device Vibration Control of two Cantilever Timoshenko Beams	70
3.4.1	Description of the physical model	70
3.4.2	Passive on control	74
3.4.3	Fuzzy Logic Control	78
3.5	Reduction of vibration with MR Outriggers	81
3.5.1	Description of Physical system and Dynamic model formulation	81
3.5.2	Semi-active controller	84
3.6	Conclusion	90
	General Conclusion	91
	List of Publications	106

Résumé

Cette thèse traite de la réponse dynamique des structures soumises aux charges sismiques. De ce fait, les structures employées pour cette étude sont les bâtiments. Ces derniers sont considérés comme des poutres porte-à-faux, encastées à la base et libres au sommet. L'approche de la théorie de Timoshenko basée sur les équations différentielles partielles est utilisée pour modéliser lesdites structures. Un amortisseur magneto-rhéologique (MR) est employé pour modifier la réponse dynamique du système structurel.

Une analyse théorique d'un bâtiment sous excitation sismique est menée. Une attention particulière est accordée à la détermination des valeurs propres de la forme spatiale. Il est observé que la réponse du système structurel est grandement influencée par la présence d'un dispositif de contrôle fixé à un point spécifique de la structure. La condition de stabilité du système contrôlé est établie grâce au critère de Routh-Hurwitz. Les réponses statistiques de deux bâtiments connectés soumis à une excitation à séquence répétée sont décrites. Il est observé que les stratégies Lyapunov et logique floue adoptées pour prévoir la dynamique de la tension d'alimentation du dispositif magnéto-rhéologique, augmentent la performance du contrôle du système structurel. En plus, la condition d'action du dispositif de contrôle est présentée à chaque mode de vibration.

Mots Clés: Poutre porte-à-faux de Timoshenko , Amortisseur MR, Excitation sismique, Théorie de Lyapunov, Contrôle de logique floue.

Abstract

This thesis deals with the dynamic response of structures subjected to seismic loads. As a result, the structures used for this study are buildings. They are considered cantilever beams, clamped at the base and free at the top. The Timoshenko theory based on partial differential equations is used to model these structures. A magneto-rheological (MR) device is used to modify the dynamic response of the structural system.

A theoretical analysis of a building connected under seismic excitation is carried out. Particular attention is paid to the determination of eigenvalues of the spatial form. The response of the structural system is greatly influenced by the presence of a control device attached to a specific point of the structure. The stability condition of the controlled system is established by the Routh-Hurwitz criterion. The statistical responses of two interconnected buildings subjected to the repeated sequence of excitation are described. It is observed that the adopted Lyapunov and fuzzy logic strategies to foresee the dynamic of the voltage, increase the performance of the control the structural system. Moreover, the condition of the action time of the control device is presented at each mode of vibration.

Keywords: Timoshenko cantilever beam, MR device, Earthquake excitation, Lyapunov theory, Fuzzy logic control.

List of Abbreviations

AMD : Active mass damper

EL : Extreme Large

ER : Electro-Rheological

HMD : Hybrid mass damper

M : Medium

MF : Modification Factor

MR : Magneto-Rheological

NM : Negative Medium

NL : Negative Large

NS : Negative Small

PM : Positive Medium

PS : Positive Small

PL : Positive Large

RMS : Root-Mean-Square

TMD : Tuned mass damper

VL : Very Large

ZE : Zeros

List of Figures

Figure 1	element of a beam in the deformed and undeformed positions	9
Figure 2	Structure with Passive Energy Dissipation [40].	14
Figure 3	Base isolator systems[43, 44]	15
Figure 4	Taipei 101 in Taiwan.[46]	15
Figure 5	Viscous Fluid dampers[47]	16
Figure 6	Friction damper	16
Figure 7	Metallic damper	16
Figure 8	Petronas twin towers Malaysia	17
Figure 9	Structure with Active Control.	17
Figure 10	Triton square office complex in Japan	18
Figure 11	Structure with Semi Active Control.	19
Figure 12	Schematic configuration of the ER damper[53]	19
Figure 13	MR device[51]	20
Figure 14	Structure with Hybrid Control.	20
Figure 15	Modified Bouc-Wen model	22
Figure 16	Seismology [85]	25
Figure 17	Seismograph [79]	26
Figure 18	Italy-earthquake [50]	27
Figure 19	El centro earthquake, 1949 [78]	27
Figure 20	Algorithm for regenerating the nonstationary earthquake.	28
Figure 21	Kanai-Tajimi model	30
Figure 22	Clough-Penzei model	31
Figure 23	Envelope function of Shinozuka and Sato model	32
Figure 24	Envelope function of Amin and Ang model	33
Figure 25	Envelope function of Boore model	34
Figure 26	Simulation of El Centro 1940 Earthquake	35
Figure 27	Simulation of the Mexico City 1985 earthquake	35
Figure 28	Sample simulated acceleration sequences.	37
Figure 29	deterministic ground motion	38
Figure 30	Fuzzy inference system.	45
Figure 31	Input and output membership functions.	45
Figure 32	Time history response of the relative displacement	53
Figure 33	Frequency response curve	53
Figure 34	Modified Bouc-Wen model	54
Figure 35	Simplified model structure under control	55
Figure 36	Effects of the input voltage	58
Figure 37	Effects of the position of contact	58
Figure 38	Stability diagram in the space	61

Figure 39	Simplified model	62
Figure 40	Time history of buildings Bg_1 and Bg_2	68
Figure 41	Root square response Bg_1 and Bg_2 , $V_{max} = 2.0$, MF=12090	69
Figure 42	The simplified model of the interconnected buildings	70
Figure 43	First mode $X_c = 0.3$, MF= 1000	75
Figure 44	Second mode $X_c = 0.3$, MF= 1000	76
Figure 45	Limit value of the MR damper	76
Figure 46	Location point of the MR device	77
Figure 47	Membership functions for Input and Output	79
Figure 48	Time histories of structures Bg_1 and Bg_2	79
Figure 49	Force generated by the MR damper	80
Figure 50	Applied voltage to the MR damper	80
Figure 51	Cantilever beam with MR outriggers	81
Figure 52	Cross-section of the core tube	82
Figure 53	Optimal position of damped outriggers, $\zeta_a = 0.762$ and MF=1.0	86
Figure 54	Optimal position of damped outriggers, $\zeta_a = 0.095$ and MF=1.0	86
Figure 55	Optimal scale coefficient MF	87
Figure 56	Time histories at the first mode of the vibration.	88
Figure 57	Time histories at the second mode of the vibration.	88
Figure 58	Time histories at the third mode of the vibration	89

List of Tables

Table 1	Parameters of the filter soil of Clough-Penzien [84]	30
Table 2	Runge-Kutta coefficients fourth-order time-invariant	42
Table 3	Geometric and material properties	52
Table 4	Dimensionless values	52
Table 5	Modified MR damper parameters	55
Table 6	Geometric and material properties	65
Table 7	Model parameters of the MR damper.	66
Table 8	Model parameters of the MR damper.	66
Table 9	parameter values of Bg_1 and Bg_2	74
Table 10	Max RMS Bg_1 and Bg_2 versus location points.	77
Table 11	Fuzzy control rules	79
Table 12	parameters of the structural system.	85
Table 13	Model parameters of the MR damper.	86

General Introduction

In the last decades, environment loads [1] such as strong winds, large waves, severe earthquakes continue to affect the human comfort and even structural. Many countries in the World such as Haiti in 2010, Japan in 2011, China in 2008, 2014 and in 2016, Nepal in 2015, Ecuador in 2016, Italy in 2016. They triggered the quakes which cause a great deal of human and animal injuries and death, and left behind a weak economy or heavy financial loss. The main vulnerable fixed targets which have the problem to withstand of those disturbances induced the excessive vibration, are always the engineering structures, such as the residential buildings, roads, railways, earth dams, nuclear power plants and long-span bridges. They are not the only to be affected by those natural disasters, other public and private sectors such as the communication lines, electrical systems can also be affected. The effects of that natural catastrophe on the structural and electrical sectors clearly demonstrate that is the one of the most powerful disaster worldwide.

Because of this harm, a great deal of researchers and engineers continues to multiply the intensive research efforts in civil engineering structures, in view of giving them the effective means to alter their dynamic response in order to improve the potential resistance [2]. This should be minimized the loss of life by preventing the premature collapse of buildings and other mentioned structures earlier during earthquake-induced vibration. Since earthquakes do not kill and injure people, it is rather falling buildings or other structures.

As a result, several studies in the field structural control within the experimental framework as well as theory have been well developed to improve the building performance mitigate [3–11]. In this context, some type of structural protective systems may be implemented to mitigate the damage effects of these environmental forces [12]. The mechanism should absorb the input energy and also significantly increase the damping and stability of the structural system. As an application example, one can note Triton Square office complex, in Tokyo, Japan [13]. This structural control was put in place in 2001 using two active actuators such as the coupled elements.

In the same view, other mechanical structures such as the outrigger system which is consisted of a core wall, external columns, and outriggers was designed to resist severe earthquake and strong winds[14]. This type of new structural concept is defined as a novel energy dissipation system which can mostly be used to protect high rise and tall buildings against the hazard loads,

such as severe earthquakes and strong winds [15]. It is important to note that the performance of this type of system depends on the flexural and shear stiffness of various core or wall and also of the axial stiffness of the perimeter columns and their distance from the core.

To investigate the dynamic responses different approaches were employed to model of structures, specially tall buildings. The large scale deformation can approximately be described by equivalent homogeneous elastic-continuum, although structure primarily consist of structural members (column, walls, floors, etc) separated by void spaces (rooms, doors, windows, etc.)[16]. In this context, a large number studies devoted the single or multi-degree-of-freedom approach to model elastic structures [17–19], the elastic flexural deformation beam [20–22], the shear-flexural cantilever [23]. Thus, it is important to mention that up to now there is a lack of research work in the literature that takes into account the combination of shear-type deformation and rotary inertia effects.

The case of interest in thesis is to consider the combination of underlying effects in the dynamic behaviour of structures under earthquake loading. We attempt to solve the following problems:

- **Mathematical modelling of structural systems under earthquake- induced vibration.**
- **Use mathematical and numerical tools to access the behaviour of the structural system and analyse the influence of the control device.**
- **Optimization of the control strategy (Find the best location of the control device leading to good control by guaranteeing the safety and the stability of structures).**

Thus, the organization of the thesis is structured as follows.

In **chapter one**, we present a literature review which is based on the generalities on the beam dynamics of beams, by briefly exposing the boundary conditions and some different characteristic equations. Afterwards, generalities on the vibration control of mechanical structures are given.

Chapter two presents deterministic and probabilistic mathematical models of earthquake ground motions. Moreover, an algorithm for regenerating the non-stationary earthquake is presented. The mathematical and numerical tools used to characterize the dynamic responses of the studied structural system are also illustrated in this chapter.

Our results are presented in **chapter three**. The mathematical model describing the dynamic behaviour of the structural system equipped of a magnetorheological damper under the seismic load is presented. Afterwards, a control law is defined and used to guide the voltage, with the main aim to attenuate the vibration of the structural system.

We end with a general conclusion where the main results are summarized and some perspectives mentioned.

.

LITERATURE REVIEW

1.1 Introduction

Very important in many engineering applications, beam is used as a structural element subjected to various static and dynamic loads of localized or uniform types. One of the most important problems in the vibration theory of beams is their resistance face to dynamic behaviour of environment loads. Hence, the determination of the natural frequencies and mode shapes have considerable interest in the aerospace, civil and mechanical engineering in order to foresee with a better accuracy the dynamic behaviour of several structures such as, tall buildings, bridges, helicopter rotor blades, turbine blades, propellers, railway, air-plane wings, satellite. The purpose of this chapter is to provide background information on different mathematical modelling of beams and some further details on control mechanisms. Section 1.2 presents generalities on beam models. In Section 1.3 an overview of control mechanisms employed in the literature will be presented as well as the equations describing the dynamic of MR dampers. In section 1.4 more details on the problems solved in this thesis will be given. Section 1.5 will conclude the chapter.

1.2 Generalities on beam models

In order to find better means to increase the safety such as bridges, tall buildings against severe earthquake and strong winds. Many researchers have adopted different simplified approaches based on the partial differential, single and multi-degree of freedoms equations to model these structures. This is due to their complexity, since it is well-known they have a compactness incorporating the elements of natural discontinuous. Many works in the literature have considered various engineering structures like an equivalent continuum beam characterized by either effect, flexural deformation, rotary inertia, shear influence or both. There exist in the literature four models well-known and used to characterized the dynamic response of the uniform beam [24]. The four theories are the Euler-Bernoulli, Rayleigh, shear and Timoshenko.

1.2.1 Euler-Bernoulli beam model

The Bernoulli-Euler model is defined as the context classical theory for vibration of the uniform beam. Although the effects of transverse shear deformation and rotatory inertia effect of the cross section are neglected. In spite of the correction brought by other models which are also described

in this thesis. It stays the most used in the literature because it is simple and provides reasonable engineering approximations for many problems [25–27]. It predicts the frequencies of flexural vibration of lower modes of thin beams quite accurately; and becomes inaccurate at higher modes or for deep beams where the mentioned effects become significant [28].

The mathematical formulation of motion of beam describing the classical Bernoulli-Euler model is the following form

$$\rho A \frac{\partial^2 y}{\partial t^2} + EI \frac{\partial^4 y}{\partial x^4} = 0 \quad (1)$$

In which,

EI represents the flexural rigidity of the beam, and ρA is the mass per unit length.

where E denotes the Young's modulus of elasticity of beam material, A is the cross-sectional area, $I = Ar^2$ (r = radius of gyration of the cross section) is the moment of inertia of the cross-section, ρ is the mass density of the beam material.

The bending vibration namely, transverse displacement $y = y(x, t)$ can be described by two variables depending on axial coordinate along the length of the beam x and time t .

1.2.2 Rayleigh beam model

The first correction to the classical Euler-Bernoulli beam model was considered in 1877 by Lord Rayleigh [29]. The contribution takes into consideration of rotational energy of a beam cross-section. Because the rotary inertia which becomes increasingly important for shorter bending wavelengths, and the the cross section remains perpendicular to the neutral plane.

The equation (1) is rewritten as follows

$$\rho A \frac{\partial^2 y}{\partial t^2} + EI \frac{\partial^4 y}{\partial x^4} - \rho I \frac{\partial^4 y}{\partial x^2 \partial t^2} = 0. \quad (2)$$

The last term of this equation (2) denotes the presence of the rotary inertia effect.

1.2.3 Shear beam Model

In this case, only the effect of the shear is considered in investigation of transverse vibrations of the structural engineering [30].

The following mathematical formulation describing the behaviour is

$$\rho A \frac{\partial^2 y}{\partial t^2} - k_s AG \left(\frac{\partial^2 y}{\partial x^2} - \frac{\partial \theta}{\partial x} \right) = 0 \quad (3)$$

$$\rho I \frac{\partial^2 \theta}{\partial t^2} + k_s AG \left(\frac{\partial^2 y}{\partial x^2} - \frac{\partial \theta}{\partial x} \right) = 0 \quad (4)$$

We can notice that unlike to the Euler-Bernoulli and Rayleigh model beams, the shear beam model is characterized by two dependant variables.

By definition an ideal shear beam exhibits no flexural deformations, but deforms in shear only[31]. This leads to considering the shear beam in the technical note[32]

$$\frac{\partial \theta}{\partial x} = 0$$

In the context, the equation (3) can be given as follows

$$\rho A \frac{\partial^2 y}{\partial t^2} - k_s AG \frac{\partial^2 y}{\partial x^2} = 0 \quad (5)$$

$$(6)$$

One can notice that the presence of the variable θ due to shear deformation effect.

1.2.4 Timoshenko beam model

In the 20th century Timoshenko was the pioneer in this field to demonstrate the importance of shear deformation and rotational inertia effect in the dynamics of elastic beams [33]. He introduced a shear coefficient to account for the variation of the shear stress across the cross section [34]. The Timoshenko theory is also defined as an expansion of that classical Euler-Bernoulli model, since these two quoted effects are ignored. In other words, the Timoshenko beam includes of shear deformation in a Rayleigh beam.

The effect of rotation is large when the curvature of the beam is large relative to its thickness [35]. Two instances where this is true are

(i) a beam that is short in length relative to its thickness,

(ii) a long beam vibrating in a higher mode so that the nodal points are close together

Consequently, the Timoshenko beam model is suitable for describing the behaviour of short beams, sandwich composite beams, or beams subject to high-frequency excitation. The quoted effects require that the deformation of the cross section is now no perpendicular or longer normal to the

deformed neutral axis.

Thus, the angle $\frac{\partial y}{\partial x}$ between the beam axis and x axis, also known as the

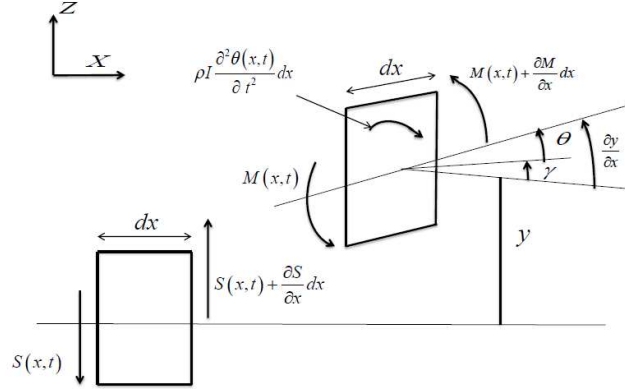


Figure 1: element of a beam in the deformed and undeformed positions

slope of the centerline of the beam.

The angle $\theta = \theta(x, t)$ is defined as the transverse rotation of the beam cross-section due to the bending moment

$$\frac{\partial y}{\partial x} = \theta + \gamma \quad (7)$$

The difference of the above equation gives us a measure of the shearing angle.

The shear force is defined by

$$M = -EI \frac{\partial \theta}{\partial x} \quad (8)$$

and the bending moment by

$$S = k_s GA \gamma = k_s GA \left(\frac{\partial y}{\partial x} - \theta \right) \quad (9)$$

in which $k_s GA$ represents the shear rigidity of the beam

where,

$G = \frac{E}{2(1+\nu)}$ is the shear modulus of the beam material.

k_s the so-called shear correction coefficient, is depending on the geometric of the cross section of the beam (For instance, $k_s = \frac{10(1+\nu)}{12+11\nu}$ for rectangular cross sections and $k_s = \frac{6(1+\nu)}{7+6\nu}$ for circular ones.) and also of the Poisson's ratio ν as discussed in ref [36].

This coefficient is introduced to take into account the fact that the shear

stress and shear strain are not uniformly distributed over the cross section.

For translation in the direction of OZ , one obtains

$$\frac{\partial S}{\partial x} dx = \rho A \frac{\partial^2 y}{\partial t^2} dx \quad (10)$$

$$-\frac{\partial M}{\partial x} + S dx = \rho I \frac{\partial^2 \theta}{\partial t^2} dx \quad (11)$$

The following set of coupled differential equations in terms of the beam displacement $y(x, t) = y$ and rotation $\theta(x, t) = \theta$ of the cross-section is thus expressed as follows

$$\rho A \frac{\partial^2 y}{\partial t^2} = k_s AG \left(\frac{\partial^2 y}{\partial x^2} - \frac{\partial \theta}{\partial x} \right) \quad (12)$$

$$\rho I \frac{\partial^2 \theta}{\partial t^2} = k_s AG \left(\frac{\partial y}{\partial x} - \theta \right) + EI \frac{\partial^2 \theta}{\partial x^2} \quad (13)$$

Eliminating θ , we obtain the uncoupled equations of motion in the form

$$EI \frac{\partial^4 y}{\partial x^4} + \rho A \frac{\partial^2 y}{\partial t^2} - \rho I \left(1 + \frac{E}{k_s G} \right) \frac{\partial^4 y}{\partial x^2 \partial t^2} + \frac{\rho^2 I}{k_s G} \frac{\partial^4 y}{\partial t^4} = 0 \quad (14)$$

The two first expressions of the Equation (14) represent those defined by Euler-Bernoulli model.

The third term represents the correction for rotary inertia while the fourth term represents the shear deformation effect.

The last term represents the joint action of rotary inertia and shear deformation effects.

One can summarize the four model of beam theories as follows

- **Euler-Bernoulli** = Bending moment + Lateral deformation
- **Rayleigh** = Euler-Bernoulli + Rotary inertia
- **Shear** = Euler-Bernoulli + Shear deformation
- **Timoshenko** = Rayleigh + Shear deformation

From summary one can observe the difference between Timoshenko model and other theories. Since the Timoshenko model is an extension of the Euler-Bernoulli model by combining the shearing force and rotary motion effect.

1.2.5 Boundary conditions of the beam

Conditions along edges of a beam will be illustrated here, in order to reduce the partial differential forms to a set of ordinary differential equations. To

reach to this objective, one needs to employ the boundary conditions. The ends of the beam is referred to 0 that in other case of boundary conditions can be defined as the bottom and L as the top of beam.

The boundary conditions can be written as follows:

Free-Free boundary condition: shearing forces and moments are assumed to be zero at each end of the beam,

$$\frac{\partial y}{\partial x}(0, t) - \theta(0, t) = 0, \quad \frac{\partial \theta}{\partial x}(0, t) = 0 \quad (15)$$

$$\frac{\partial y}{\partial x}(L, t) - \theta(L, t) = 0, \quad \frac{\partial \theta}{\partial x}(L, t) = 0 \quad (16)$$

clamped at both ends: the rotation of the beam section and traversal displacement are assumed to be zero at each end of the beam.

$$y(0, t) = \theta(0, t) = 0 \quad (17)$$

$$y(L, t) = \theta(L, t) = 0 \quad (18)$$

Hinged at both ends: the traversal displacement and the bending moment M at each end of the beam are assumed to be zero

$$y(0, t) = 0, \quad \frac{\partial \theta}{\partial x}(0, t) = 0 \quad (19)$$

$$y(L, t) = 0, \quad \frac{\partial \theta}{\partial x}(L, t) = 0 \quad (20)$$

Cantilever (defined as at clamped end and at free end). As a result each of aforementioned boundaries is considered to defined the cantilever conditions

$$y(0, t) = \theta(0, t) = 0, \quad \text{at the clamped end} \quad (21)$$

$$\frac{\partial y}{\partial x}(L, t) - \theta(L, t) = 0, \quad \text{and the free} \quad (22)$$

We can note that each configuration of boundary conditions leads to a particular dynamic of beams.

1.2.6 Characteristic Equations of the beam

The solutions of (12) and (13) can be taken as the product of the two functions therefore expressions are under the form [37]

$$y(x, t) = \Phi(x) \sin(\omega_n t) \quad (23)$$

$$\theta(x, t) = \Psi(x) \sin(\omega_n t) \quad (24)$$

by inserting (24) into (14) and also introducing the following new variables

$$X = \frac{x}{L}, \quad \phi = \frac{\Phi}{L} \quad (25)$$

we get to the following equation defined as follows

$$\frac{d^4\phi}{dX^4} + \rho\omega_n^2 L^2 \left(\frac{1}{E} + \frac{1}{k_s G} \right) \frac{d^2\phi}{dX^2} - \frac{\rho A \omega_n^2 L^4}{EI} \left(1 - \frac{\rho r^2 \omega_n^2}{k_s G} \right) \phi = 0 \quad (26)$$

The solution of (26) is under the form.

$$\phi(X) = C \exp(\lambda X) \quad (27)$$

in what follows, the following polynomial is obtained after substituting of (27) into (26)

$$\lambda^4 + \alpha^2 \omega_n^2 \left(1 + \frac{1}{\mu} \right) \lambda^2 - \left(\beta^2 \omega_n^2 - \frac{1}{\mu} \alpha^4 \omega_n^4 \right) = 0 \quad (28)$$

in which

$$\alpha = L \sqrt{\frac{\rho}{k_s G}}, \quad \mu = \frac{E}{k_s G} \quad (29)$$

The resolution of (28) gives four roots that are defined as follows

$$\lambda_1 = \pm j \delta_n, \quad \lambda_2 = \pm \varepsilon_n \quad (30)$$

with

$$\delta_n = \frac{\sqrt{2} \alpha \omega_n}{2} \sqrt{\left(1 + \frac{1}{\mu} \right) + \sqrt{\left(1 - \frac{1}{\mu} \right)^2 + \frac{4\eta^2}{\alpha^2 \omega_n^2}}} \quad (31)$$

$$\varepsilon_n = \frac{\sqrt{2} \alpha \omega_n}{2} \sqrt{-\left(1 + \frac{1}{\mu} \right) + \sqrt{\left(1 - \frac{1}{\mu} \right)^2 + \frac{4\eta^2}{\alpha^2 \omega_n^2}}} \quad (32)$$

where $\eta = L \sqrt{\frac{k_s G A}{EI}}$

the following equation in terms of eigenvalues δ_n and ε_n is obtained:

$$(\delta_n^2 - \varepsilon_n^2) \left[\eta^2 - \frac{1}{\mu + 1} (\delta_n^2 - \varepsilon_n^2) \right] \varepsilon_n^2 \delta_n^2 = 0 \quad (33)$$

The function of the lateral deflection is expressed as

$$\phi(X) = C_1 \sin(\delta_n) + C_2 \cos(\delta_n) + C_3 \sinh(\varepsilon_n) + C_4 \cosh(\varepsilon_n) \quad (34)$$

thus, the shape function of the rotation ψ is written as follows

$$\psi(X) = C_5 (C_1 \sin(\delta_n) - C_2 \cos(\delta_n)) + C_6 (C_3 \sinh(\varepsilon_n) + C_4 \cosh(\varepsilon_n)) \quad (35)$$

in which

$$C_5 = \delta_n + \frac{\mu(\delta_n^2 - \varepsilon_n^2)}{\delta_n(\mu + 1)}, \quad C_6 = \varepsilon_n + \frac{\mu(\delta_n^2 - \varepsilon_n^2)}{\varepsilon_n(\mu + 1)} \quad (36)$$

C_1, C_2, C_3 and C_4 are coefficients that depend on the following boundary conditions.

Let note in passing that the length of beam varied at 0 to 1. This consideration will automatically modify the obtained form from the boundary conditions.

(a) Cantilever beam

$$\begin{aligned} & \left[(\delta_n^2 + \mu\varepsilon_n^2)^2 + (\varepsilon_n^2 + \mu\delta_n^2)^2 \right] \cos(\delta_n) \cosh(\varepsilon_n) + (\delta_n^2 + \mu\varepsilon_n^2) \times \\ & (\varepsilon_n^2 + \mu\delta_n^2) \left(-2 + \frac{\delta_n^2 - \varepsilon_n^2}{\delta_n \varepsilon_n} \sin(\delta_n) \sinh(\varepsilon_n) \right) = 0 \end{aligned} \quad (37)$$

(b) Clamped-clamped beam

$$\begin{aligned} & 2(\varepsilon_n^5 \delta_n \mu + (1 + \mu^2) \delta_n^3 \varepsilon_n^3 + \varepsilon_n \delta_n^5 \mu) \cos(\delta_n) \cosh(\varepsilon_n) + \\ & (\varepsilon_n^6 \mu^2 + (-1 + 2\mu) \delta_n^2 \varepsilon_n^4 + (1 - 2\mu) \delta_n^4 \varepsilon_n^2 - \delta_n^6 \mu^2) \times \\ & \sin(\delta_n) \sinh(\varepsilon_n) - 2\varepsilon_n^5 \delta_n \mu - 2(1 + \mu^2) \varepsilon_n^3 \delta_n^3 - 2\varepsilon_n \delta_n^5 \mu = 0 \end{aligned} \quad (38)$$

(b) Hinged-Hinged beam

$$(\delta_n^2 + \varepsilon_n^2)^2 \sin(\delta_n) \sinh(\varepsilon_n) = 0 \quad (39)$$

One should note that the determination of eigenvalues requires an appropriated algorithm by using of (33).

1.3 Generalities on the vibration control of mechanical structure

Many structural systems are affected by increasing of the energy from environmental loads such as the severe earthquakes, strong winds and other types of dynamic loads. In order to stabilize the structural health, a part of this energy should be dissipated to avoid the structural damages. In this sense, the new concepts of control mechanisms have been developed and

incorporated into structures to absorb the input energy by minimizing excessive vibration.

1.3.1 Concepts of control mechanisms

Mechanisms for control of structural response can be classified into four main groups: passive, active, hybrid, and semi-active.

1.3.1.1 Passive control

A passive control system is a mechanism that does not require an external power source to operate and has limited ability. Because it is not able to adapt to structural change [38].

The control device has no sensors, controllers and cannot respond to variations in the parameters of the object being controlled [39].

The configuration of this structural control system is illustrated in Figure 2.

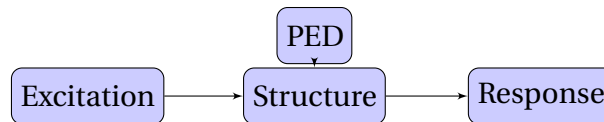


Figure 2: Structure with Passive Energy Dissipation [40].

The major advantage of passive control systems is their manner to work at no operational cost (no consumption of energy) and with minimum requirements on maintenance [41]. As example,

(a) **Base isolator systems**(Figure 3), also known as seismic base isolation, defined as one of the most used mechanism of protecting of structures against the earthquake loadings. These systems are effective in reducing the inter-story displacements against vibrations transmitted through the ground, such as seismic vibrations but it is not efficient to resist wind loading due to the flexibility in the horizontal direction [42].

(b) **Tuned mass dampers** consisting of components such as mass, springs and viscous dampers. The effectiveness of these devices is relatively limited. Because the tuning frequency of the mass damper differs from the main frequency of the structure, tuned mass damper will have little effect in reducing the seismic responses[45].

So one can define the Taipei 101 as an example of design and construction practice in the world. The control system was installed at the top of the structure (as seen in Figure4).

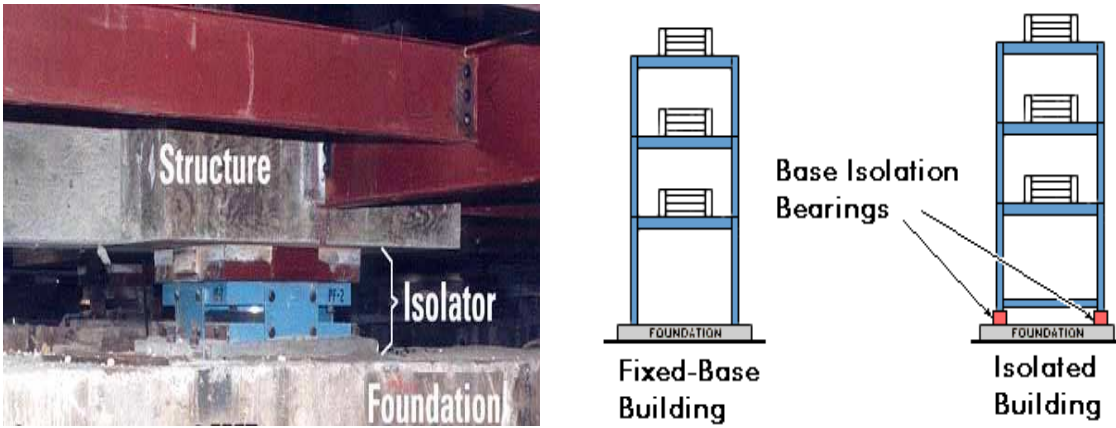


Figure 3: Base isolator systems[43, 44]



Figure 4: Taipei 101 in Taiwan.[46]

This structure has been designed to withstand typhoons and frequent earthquakes in the Asia Pacific region.

- (d) **Viscous Fluid dampers** (see Figure5) are commonly used as passive energy dissipation devices for seismic protection of structures. Such dampers consist of a hollow cylinder filled with fluid, the fluid typically being silicone based.
- (c) **Friction dampers** as shown in Figure6, exhibit perfect rectangular hysteretic behaviour.
- (e) **Metallic Yied dampers**(Figure 7), in this configuration the energy is absorbed by metallic components. They utilize the hysteretic behaviour of metals in the inelastic range and can be fabricated from steel, lead or spherical shape memory alloys.

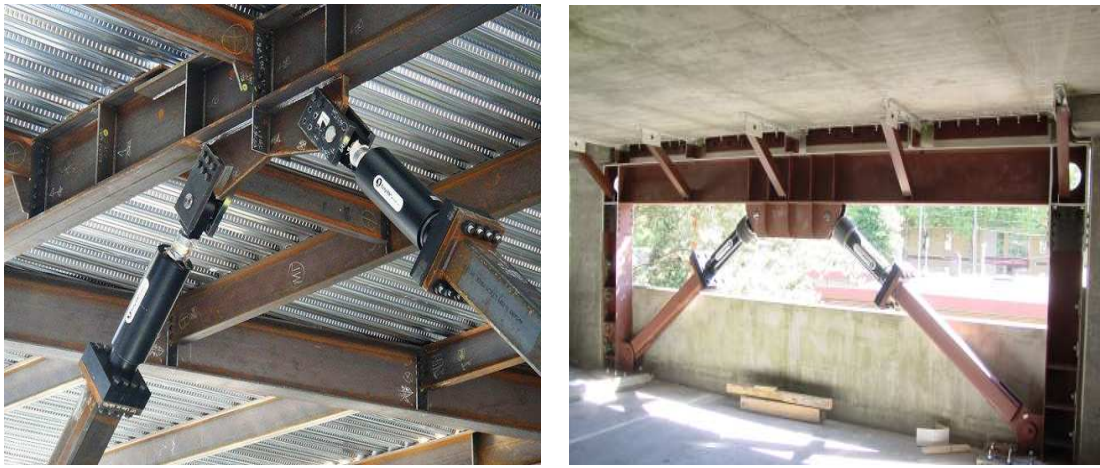


Figure 5: Viscous Fluid dampers[47]

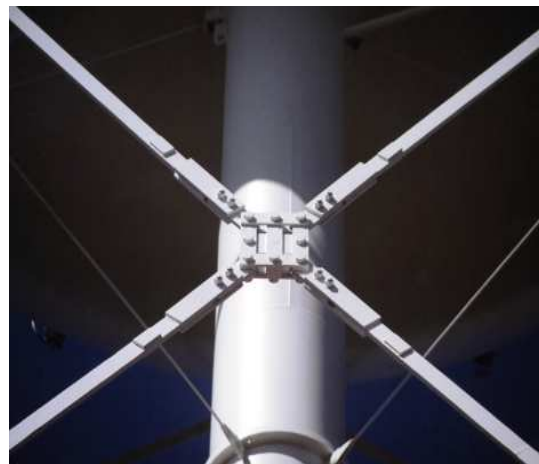


Figure 6: Friction damper

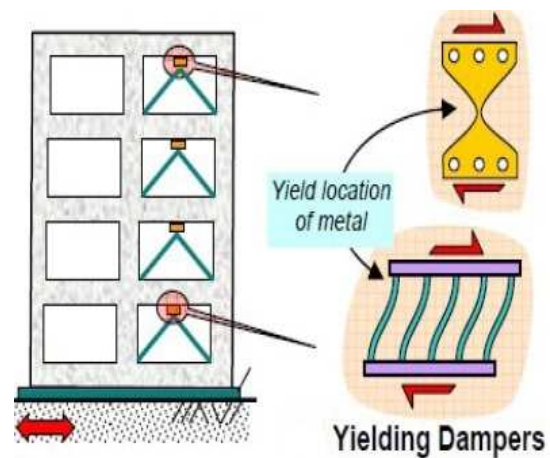
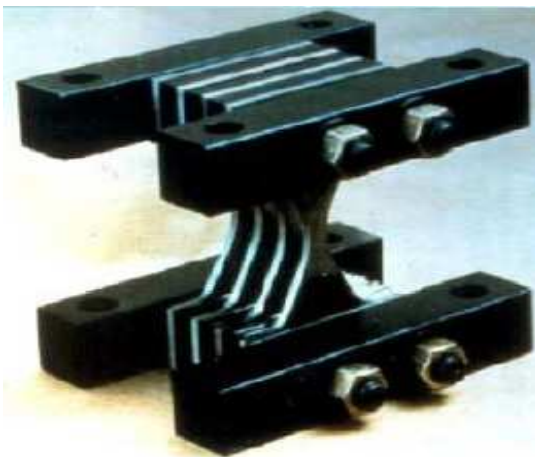


Figure 7: Metallic damper

One can also note in passing the interconnected tall buildings by a passive coupling element was built in the world. The case well-known is Petronas Towers in Malaysia, also known as the Petronas twin tower as illustrated in

Figure 8.



Figure 8: Petronas twin towers Malaysia

1.3.1.2 Active control

An active control system is a control mechanism that modified the dynamic response of a structure by means of the application of an external large power source. It is designed to absorb a wide band of frequencies, and needs high operational cost. The scheme of Active control system is displayed in Figure9. This system consists of:

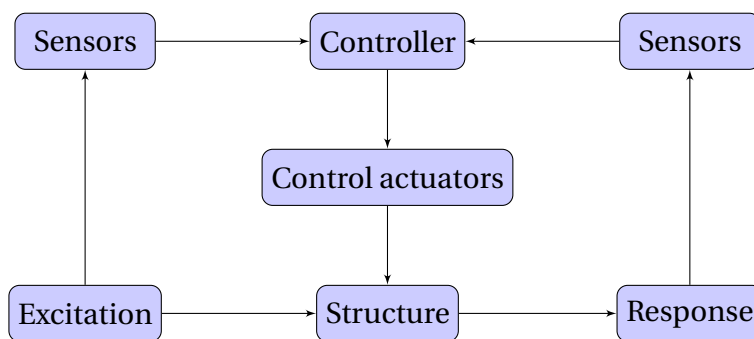


Figure 9: Structure with Active Control.

- * Sensors located about structure and are used to measure either external excitation or structural response, or both
- * Controllers process the measured information by sensors and compute necessary control forces based on given algorithm.
- * Actuators are used to produce the required force and usually powered by external energy sources

Moreover the injection of the energy can destabilize the structural system. We can note[40]

- (a) **Active Variable stiffness,**
- (b) **Active mass dampers,**
- (c) **Active bracing systems.**
- (d) **Active Tendon systems**

As practice example, one can note Triton Square office complex, in Tokyo, Japan [13]. This structural control executed in 2001 using two active actuators like the coupled element as seen in Figure 10.

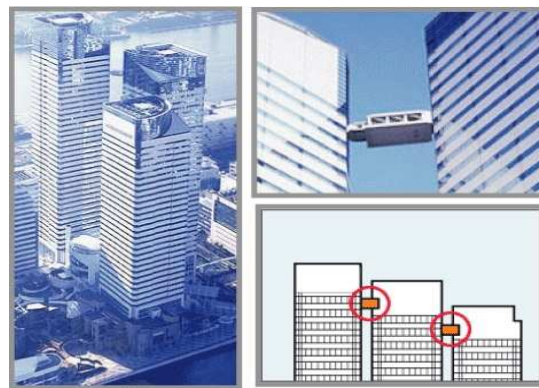


Figure 10: Triton square office complex in Japan

1.3.1.3 Semi-active control

Semi active control system combines features of passive and active control systems without requiring a large power source to change its mechanical properties.

A semi-active control device is a system therefore physical properties of dissipation can be adjusted in real time but cannot input mechanical energy into the system being controlled in contrast to active control devices.

The one of particularities of the semi-active devices is its capacity to adapt its dynamics related to the effects of environmental loadings. The semi active control system is displayed in figure 11 Moreover they can also achieve the majority of the performance of passive and active control systems. Some examples of these kind devices are

- (a) **Electroheological dampers (ER)** as illustrated in Figure 12: ER contain dielectric particles suspended that offer resistance when are subjected to an electric field.

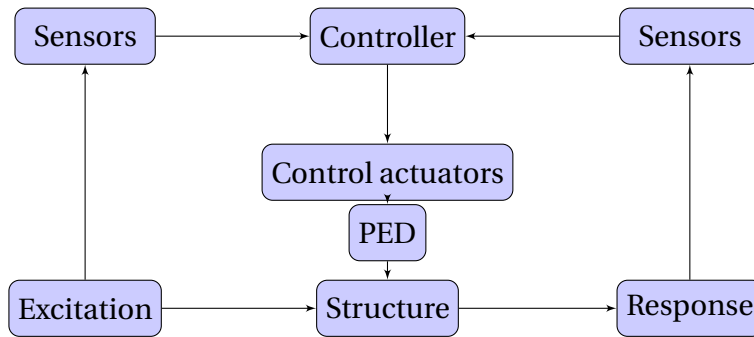


Figure 11: Structure with Semi Active Control.

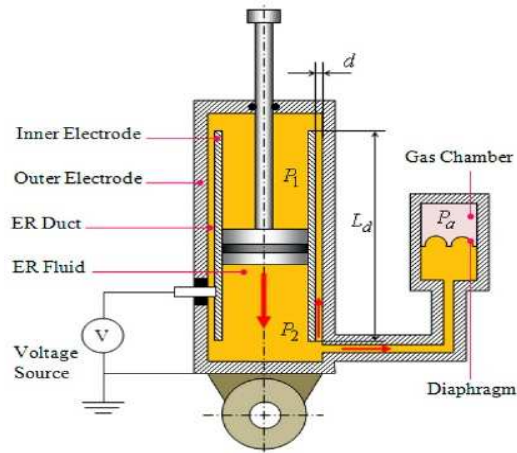


Figure 12: Schematic configuration of the ER damper[53]

(b) **Magnetorheological dampers** (Figure 13b) employ MR fluids to change its force. This appears when the magnitude of applied magnetic modifies the liquid state.

(c) **Continuous variable stiffness.**

(d) **Tuned mass dampers**

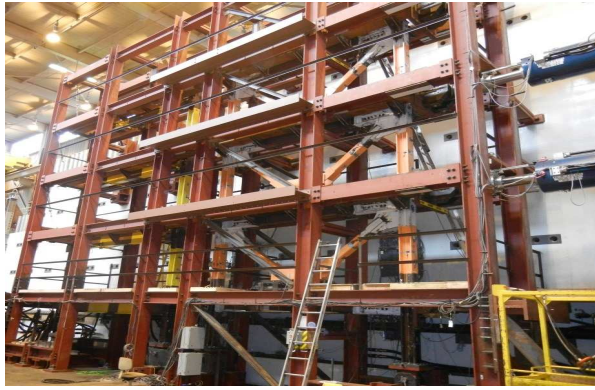
1.3.1.4 Hybrid control

Hybrid control (see Figure 14) implies the combined use of active and passive control systems.

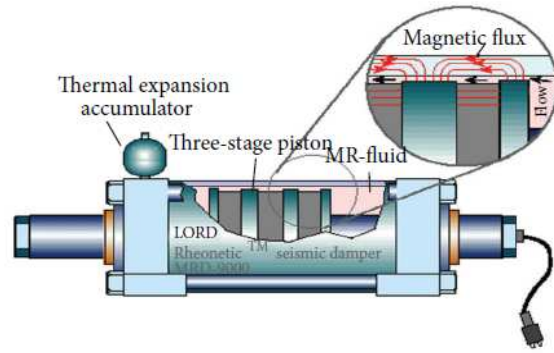
Advantage with this kind control approach is that the multiple control devices are operating and higher levels of performance may be achievable. For example, a structure equipped with distributed visco-elastic damping supplemented with active mass damper on the top of the structure [52].

In what follows, some hybrid control systems can be presented[42]

(a) **Hybrid base isolation system.** This system can be composed of Base isolation system and active tendon control system, or combined the Base isolation system + MR fluid dampers.



(a) A prototype steel frame with MR dampers



(b) Schematic of the prototype 20 ton large-scale MR fluid damper

Figure 13: MR device[51]

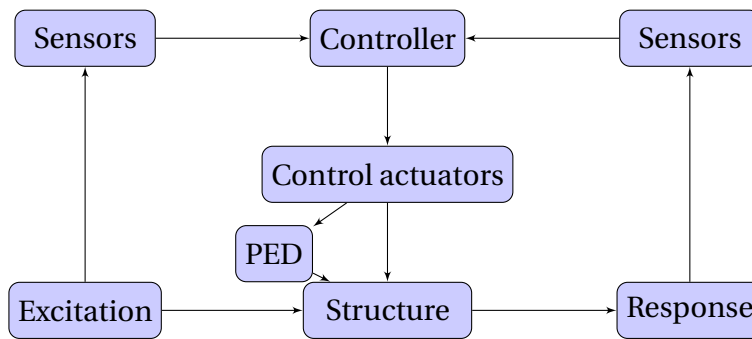


Figure 14: Structure with Hybrid Control.

- (b) **Hybrid damper actuator bracing control.** This system can be used the Hydraulic actuators and passive device.
- (c) **Hybrid mass damper (HMD).** This device is composed of either a combination of a passive TMD (Tuned Mass Damper) and an active control actuator, or a combination of an AMD (Active mass damper) to a TMD.

Thus Hybrid control systems can alleviate some of the restrictions and limitations that exist when each system is acting alone.

1.3.2 Dynamic modelling of MR dampers

Most of the studies in the literature are based on two kind categories of devices using controllable fluid-based systems, Electrorheological(ER) and Magnetorheological (MR) fluids. Despite their different properties, these ones have useful common features such as fast response time and continuously controlled rheological characteristics [75].

Need a cost high voltage (e.g. 4000 volts) to generate the electric field which applied to ER fluid changes its apparent viscosity. Moreover the fluids have a

very limited yield stress and sensitive to temperature.

When a magnetic field is applied to the fluids, particle chains form. As a result, the fluid becomes a semi-solid, exhibiting Bingham plastic behaviour. Transition to rheological equilibrium can be achieved in a few milliseconds, providing devices with high bandwidth.

The MR damper consists of a hydraulic cylinder that contain micrometer-sized magnetically polarizable particles dispersed in hydrocarbon oil and can operate at temperatures from $-40^{\circ}C$ to $150^{\circ}C$ with only modest variations in the yield stress.

Nowadays MR dampers are used for full-scale applications in the world-wide, due to inherent stability, mechanical simplicity, high-dynamic range, large temperature operating range, low power requirement, large force capacity and robust performance. Consequently, different models have been developed in ref [91] to describe the behaviour of the MR damper. One can note

- Bingham model, defined by a Coulomb friction element placed in parallel with a viscous damper.
- Gamato and Filisko model that is consisted of the Bingham model in series with a standard model of a linear solid.
- Bouc-Wen model that is extremely versatile and can exhibit a wide variety of hysteretic behaviour.

Thus, Spencer et al. [91] through the experimental analysis have showed that all these mentioned models do not describe very-well the reel behaviour of the MR damper. As a result, authors have proposed a mechanical model based on the Bouc-Wen hysteresis. From the obtained results, the authors have concluded that the approach is numerically tractable and effectively portrays the behaviour of a MR damper. The schematic of the model is shown in Figure 15.

The equation governing the force predicted by this model is

$$f = c_1 \dot{y} + k_1(x - x_0) \quad (40)$$

where x is the displacement of the damper; x_0 is the initial displacement of spring k_1 , and k_1 is defined as the accumulator stiffness.
and

$$\dot{y} = \frac{1}{c_1 + c_0} [\alpha z + c_0 \dot{x} + k_0(x - y)] \quad (41)$$

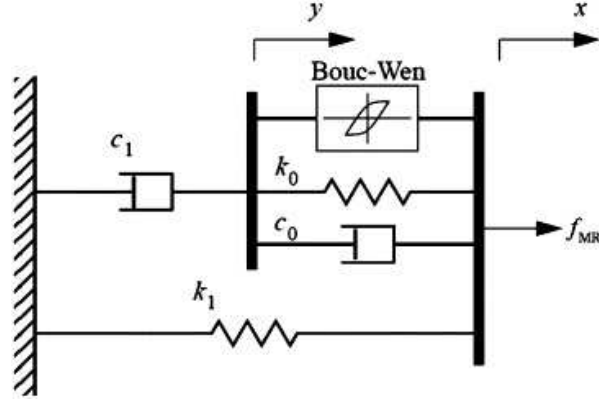


Figure 15: Modified Bouc-Wen model

where, y is the internal movement of the MR damper. The evolutionary variable z is governed by

$$\dot{z} = -\gamma|\dot{x} - \dot{y}|z|z|^{n-1} - \beta(\dot{x} - \dot{y})|z|^n + A(\dot{x} - \dot{y}) \quad (42)$$

k_0 is the control stiffness at large velocities, c_0 and c_1 represent viscous damping coefficients at high and low damper velocities, respectively. α is the evolutionary coefficient. These characteristic parameters γ , β and A can control the linearity and the smoothness of the transition from the pre-yield to the post-yield region.

Some parameters of equations (41) and (42) depend on the command voltage

$$\alpha = \alpha_a + \alpha_b u, \quad c_0 = c_{0a} + c_{0b} u, \quad c_1 = c_{1a} + c_{1b} u \quad (43)$$

The dynamics involved in the MR fluid reaching equilibrium are accounted for through the first order filter [82]

$$\dot{u} = -\eta(u - v) \quad (44)$$

in which v is the command voltage applied to the current driver.

Despite all that the MR dampers are characterized by the intrinsically non-linear behaviour which stays a mayor disadvantage. It is raison why the one of the main challenge is the development of an appropriate control algorithm that can take full advantage of the unique features of the MR damper, in view of obtaining the optimal input voltage corresponding to the desired damper force. We have some examples based on Lyapunov stability theory, Decentralized Bang-Bang Control, Clipped-Optimal Control, Fuzzy logic control, modulated homogeneous friction, Sliding mode, Genetic algorithm etc.

1.4 Problem of the thesis

As mentioned earlier, the semi-active devices have several advantages over other types. Because they combine the best features of both passives as well as actives and require a low voltage that changes the physical system properties. All aforementioned studies on reduction of vibration of buildings only considered the simple-flexure or shear deformations in neglecting the combination of both rotary inertia and shear effects to model the engineering structures. The approach displays single and multi-modes by taking into account the neglected mentioned effects will be used to model the mechanical structures. Moreover, a magneto-rheological damper will be used as the integral part of the structural system to attenuate the vibration mode induced by earthquake action.

1.5 Conclusion

In this chapter, the theories for the vibrating uniform beams were provided. As a result, the Timoshenko model which takes into account the shear and rotational effects was adopted to model the employed structures in this work. The description of concepts of control mechanisms was presented as well as the equations describing the dynamics of the MR damper. The following chapter will be devoted to mathematical models of earthquake ground motions, analytical and numerical formalism used to solve the problem of the thesis.

**MATHEMATICAL MODELS OF GROUND
MOTIONS, ANALYTICAL AND NUMERICAL
FORMALISMS**

2.1 Introduction

This chapter deals with the different mathematical modellings of earthquake ground and provides the different analytical and numerical methods that will be used to solve the problem statement of the thesis. Section 2.2 presents the recorded ground motions used in the iteration to solve the design earthquake-resistant problem. In section 2.3, the stochastic method employed to model the acceleration ground motion. Section 2.4 is devoted the deterministic approach for generating the nonstationary earthquake. In Section 2.5 the tool for analytical and numerical methods explored to assess the dynamic response of the physical system are given. The conclusion of the chapter appears in section 2.6.

2.2 The recorded ground motions

Earthquakes refer to sudden movements of the soil conducted by a sequence of vibrations due to discharge of the strain energy accumulate in the earth's crust. Also defined as a natural phenomenon that usually starts at a depth of less than 100 Km below the ground [69].

Mainly cause by slip along faults, the energy from an earthquake propagate as body waves and surface waves.

Magnitude of earthquake measures the energy of an earthquake. So, each earthquake is characterized by a unique release of strain energy. This is calculated from Richter scale. Intensity of earthquake is based on observation of damaged engineering structures as well as reactions of people. The point

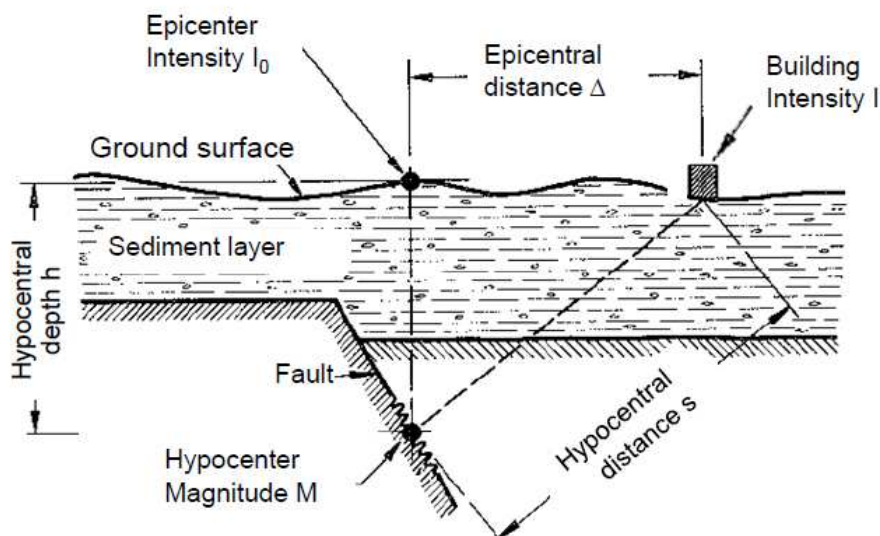


Figure 16: Seismology [85]

of origin or the point where an earthquake or underground explosion originates, called the seismic focus or hypocenter, is located with the help of seismograph (as seen in Figure16).

The point on Earth's surface directly above the hypocenter is called the epicentre [70].

The epicentral distance is the distance from the epicenter or epicentre to the point of interest on the surface of the earth.

Thus, to have other information from earthquake, such as

- peak ground acceleration (PGA) is the maximum amplitude of ground acceleration.
- peak ground velocity (PGV) is the maximum amplitude of velocity.
- peak ground displacement (PGD) is the maximum respective amplitude of displacement.

One needs to record seismic waves cause by that earth-shaking phenomenon. As a result, the device employed by scientists is a seismograph as presented in Figure17. It is an instrument that records the shaking of the earth's surface caused by seismic waves, and is to accurately record the motion of the ground during a quake.

One of the recent case is the earthquake that hit central Italy on 24 August

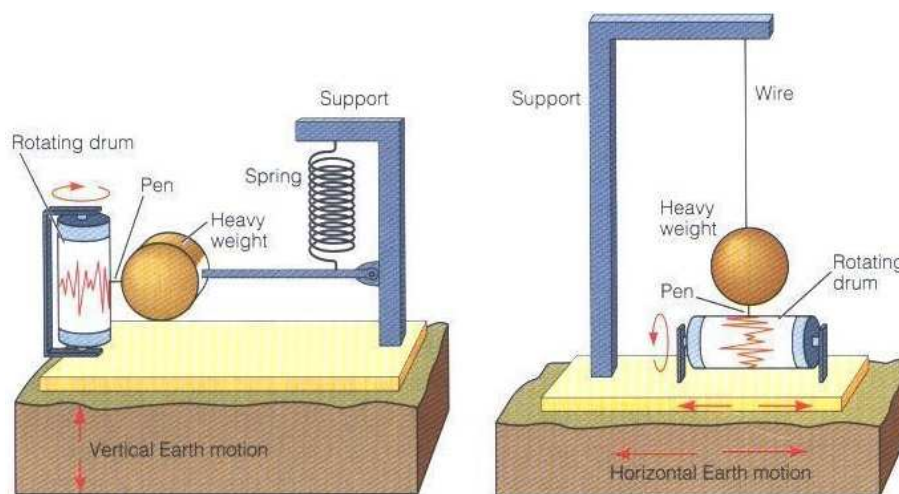


Figure 17: Seismograph [79]

2016 with its hypocenter at a depth of 4 ± 1 km. This catastrophic caused heavy destruction as indicated in Figure 18.

It must stand on Earth's vibrating surface, and it will therefore vibrate along with that surface. This means that there is no fixed frame of reference for making measurements. El Centro earthquake 1940 in the Imperial Valley is



Figure 18: Italy-earthquake [50]

an example of recorded ground motion in south eastern Southern California (see Figure 19). In fact, Figures 19a and 19b display the record data from same place at different component or position of the seismograph.

It is important to note that extension of significant damages of engineer-

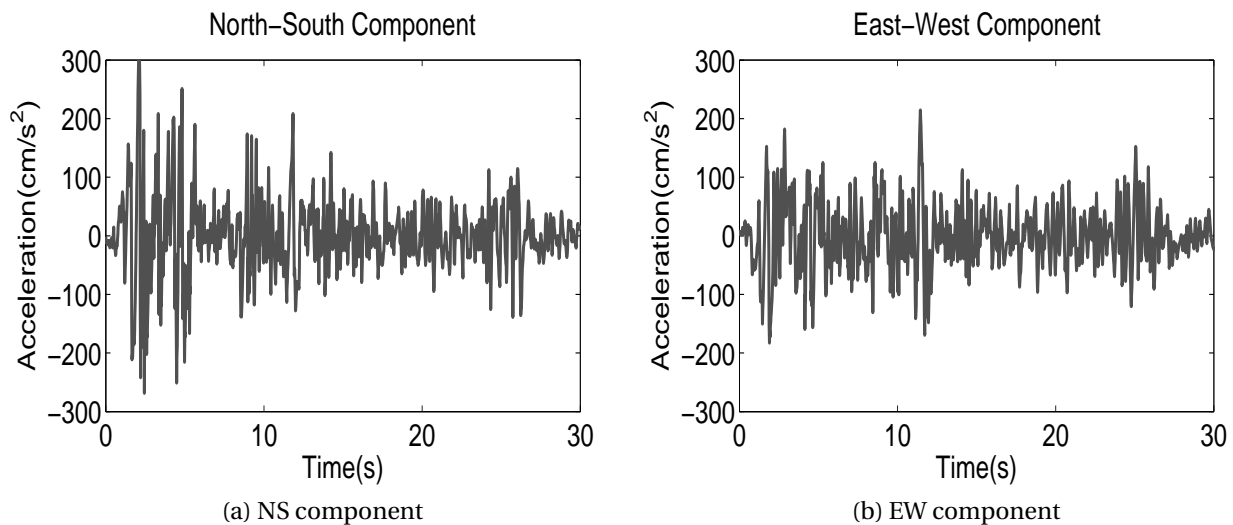


Figure 19: El centro earthquake, 1949 [78]

ing structures caused by earthquake, depends on the nature of the soil. The precise prediction of seismic events remains elusive and unattainable goal in spite of these efforts. Many researchers have employed of recorded ground motion of different sites as the input earthquake ground acceleration to assess of impact of earthquake loads on the structures.

Although consideration of an actual earthquake ground motion record as the input has the advantage of having occurred in a past earthquake at a cer-

tain location, it is certainly insufficient since the future earthquake strong motion at the site of interest could have completely different characteristics [81]. As a result, Recent earthquakes have demonstrated the vulnerability of buildings.

There are two methods used to estimate ground motion in engineering practice [62].

- Deterministic seismic hazard analysis defined as the first method
- probabilistic seismic hazard analysis, referred to as the second method.

2.3 The Probabilist ground motions

various mathematical models in the literature for estimating the acceleration ground motion, include the soil characteristics at a side. The modelling of the earthquake excitation require to take into account many aspects such as the peak ground acceleration, magnitude, intensity, epicentre distance and frequency content. Advantage with the mathematical approach is that, we can generate many forms of recorded ground motion at different sites by adjusting on the intensity and frequency content varies with time. Since the nonstationary earthquakes are focused on these two mentioned parameters.

Figure 20 presents different steps to generate of the numerical way a non-

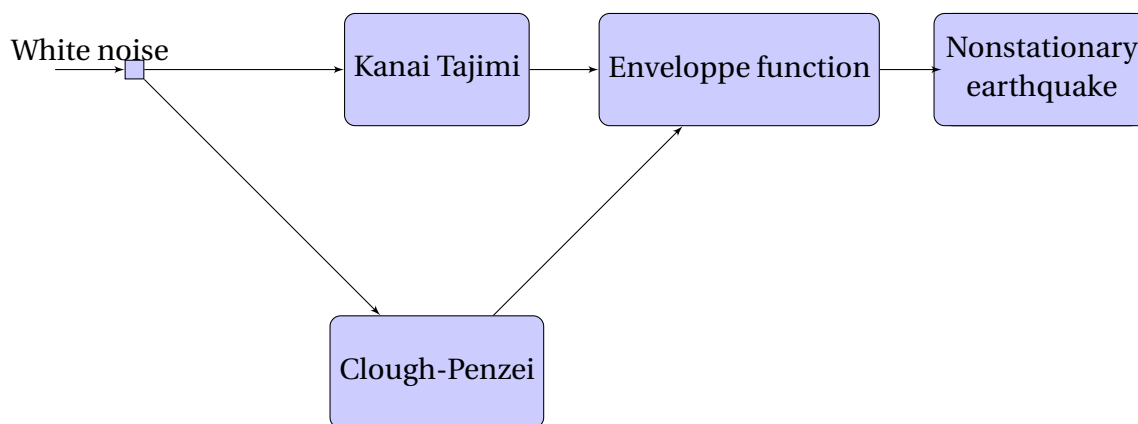


Figure 20: Algorithm for regenerating the nonstationary earthquake.

stationary earthquake. Each block is defined as follows

2.3.1 White-noise

Let $\eta(t)$ be defined as white noise. It is a random process and described as Gaussian whether checked the following properties

a zero mean value

$$E[\eta(t)] = 0 \quad (45)$$

and has an auto-correlation function defined by

$$R(t_1, t_2) = E[\eta(t_1)\eta(t_2)] = \delta(\tau) \quad (46)$$

where $\tau = t_2 - t_1$, and $\delta()$ is the Dirac delta function.

2.3.2 Kanai-Tajimi

The analyse of recorded data from strong ground motion demonstrates that earthquake power spectra are not independent of frequency [93]. The Kanai-Tajimi (Kanai 1957; Tajimi 1960) model is well-known and used very widely in the analysis of engineering structures under earthquake excitation [115]. Thus, the power spectral intensity of the ground acceleration is given by

$$S(\omega) = S_0 \frac{\omega_g^4 + (2\zeta_g \omega_g \omega)^2}{(\omega_g^2 - \omega^2)^2 + (2\zeta_g \omega_g \omega)^2} \quad (47)$$

In which

ζ_g and ω_g are damping coefficient and frequency. They are defined as filter parameters which depend on the site soil characteristics. S_0 is the constant spectral intensity.

Figure 21 illustrates different forms of Kanai-Tajimi model for $\zeta_g = 0.4$, $\omega_g = 3\pi$ rad/s (a) $S_0 = 0.02 \text{ m}^2/\text{s}^3$, (b) $S_0 = 0.015 \text{ m}^2/\text{s}^3$.

The site soil is considered as the place where a white noise disturbance is applied at bedrock and the motion is transmitted to the ground surface through a soil layer.

The following equations can be used

$$\begin{aligned} a(t) &= -2\zeta_g \omega_g \dot{x} - \omega_g^2 x \\ \ddot{x} + 2\zeta_g \omega_g \dot{x} + \omega_g^2 x &= \eta(t) \end{aligned} \quad (48)$$

$\eta(t)$ is the Gaussian white noise process, as pointed out in Equations (45) and (46).

This Kanai-Tajimi model has the attractive feature because it is the ability to simulate ground acceleration in a very simple way. The most serious short-coming of the original Kanai-Tajimi model is its treatment of earthquakes as stationary random processes [89].

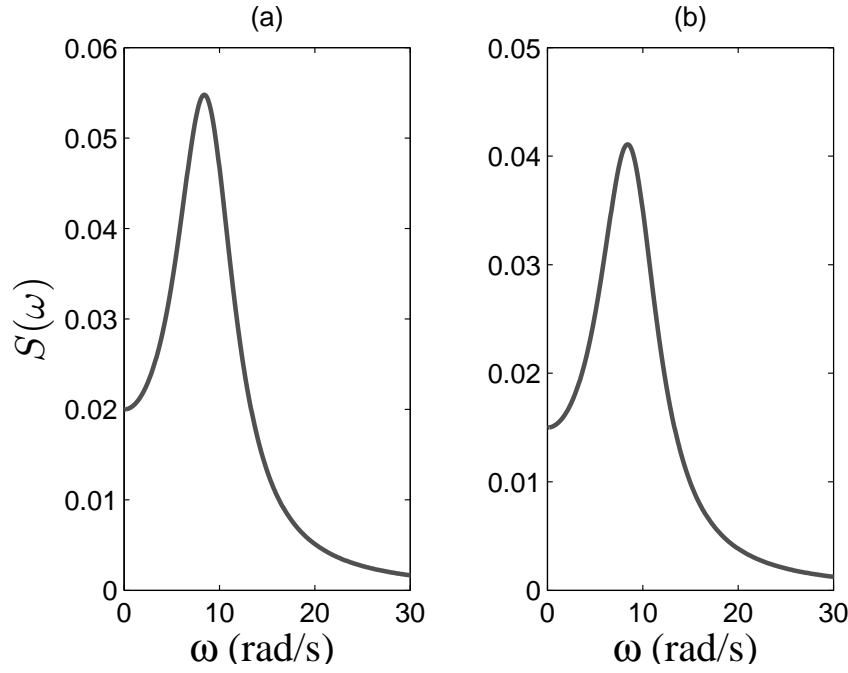


Figure 21: Kanai-Tajimi model

2.3.3 Clough-Penzien

Despite of the fact that the Kanai-tajimi shows advantage of the simple way for the simulation of the stationary ground motion but presents a drawback specially, in low frequency in which the variances of ground velocity and ground displacement become infinite ($\omega \rightarrow \infty$). These can be seen from the relationships between power spectra for ground acceleration, velocity and displacement.

To remedy to this noticed problem therefore the concept consists to remove the singularity at $\omega = 0$, Clough and Penzien modified the Kanai-Tajimi formulation by adding an another term.

Hence, the mathematical expression has been rewritten and given as follows

$$S(\omega) = S_0 \left[\frac{\omega_g^4 + 4\zeta_g^2 \omega_g^2 \omega^2}{(\omega_g^2 - \omega^2)^2 + 4\zeta_g^2 \omega_g^2 \omega^2} \right] \left[\frac{\omega^4}{(\omega_f^2 - \omega^2)^2 + 4\zeta_f^2 \omega^2 \omega_f^2} \right] \quad (49)$$

Figure 22 displays the different forms of Clough-Penzien model for $\zeta_g = 0.4$,

Table 1: Parameters of the filter soil of Clough-Penzien [84]

Soil	$\omega_g(rad/s)$	ζ_g	$\omega_f(rad/s)$	ζ_f
Hard	15.0	0.6	1.5	0.6
Medium	10.0	0.4	1.0	0.6
Soft	5.0	0.2	0.5	0.6

$$\omega_g = 3\pi \text{ rad/s}, S_0 = 0.02 \text{ m}^2/\text{s}^3.$$

where ω_f and ζ_f are high-pass filter parameters

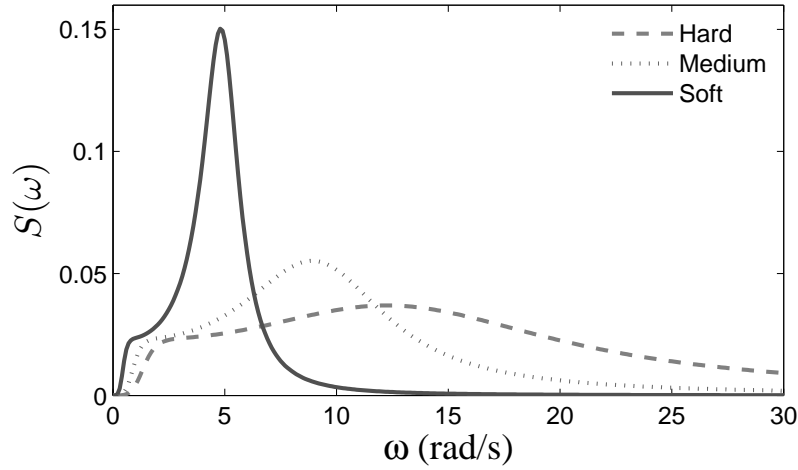


Figure 22: Clough-Penzel model

2.3.4 Envelope Functions

The envelope function $Env(t)$ describes the variation of ground motion intensity with time [93]. Various models have extensively been suggested in the literature to illustrate time-varying intensities.

2.3.4.1 Shinozuka and Sato model

The Shinozuka and Sato model (Figure 23) is based on the difference between two exponential function given as follows [93]

$$Env(t) = c_e(e^{-\alpha t} - e^{-\beta t}) \quad (50)$$

in which

$$c_e = \frac{1}{\left(\frac{\alpha}{\beta}\right)^{\frac{\alpha}{\beta-\alpha}} - \left(\frac{\alpha}{\beta}\right)^{\frac{\beta}{\beta-\alpha}}}$$

The time at which the envelope function reaches the maximum value, $Env(t_{max}) = 1$ is

$$t_{max} = \frac{\ln\left(\frac{\beta}{\alpha}\right)}{\beta - \alpha} \quad (51)$$

It can observe from (51) that the time duration depends on the choice of parameters α and β , and by changing the values of these ones we have of

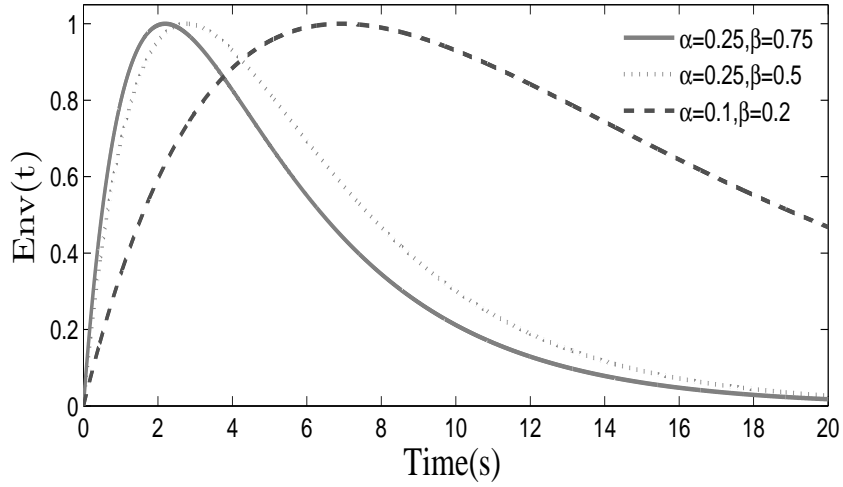


Figure 23: Envelope function of Shinozuka and Sato model

different time-modulating functions.

The short duration ($\alpha = 0.10, \beta = 0.20$), and the long duration ($\alpha = 0.25, \beta = 0.75$). From Figure 23 it is observed that the time at which the envelope function reaches to 1 really matches with Equation 51.

2.3.4.2 Amin and Ang model

The mathematical expression of Amin and Ang model is generalised by Jennings *et al.* [87], therefore the equation is

$$Env(t) = \begin{cases} t^2/4, & 0 \leq t \leq 2 \\ 1.0, & 2 < t \leq 4 \\ \exp(-0.268(t-4)), & 4 < t \leq 12 \end{cases} \quad (52)$$

by taking account of this form, we have the Figure 24 which illustrates the envelope function of Amin and Ang.

2.3.4.3 Boore model

The mathematical model described by Boore[48] is expressed as follows

$$Env(t) = at^b e^{-ct} H(t) \quad (53)$$

where $H(t)$ is the unit-step function. a is the normalizing factor, and b and c are the shape parameters.

These conditions yield

$$b = -\epsilon \frac{\ln(\eta)}{[1 + \epsilon(\ln \epsilon - 1)]} \quad (54)$$

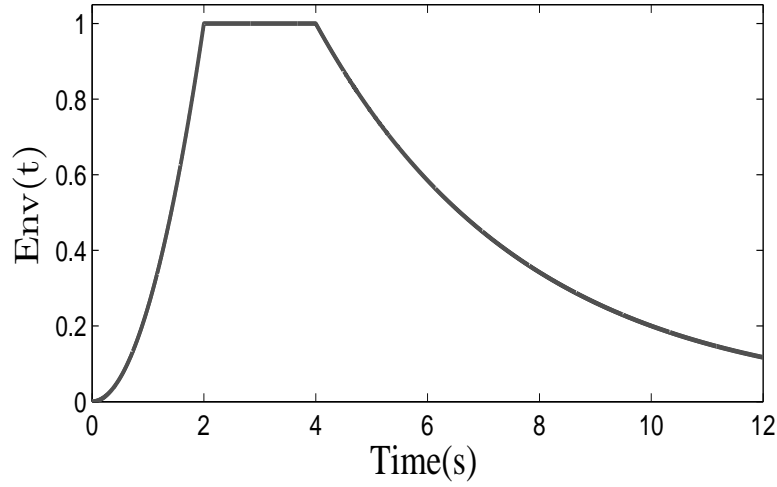


Figure 24: Envelope function of Amin and Ang model

and

$$c = b/\epsilon T_w \quad (55)$$

where ϵ and η are constants and T_w is the specified duration. The normalizing factor a can be chosen in several ways

$$a = (e/\epsilon T_w)^b \quad (56)$$

gives a maximum amplitude of unity, and

$$a = \left[\frac{(2c)^{2b+1}}{\Gamma(2b+1)} \right]^{1/2}$$

results in an envelope with unit squared area.

By taking the values of parameters $a = 0.117$; $b = 1.825$; $c = 0.277$ obtained by Saragoni and Hart[49]. We have the Figure 25 that shows the Envelope function of Boore model.

The chosen envelope function depends on the form of observed ground motions. Since the mentioned function describes the manner in which the intensity of the stochastic process varies with time.

2.3.5 Excitation Earthquake models

The nonstationary Kanai-Tajimi model has been used by the researchers [89, 94] to produce artificial records of the ground motion time histories. In other words this one allows to generate the artificial accelerograms with a single dominant frequency.

The mentioned model only illustrates the stationary random aspect, which

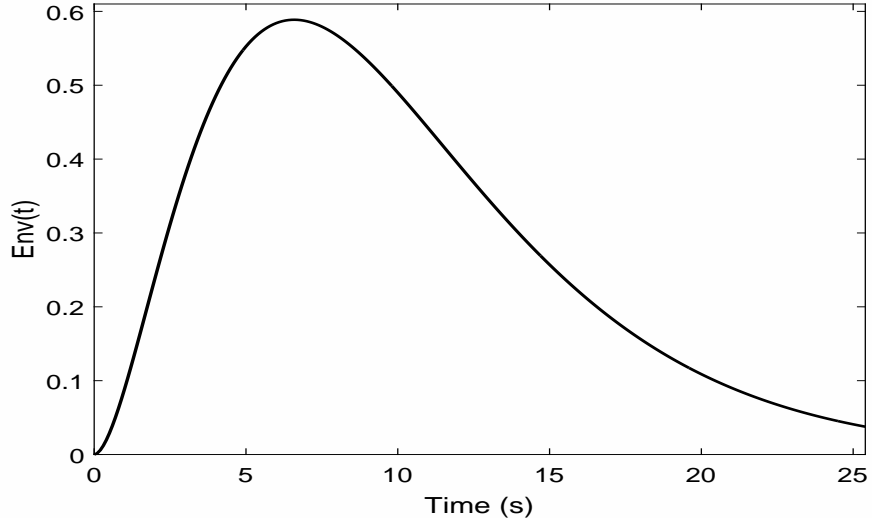


Figure 25: Envelope function of Boore model

is not the real nature of the ground excitation because it includes the time-varying intensity and frequencies [94]

$$\ddot{X}_g = -(-2\zeta_g(t)\omega_g(t)\dot{X}_f + \omega_g^2(t)X_f)Env(t) \quad (57)$$

$$\ddot{X}_f + 2\zeta_g(t)\omega_g(t)\dot{X}_f + \omega_g^2(t)X_f = n_1(t) \quad (58)$$

where \ddot{X}_g is the ground acceleration, X_f is the filter response, $\omega_g(t)$ is the time dependent predominant ground, $Env(t)$ is the amplitude envelope function

2.3.5.1 El Centro 1940 earthquake

The envelope function is given by

$$Env(t) = 9.44t^3 e^{-1.17t} + 3.723 \quad (59)$$

The content frequency is described by

$$\omega_g(t) = 9.425 + 59.722(e^{-0.0625t} - e^{-0.15t}) \quad (60)$$

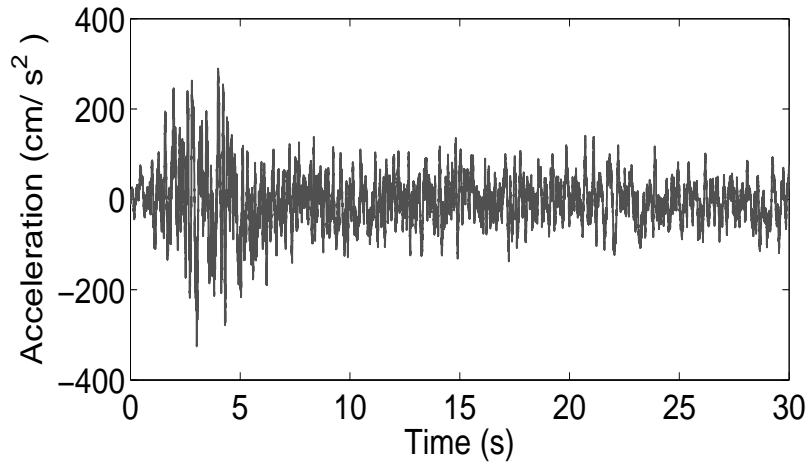


Figure 26: Simulation of El Centro 1940 Earthquake

2.3.5.2 Mexico City 1985 earthquake

The envelope function adapted to this type earthquake is

$$Env(t) = \begin{cases} 0.3915t + 1.45 & \text{for } 0 \leq t \leq 32 \\ 13.978 - 1.073(t - 32), & \text{for } 32 < t \leq 42.9 \\ 2.2823, & \text{for } t \geq 42.9 \end{cases} \quad (61)$$

The content frequency is given

$$\omega_g(t) = 3.456 + 3.77 \sin(0.17(t - 2)) \quad (62)$$

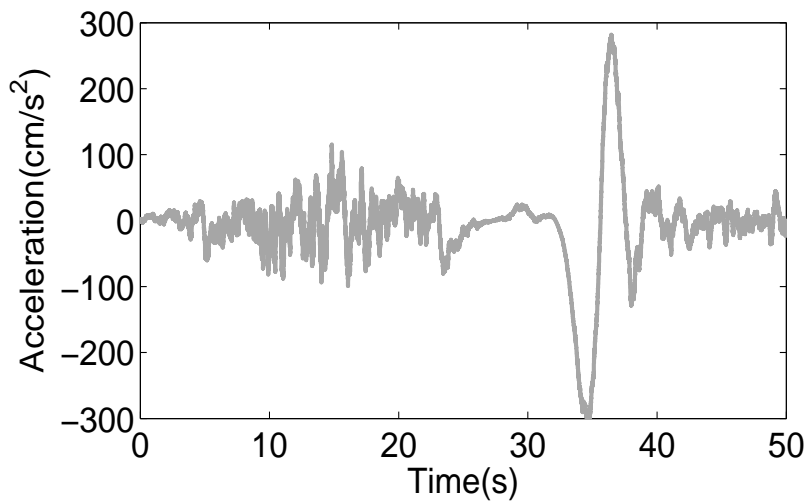


Figure 27: Simulation of the Mexico City 1985 earthquake

2.3.6 Abbas and Takewaki

The nonstationary ground acceleration \ddot{X}_g of n sequences is presented by Abbas and Takewaki [92]. Authors pointed up, ground acceleration of multiple sequences could result in more damage to the structure than a single ordinary event. Because the structure gets damaged in the first sequence, and additional damage accumulates from secondary sequences before any repair is possible.

The acceleration expression proposed to take the form of a filtered Gaussian stationary white noise modulated by a deterministic envelope function of time, as defined

$$\ddot{X}_g(t) = \begin{cases} En\nu_1(t)\ddot{w}_1; & 0 \leq t \leq T_1 \\ 0; & T_1 < t \leq T_1 + T_2 \\ En\nu_2(t - T_1T_2); \ddot{w}_2(t) & T_1 + T_2 \leq t \leq T_1 + T_2 + T_3 \\ \dots & \\ En\nu_n(t - \sum_{i=1}^{n+1} T_i)\ddot{w}_n(t); & \sum_{i=1}^{n+1} T_i \leq t \leq \sum_{i=1}^{n+2} T_i \end{cases} \quad (63)$$

where

$e_1(t), e_2(t) \dots e_n(t)$ are the envelope functions associated with the acceleration sequences 1, 2 ... n ,

$\ddot{w}_1(t), \ddot{w}_2(t) \dots \ddot{w}_n(t)$ are stationary random processes.

$T_1, T_2 \dots T_{n+2}$ are the time durations of the acceleration sequences.

The envelope function for the i th sequence is expressed as

$$En\nu_i(t) = A_i \left(t - \sum_{i=1}^n T_i \right) \exp \left[-\alpha_i \left(t - \sum_{i=1}^n T_i \right) \right] \quad (64)$$

where e_{0i} and α_i are $2n$ positive constants that control the intensity and the non-stationarity trend of the i th acceleration sequence.

The parameters of envelope function are $\alpha_1 = 0.3$, and $\alpha_2 = 0.35$, $A_1 = 0.8155$, $A_2 = 0.9514$, $\omega_g = 3\pi$ rad/s, $\eta_g = 0.4$, (the time duration of the sequences is about 25 s, and 20 s respectively) and the separating time interval between the sequences is 40 s.

The dimensionless nonstationary ground acceleration for two sequences with the separating time interval both of them, is shown in Figure 28.

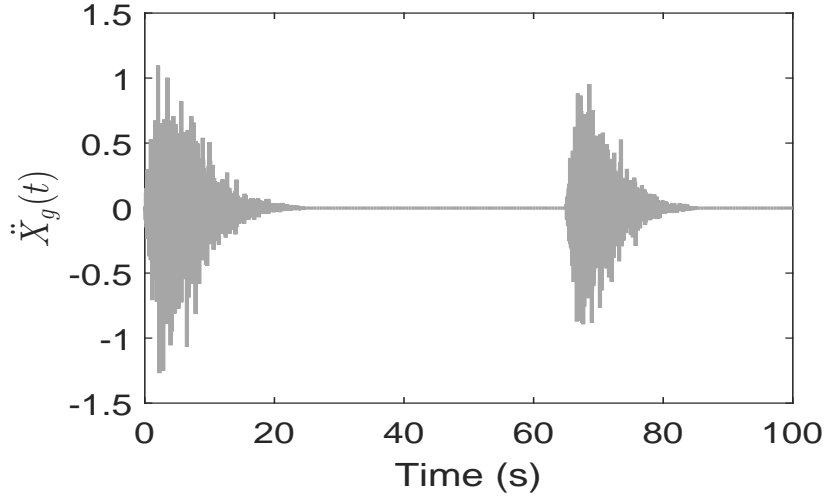


Figure 28: Sample simulated acceleration sequences.

2.4 The deterministic ground motion

The earthquake load is modelled as a deterministic time history which is expressed in terms of a Fourier series that is modulated by an enveloping function [90].

The main difference with section 2.3 is that, the random process does not employ to generate the earthquake motion. The common characteristic between the two types of modelling is the non-stationary deterministic function of time. Since its presence of this one allows to adjust the duration of ground motion.

$$\ddot{X}_g(t) = e(t) \sum_{i=1}^{N_f} [A_i \cos(\omega_i t) + B_i \sin(\omega_i t)] \quad (65)$$

where

$A_i ; B_i$, are $2N_f$ unknown constants and ω_i , $i = 1, 2, \dots, N_f$ are the frequencies presented in the ground acceleration \ddot{X}_g which are selected such that they span satisfactory the frequency range $[0, 25] Hz$.

The function $e(t) = e_0(e^{-\alpha t} - e^{-\beta t})$ represents the enveloping function that imparts transient nature to the earthquake acceleration. The deterministic expression does not reflect the real nature of ground motions.

Figure 29 is an example of deterministic ground motion with the values defined as follows

$e_0 = 2.17$; $\alpha = -0.13$; $\beta = -0.5$, $A_1 = 0.71$; $\omega_1 = 11.42$; $B_1 = 0.025$; $A_2 = 0.065$; $\omega_2 = 13.56$; $B_2 = 0.055$; $A_3 = .25$; $\omega_3 = 14.7$; $B_3 = 0.015$; $A_4 = 0.06$; $B_4 = 0.015$; $\omega_4 = 15.15$.

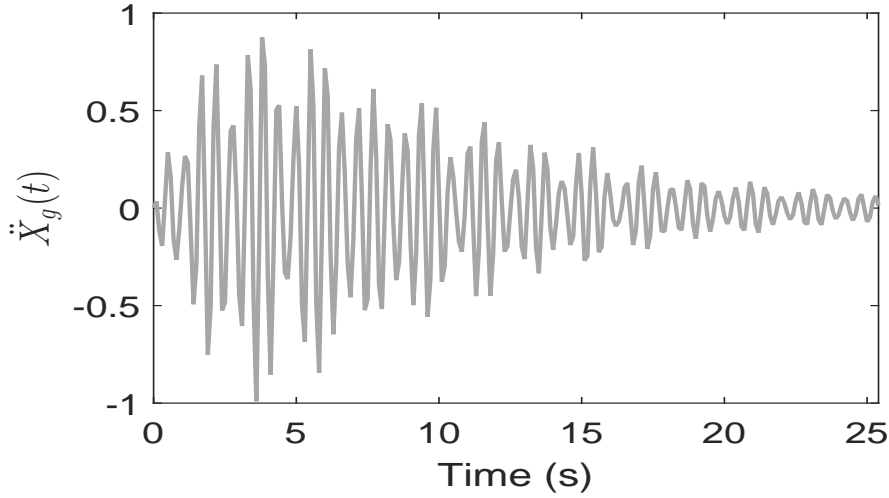


Figure 29: deterministic ground motion

2.5 Analytical and Numerical formalisms

2.5.1 Method of lines

The "method of lines" or "semi-discretisation" is defined as a method for the approximate solution of parabolic partial differential equations [88].

In this part, we describe an implementation of the method applied to non-linear parabolic partial differential equations.

$$\frac{\partial^2 u}{\partial t^2}(x, t) = f\left(t, x, \frac{\partial u}{\partial x}(x, t), \frac{\partial u}{\partial t}(x, t), \frac{\partial^2 u}{\partial x^2}(x, t)\right) \quad (66)$$

Consider for example the below equation given

$$\frac{\partial^2 u}{\partial t^2}(x, t) = \frac{\partial^2 u}{\partial x^2}(x, t) + c_1 \frac{\partial u}{\partial t}(x, t) \quad (67)$$

over $0 \leq x \leq 1$, $t > 0$

subject to

- initial conditions

$$u(x, 0) = 0, \quad \frac{\partial u}{\partial t}(x, 0) = 0, \quad 0 \leq x \leq 1, \quad (68)$$

- and boundary conditions

$$u(0, t) = 0, \quad u(1, t) = 0, \quad t > 0 \quad (69)$$

$$\frac{\partial u}{\partial x}(0, t) = g(x), \quad \frac{\partial u}{\partial x}(1, t) = 0, \quad t > 0 \quad (70)$$

The adopted standard second order finite difference approximations given as follows

$$\frac{\partial u(x, t)}{\partial x} = \frac{u(i-1, j) - u(i+1, j)}{2\Delta x}, \quad (71)$$

$$\frac{\partial^2 u(x, t)}{\partial x^2} = \frac{u(i-1, j) - 2u(i, j) + u(i+1, j)}{(\Delta x)^2} \quad (72)$$

and

$$\frac{\partial u(x, t)}{\partial t} = \frac{u(i, j-1) - u(i, j+1)}{2\Delta t} \quad (73)$$

by introducing the new variables, we have

$$v_1(i) = u(i, j), \quad v_2(i) = u(i, j+1), \quad v_3(i) = u(i, j-1) \quad (74)$$

this yields the expressions defined as follows

$$\frac{\partial u(x, t)}{\partial x} = \frac{v_1(i-1) - v_1(i+1)}{2\Delta x}, \quad (75)$$

$$\frac{\partial^2 u(x, t)}{\partial x^2} = \frac{v_1(i-1) - 2v_1(i) + v_1(i+1)}{(\Delta x)^2} \quad (76)$$

$$\frac{\partial u(x, t)}{\partial t} = \frac{v_3(i) - v_2(i)}{2\Delta t} \quad (77)$$

Equations (75) and (76) are inserted in the relation (67), one gets

$$\left\{ \begin{array}{l} \frac{du_1}{dt} = v_0(i) \\ \frac{dv_0}{dt} = \frac{v_1(i-1) - 2v_1(i) + v_1(i+1)}{(\Delta x)^2} + c_1 \left(\frac{v_3(i) - v_2(i)}{2\Delta t} \right) \end{array} \right. \quad (78)$$

We set $\Delta x = 1/N$, $x_i = (i-1)\Delta x$ and $t = j\Delta t$ where Δx and Δt are the spatial and temporal steps, i and j are integer variables relative to position and time. N is the number of discrete points considered along the beam length.

Initial conditions are

$$v_0(i) = 0, \quad , v_1(i) = 0, \quad v_2(i) = v_3(i) = 0.0, \quad \text{for } i = 1, \dots, m \quad (79)$$

The boundary conditions become

$$v_1(1) = 0.0, \quad v_1(m) = 0. \quad (80)$$

$$v_1(2) = v_1(0) + 2\Delta x g(x_1), \quad v_1(m+1) = v_1(m-1) + 2\Delta x g(x_m) \quad (81)$$

Equation (78) can be solved using initial and boundary conditions.

2.5.2 Routh-Hurwitz Stability Criterion

Routh-Hurwitz stability criterion is a method for stability analysis of linear systems. This approach is a necessary and sufficient condition for the stability of a system, since it has bounded output for bounded inputs, if the roots of its characteristic equation have negative real parts only.

The characteristic equations is given by

$$f(\lambda) = a_0\lambda^n + a_1\lambda^{n-1} + \dots + a_{n-1}\lambda + a_n = 0 \quad (82)$$

where the coefficients a_i are real constants.

The main diagonal of the Hurwitz's matrix are the form

$$\Delta_1 = a_1, \quad \Delta_2 = \begin{vmatrix} a_1 & a_0 \\ a_3 & a_2 \end{vmatrix},$$

$$\Delta_3 = \begin{vmatrix} a_1 & a_0 & 0 \\ a_3 & a_2 & a_1 \\ a_5 & a_4 & a_3 \end{vmatrix}, \quad \dots, \quad \Delta_n = \begin{vmatrix} a_1 & a_0 & 0 & \dots & 0 \\ a_3 & a_2 & a_1 & \dots & 0 \\ a_5 & a_4 & a_3 & \dots & 0 \\ \dots & \dots & \dots & \dots & \dots \\ 0 & 0 & 0 & \dots & a_n \end{vmatrix}$$

In general, Hurwitz condition states: all of the roots of the polynomial have negative real part if the determinant of all Hurwitz matrix are positive. That is, none of them are zero or negative.

$$\Delta_1 > 0, \quad \Delta_2 > 0, \quad \dots, \quad \Delta_n > 0 \quad (83)$$

Since, $\Delta_n = a_n\Delta_{n-1}$, the condition $\Delta_n > 0$ can be changed by a_n

$$n = 2; \quad a_1 > 0 \quad \text{and} \quad a_2 > 0 \quad (84)$$

$$n = 3; \quad a_1 > 0, a_3 > 0 \quad \text{and} \quad a_1 a_2 > a_3 \quad (85)$$

$$n = 4; \quad a_1 > 0, a_3 > 0, a_4 > 0 \quad \text{and} \quad a_1 a_2 a_3 > a_3^2 + a_1^2 a_4 \quad (86)$$

Thus, conditions checked the system is considered stable.

Numerical formalism can be defined as an approximate solution of problems occur for instance in physics, chemistry, biology, economics and in many field of engineering.

The numerical analysis is adopted in the many case to obtain information about the response dynamics of the physical system. It is impossible to have analytical solution. The selection of integration algorithms using numerical approximation depends on of the complexity of problems and the scientific disciplines.

2.5.3 Fourth-order Runge-Kutta methods

Runge-kutta algorithm is an integrator method the most well-known. It is employed to approximate numerical solution the higher order ordinary differential equations. This mentioned algorithm is also defined as implicit and explicit iterative methods. The method can be used within stochastic and deterministic differential equation frameworks.

However there are many modified version of the Runge-kutta algorithm within the deterministic framework as well as stochastic. The new Runge-Kutta (RK) algorithm described by Kasdin [80] is used for the integration of stochastic differential equations. This approach improves the accuracy of stochastic simulations over the traditional approaches.

2.5.3.1 The deterministic version

As above mentioned, the algorithm can also employ within deterministic. The general deterministic algorithm is given as follows.

$$\dot{\mathbf{X}}(t) = \mathbf{F}(X, t) \quad (87)$$

The solution of 87 is approximated at time, as described by following set of equations:

$$X_{k+1}(t) = X_k + a_{51}k_1 + a_{52}k_2 + a_{53}k_3 + a_{54}k_4 \quad (88)$$

in which

$$k_1 = hF(X_k, t_k) \quad (89)$$

$$k_2 = hF(X_k + a_{21}k_1, t_k + c_2h) \quad (90)$$

$$k_3 = hF(X_k + a_{31}k_1 + a_{32}k_2, t_k + c_3h) \quad (91)$$

$$k_4 = hF(X_k + a_{41}k_1 + a_{42}k_2 + a_{43}k_3, t_k + c_4h) \quad (92)$$

where h is the time step size. These equations are an order-n RK integrator. The coefficients c_2, c_3, c_4 and $a_{21}, a_{31}, a_{32}, a_{41}, a_{42}, a_{43}, a_{51}, a_{52}, a_{53}, a_{54}$ are constant defined.

2.5.3.2 The stochastic version

Stochastic differential equations (SDE) become an important tool in many scientific areas due to its application for modelling dynamical systems. The mathematical expression is given by

$$\dot{\mathbf{X}}(t) = \mathbf{F}(X, t) + G(X, t) w(t) \quad (93)$$

where

$w(t)$ is a vector of Gaussian.

$F(X, t)$ and $G(X, t)$ are the dynamic and input distribution matrix, respectively.

Thus, the Kasdin's scheme is described as follows

$$X_{k+1}(t) = X_k + a_{51}k_1 + a_{52}k_2 + a_{53}k_3 + a_{54}k_4 \quad (94)$$

in which

$$\begin{aligned} k_1 &= hF(X_k, t_k) + hG(X_k, t_k) w_1 \\ k_2 &= hF(X_k + a_{21}k_1, t_k + c_2h) + G(X_k + a_{21}k_1, t_k + c_2h) w_2 \\ k_3 &= hF(X_k + a_{31}k_1 + a_{32}k_2, t_k + c_3h) + G(X_k + a_{31}k_1 + a_{32}k_2, t_k + c_3h) w_3 \\ k_4 &= hF(X_k + a_{41}k_1 + a_{42}k_2 + a_{43}k_3, t_k + c_4h) + \\ &\quad G(X_k + a_{41}k_1 + a_{42}k_2 + a_{43}k_3, t_k + c_4h) w_4 \end{aligned}$$

c is a constant that can be obtained by

$$c_2 = a_{21} \quad (95)$$

$$c_3 = a_{31} + a_{32} \quad (96)$$

$$c_4 = a_{41} + a_{42} + a_{43} \quad (97)$$

Let us consider a vectorial variable $X(t) = (x_1(t), x_2(t), \dots, x_n(t))$

Table 2: Runge-Kutta coefficients fourth-order time-invariant

a_{32}	0.00342761715422	a_{41}	- 2.32428921184321
a_{42}	2.69723745129487	a_{43}	0.29093673271592
a_{51}	0.25001351164789	a_{52}	0.67428574806272
a_{53}	-0.00831795169360	a_{54}	0.08401868181222

- Mean

$$\bar{X} = \frac{1}{n} \sum_{m=1}^n x_m(t) \quad (98)$$

- Mean square

$$\bar{X}_2 = \frac{1}{N} \sum_1^m x_m(t)^2 \quad (99)$$

2.5.4 Newton-Raphson Method for system of equations

Due to the encountered difficulties for solving the nonlinear system of equations. Many iterative methods are employed in the literature to remedy to

this problem. The Newton-Raphson method is defined as an iterative procedure for finding zeros of an equation or the system of nonlinear equations. To illustrate this principle, the system of equations is defined as follows

$$\begin{cases} f(x, y) = 0 \\ g(x, y) = 0 \end{cases} \quad (100)$$

The functions $f(x, y)$ and $g(x, y)$ are two arbitrary functions

$$f(x, y) = f(x_0, y_0) + \frac{\partial f}{\partial x}(x - x_0) + \frac{\partial f}{\partial y}(y - y_0) + o(x, y) \quad (101)$$

$$g(x, y) = g(x_0, y_0) + \frac{\partial g}{\partial x}(x - x_0) + \frac{\partial g}{\partial y}(y - y_0) + o(x, y) \quad (102)$$

The Jacobian matrix associated with above equations is found as follows

$$\mathbf{J}(x, y) = \begin{pmatrix} \frac{\partial f}{\partial x} & \frac{\partial f}{\partial y} \\ \frac{\partial g}{\partial x} & \frac{\partial g}{\partial y} \end{pmatrix} \quad (103)$$

if $\det(J) \neq 0$, the iterative method is written as

$$\mathbf{X}_{n+1} = \mathbf{X}_n - J^{-1}(\mathbf{X}_n)F(\mathbf{X}_n) \quad (104)$$

A convergence criterion for the solution of a system of non-linear equation could be, for example, the magnitude of the absolute values of the functions $F(\mathbf{X}_n)$ is smaller than a certain tolerance

$$|F(\mathbf{X}_n)| < \epsilon \quad (105)$$

To get the algorithm started, we need to provide two initial values of \mathbf{X} (a vector)

2.5.5 Hardware and Software

During the course of this work, we used a Laptop computer running Windows 7 operating system and three major software's: Fortran, Matlab and Maple.

2.5.6 Box-Muller Method

The Box-Muller method will be used for generating standard Gaussian pseudo-random numbers. It is based on the observation that if U_1 and U_2 are two independent $U(0, 1)$ uniformly distributed random variables, then G_1 and G_2

are defined by [101]

$$G_1 = \sqrt{-2\ln(U_1)} \sin(2\pi U_2) \quad (106)$$

$$G_2 = \sqrt{-2\ln(U_1)} \sin(2\pi U_2) \quad (107)$$

are two independent standard Gaussian random variables

2.5.7 Fuzzy Logic

The Fuzzy Logic tool was introduced in 1965 by Lotfi Zadeh. Known as the father of fuzzy logic, he was instrumental in making fuzzy logic a major field of study to complement probability theory.

Defined as a mathematical tool of reasoning that resembles human reasoning. By helping to deal with uncertainty in engineering and working on the levels of possibilities of input to achieve the definite output, the fuzzy logic offers to a soft computing partnership the important concept of computing with words [74].

There is a wide variety of application domains of the Fuzzy logic, from control theory to artificial intelligence. It can be implemented in hardware, software, or a combination of both and can also be implemented in systems with various sizes and capabilities ranging from small micro-controllers to large, networked, workstation-based control systems.

Fuzzy logic Architecture

- **Fuzzification Module**, it transforms the system inputs, which are crisp numbers, into fuzzy sets. It splits the input signal into seven steps such as Negative Large(NL), Negative Medium (NM), Negative Small (NS), Zeros (ZE), Positive Small (PS), Positive Medium (PM), Positive Large(PL), as displayed in figure 31b.
- **Knowledge Base**, this block contains the base section described by IF-THEN rules and database which defines the membership functions of the fuzzy sets used in the fuzzy rules.
- **Inference Engine**, this block performs the crisp inputs into degrees of matching with linguistic values.
- **Defuzzification Module**, it transforms the fuzzy set obtained by the inference engine into a crisp value. This mentioned module reduces the collection of membership function values in to a single scalar quantity.

The different defuzzification methods are available in the literature. It is therefore important to select the appropriate defuzzification method for a particular application. Unfortunately, there is no standard rule for selecting a particular defuzzification method for an application [76]. Similar to the fuzzification process, the fuzzy output variables are defined using a total of 4 output membership functions: Zero, PS, PM, PL, as pointed out in Figure 31b.

Fuzzy if-then rules are characterized by appropriate membership functions. Due to their concise form, fuzzy if-then rules are often employed to capture the imprecise modes of reasoning that play an essential role in the human ability to make decisions in an environment of uncertainty and imprecision [77]

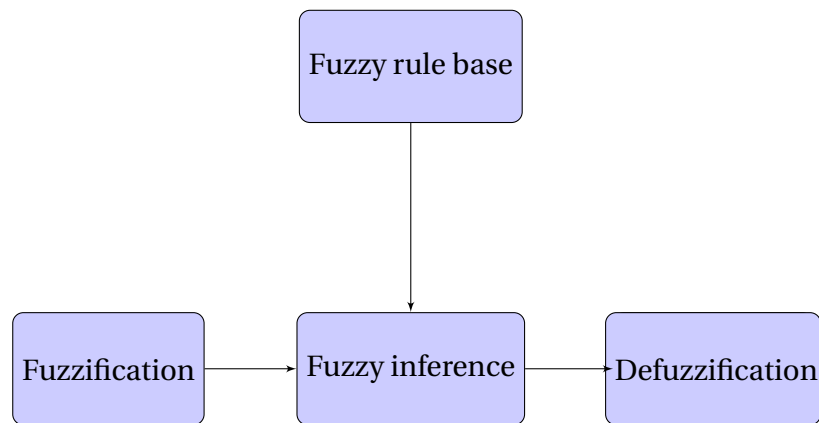


Figure 30: Fuzzy inference system.

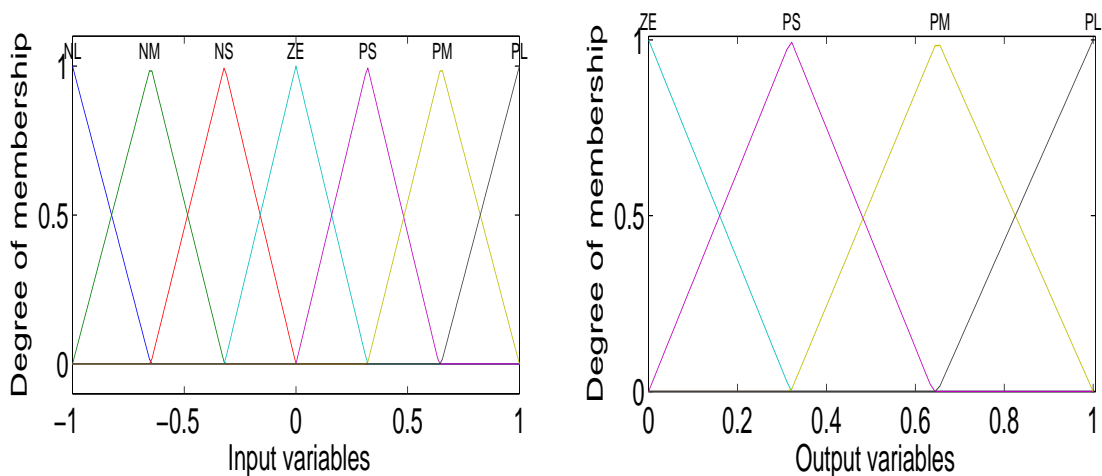


Figure 31: Input and output membership functions.

2.6 Conclusion

In this chapter, the different mathematical modellings of earthquake ground motions based on deterministic and probabilist frameworks were presented. A simple algorithm of probabilist framework for regenerating the ground motion, which maintains the nonstationary evolutions of amplitude and frequency content was detailed. Moreover, some envelope functions mentioned in the literature were enumerated. Afterwards, the mathematical and numerical simulation methods used to solve the equations subject to external perturbations such as non-stationary random process were also detailed in this chapter, as well as the hardware and software employed. As further element, a brief description was shown to determine Gaussian pseudo-random numbers. Finally, the Fuzzy Logic tool that allows of stabilizing the response dynamics of physical system were provided. The next chapter focuses on results and discussions.

RESULTS AND DISCUSSIONS

3.1 Introduction

This chapter is devoted to the results and discussions of the work carried out in this thesis. It is organized as follows. Section 3.2 deals with the general mathematical formalism, description of the control of a Timoshenko beam, and the effect of the control on the dynamics responses. Section 3.3 deals with the statistical responses of two buildings subjected to the repeated sequence of excitation. Section 3.4 deals with the influence of Fuzzy control device on the statistical response of two interconnected buildings. Section 3.5 is devoted to statistical effects of an outrigger system under seismic excitation. In this sense the description of physical system and dynamic model formulation are detailed and the performance of the employed control system to attenuate the undesirable vibration is obtained. The last section concludes the chapter.

3.2 Dynamics and MR control of vibration of cantilever Timoshenko beam under earthquake loads

Consider a Timoshenko beam of length L , with density ρ . The bending vibration can be described by two variables dependent on axial coordinate x and time t , namely, transverse displacement $y = y(x, t)$ and $\theta = \theta(x, t)$, the transverse rotation of the beam cross-section due to the bending moment.

The governing equations for the vibration of Timoshenko beam thus involve a system of two partial differential equations given by [71, 98–100]

$$\rho I \frac{\partial^2 \theta}{\partial t^2} + \alpha_2 \rho A \frac{\partial \theta}{\partial t} = EI \frac{\partial^2 \theta}{\partial x^2} + kGA \left(\frac{\partial y}{\partial x} - \theta \right) \quad (108a)$$

$$\rho A \frac{\partial^2 y}{\partial t^2} + \alpha_1 \rho A \frac{\partial y}{\partial t} = kGA \left(\frac{\partial^2 y}{\partial x^2} - \frac{\partial \theta}{\partial x} \right) + P(t) \quad (108b)$$

Where E is the Young's modulus of elasticity of beam material, G is the shear modulus of the beam material, α_1 and α_2 are the linear viscous damping coefficients, A is the cross-sectional area of the beam, k is the effective area coefficient in shear, I is the area moment of inertia and $P(t)$ is the external force.

Taking into account the following dimensionless variables:

$$\theta^* = \theta, \quad Y = \frac{y}{L}, \quad X = \frac{x}{L}, \quad \tau = \frac{t}{T}, \quad T = L \sqrt{\frac{\rho}{Gk}}$$

$$\alpha_2 = \frac{I}{A} \alpha_1, \quad \lambda = \alpha_1 T, \quad k_1 = \frac{E}{kG}, \quad k_2 = \frac{AL^2}{I}, \quad P_1(\tau) = \frac{LP(t)}{kGA}$$

Equations (108a)-(108b) are reduced to the following set of non-dimensional differential equations

$$\frac{\partial^2 \theta^*}{\partial \tau^2} + \lambda \frac{\partial \theta^*}{\partial \tau} = k_1 \frac{\partial^2 \theta^*}{\partial X^2} + k_2 \left(\frac{\partial Y}{\partial X} - \theta^* \right) \quad (109a)$$

$$\frac{\partial^2 Y}{\partial \tau^2} + \lambda \frac{\partial Y}{\partial \tau} = \left(\frac{\partial^2 Y}{\partial X^2} - \frac{\partial \theta^*}{\partial X} \right) + P_1(\tau) \quad (109b)$$

With the boundary conditions

$$Y(0, \tau) = 0, \quad \theta^*(0, \tau), \quad \frac{\partial \theta^*}{\partial X}(1, \tau) = 0, \quad \frac{\partial Y}{\partial X}(1, \tau) - \theta^*(1, \tau) = 0$$

The two expressions of the equation (109) of motion for a Timoshenko beam are combined to formulate an equation for transverse deflection Y , in the form

$$\begin{aligned} \frac{\partial^4 Y}{\partial \tau^4} + 2\lambda \frac{\partial^3 Y}{\partial \tau^3} + (k_2 + \lambda^2) \frac{\partial^2 Y}{\partial \tau^2} - (1 + k_1) \frac{\partial^4 Y}{\partial X^2 \partial \tau^2} - \lambda(1 + k_1) \frac{\partial^3 Y}{\partial X^2 \partial \tau} + \lambda k_2 \frac{\partial Y}{\partial \tau} + \\ k_1 \frac{\partial^4 Y}{\partial X^4} = k_2 P_1(\tau) + \lambda \dot{P}_1(\tau) + \ddot{P}_1(\tau) \end{aligned} \quad (110)$$

The equation.(110) is the general equation governing the transversal displacement of the damped Timoshenko beam

3.2.1 Derivation of the modal equation

To deal with the analytical analysis we resort to an assumed mode expansion. Specifically, it is assumed that Y can be written as the finite sums

$$Y(X, \tau) = \sum_{n=1}^N \Phi_n(X) Q_n(\tau) \quad (111)$$

Where

$Q_n(\tau)$ is the unknown function of time at n^{th} mode and $\Phi_n(X)$ is the solution of the eigenvalue problem obtained by solving equation (110) without damping and excitation and $\Phi_n(X)$ is given by

$$\Phi_n(X) = (C_{1n} \cos(\delta_n X) + C_{2n} \sin(\delta_n X) + C_{3n} \sinh(\epsilon_n X) + C_{4n} \cosh(\epsilon_n X)) \quad (112)$$

Where

C_{1n}, C_{2n}, C_{3n} and C_{4n} are obtained as (using the beam boundary conditions)[37]

$$C_{1n} = \frac{\cos(\delta_n) + \frac{(\varepsilon_n^2 + \mu\delta_n^2)}{(\delta_n^2 + \mu\varepsilon_n^2)} \cosh(\varepsilon_n)}{-\left(\sin(\delta_n) + \frac{\varepsilon_n}{\delta_n} \sinh(\varepsilon_n)\right)}; \quad C_{2n} = 1;$$

$$C_{3n} = -C_{1n} \frac{\left(\delta_n + \mu \frac{\varepsilon_n^2}{\delta_n}\right)}{\left(\varepsilon_n + \mu \frac{\delta_n^2}{\varepsilon_n}\right)}; \quad C_{4n} = -C_{2n}$$

The eigenvalues δ_n and ε_n of the n^{th} mode are obtained from (113) and (114), using an appropriate algorithm

$$\left[(\delta_n^2 + \mu\varepsilon_n^2)^2 + (\mu\delta_n^2 + \varepsilon_n^2)^2 \right] \cos \delta_n \cosh \varepsilon_n - (\delta_n^2 + \mu\varepsilon_n^2) (\mu\delta_n^2 + \varepsilon_n^2) \left(-2 + \frac{\delta_n^2 - \varepsilon_n^2}{\delta_n \varepsilon_n} \sin \delta_n \sinh \varepsilon_n \right) = 0 \quad (113)$$

$$(\delta_n^2 - \varepsilon_n^2) \left[\eta^2 - \frac{1}{\mu + 1} (\delta_n^2 - \varepsilon_n^2) \right] - \left(1 + \frac{1}{\mu} \right) \delta_n^2 \varepsilon_n^2 = 0 \quad (114)$$

With

$$\eta = \sqrt{\frac{k_2}{k_1}}, \quad \mu = k_1.$$

Substituting the equation.(111) into (110), multiplying (110) by $\Phi_n(X)$ the integration from 0 to 1, for the first mode of vibration ($n = 1$). We obtain the following modal equation

$$\ddot{Q}(\tau) + R_1 \ddot{Q}(\tau) + R_2 \dot{Q}(\tau) + R_3 Q(\tau) = R_5 P_1(\tau) + R_6 \dot{P}_1(\tau) + R_7 \ddot{P}_1(\tau) \quad (115)$$

with

$$R_1 = 2\lambda, \quad R_2 = k_2 + \lambda^2 - \frac{b_2}{b_1}(1 + k_1), \quad R_3 = \lambda k_2 - \lambda \frac{b_2}{b_1}(1 + k_1), \quad R_4 = \frac{b_3}{b_1} k_1,$$

$$R_5 = \frac{b_4}{b_1} k_2, \quad R_6 = \frac{b_4}{b_1} \lambda, \quad R_7 = \frac{b_4}{b_1}$$

and

$$b_1 = \int_0^1 \Phi^2(X) dX; \quad b_2 = \int_0^1 \Phi''(X) \Phi(X) dX;$$

$$b_3 = \int_0^1 \Phi''''(X) \Phi(X) dX; \quad b_4 = \int_0^1 \Phi(X) dX$$

The description of the transverse displacement of the mechanical structure

can thus be derived by solving the differential equation (115)

3.2.2 Direct numerical simulation of the partial differential equation

To validate the analytical investigation, a direct numerical simulation of the partial differential equation (109) is explored. The method of lines [88] or semi-discretization is applied.

We set $\Delta X = 1/N$, $\tau = j\Delta\tau$ where ΔX and $\Delta\tau$ are the spatial and temporal steps respectively.

i and j are integer variables relative to position and time and N is the number of discrete points considered along the beam length.

The semi-discretisation form of the equation (109a) is

$$\begin{cases} \frac{d\theta_{i,j}^*}{dt} = F_1(\theta_{i,j}^1) \\ \frac{d\theta_{i,j}^1}{dt} = F_2(\theta_{i,j}^1, \theta_{i+1,j}^*, \theta_{i,j}, \theta_{i-1,j}^*, y_{i+1,j}, y_{i-1,j}) \end{cases} \quad (116)$$

and the equation.(109b) is

$$\begin{cases} \frac{dY_{i,j}}{dt} = F_3(Y_{i,j}^1) \\ \frac{dY_{i,j}^1}{dt} = F_4(Y_{i,j}^1, Y_{i+1,j}, Y_{i,j}, Y_{i-1,j}, \theta_{i+1,j}^*, \theta_{i-1,j}^*) + P_1(\tau j) \end{cases} \quad (117)$$

The boundary conditions are

$$\theta_{0,j}^* = 0, \quad Y_{0,j} = 0, \quad \theta_{n+1,j}^* = \theta_{n-1,j}^*, \quad Y_{n+1,j} = Y_{n-1,j} + 2\Delta X\theta_{n,j}^*$$

The excitation force is taken under the form

$$P(t) = -\rho A \ddot{u}_g(t) \quad (118)$$

According to [90], the ground acceleration $\ddot{u}_g(t)$ is assumed to be represented by

$$\ddot{u}_g(t) = e_0 (e^{-\beta_1 t} - e^{-\beta_2 t}) \sum_{n=1}^{N_f} (A_n \cos(\omega_n t) + B_n \sin(\omega_n t)) \quad (119)$$

This model is expressed in terms of a Fourier series that is modulated by an enveloping function. A_n and B_n are constants, ω_n are selected such that they span satisfactorily the frequency range $(0.2, 25)Hz$. β_1 and β_2 ($\beta_2 > \beta_1 > 0$) are parameters that impart the observed transient trends in the recorded ground motion. In our study, we assume that A_n and B_n are known.

The function $P_1(\tau)$ can thus be given as

$$P_1(\tau) = -e_0 \left(e^{-\beta_{11}\tau} - e^{-\beta_{22}\tau} \right) \sum_{n=1}^{N_f} (A_{1n} \cos(\omega_{1n}\tau) + B_{1n} \sin(\omega_{1n}\tau)) \quad (120)$$

With

$$A_{1n} = \frac{\rho L}{kG} A_n, \quad B_{1n} = \frac{\rho L}{kG} B_n, \quad \beta_{11} = \beta_1 T, \quad \beta_{22} = \beta_2 T, \quad \omega_{1n} = \omega_n T$$

The geometric and material properties of the beam are defined in Table 3
This leads to $\delta_1 = 1.854172414231125$, $\varepsilon_1 = 1.725031549472968$.

Table 3: Geometric and material properties

$E = 3 \times 10^{10} Pa$ $L = 80 m,$	$G = 1.25 \times 10^{10} Pa,$ $I = 45 \times 10^3 m^4, \nu = 0.2$	$\rho = 2500 kg m^{-3}$ $k = 0.8450704225$	$A = 600 m^2,$ $\alpha_1 = 15 s^{-1}.$
--	--	---	---

(we remind the reader that δ_1 and ε_1 have been obtained after solving the system of equations (113) and (114) using Newton Raphson algorithm).

Using the relation between the dimensional and the non-dimensional parameters which we obtained before, we derive the following dimensionless values (seen Table 4) for the parameters of equation (115)

Setting ourself at a point $X = 0.5$ of the beam, we display in the Figures 32

Table 4: Dimensionless values

$b_1 = 1.111690369$ $b_4 = -0.8438165466,$ $\lambda = 0.5837807806,$ $R_3 = 48.70592206,$ $R_6 = -0.4431124853,$ $\beta_{11} = 0.00507,$ $\omega_{22} = 0.53,$ $N_f = 4,$ $A_{33} = 4.733 \times 10^{-6},$ $B_{22} = 1.041 \times 10^{-6},$	$b_2 = 0.5504788466,$ $k_1 = 2.84,$ $R_1 = 1.167561561,$ $R_4 = 28.40443194,$ $R_7 = -0.7590391804,$ $\beta_{22} = 0.0195,$ $\omega_{33} = 0.60 Hz,$ $A_{11} = 1.344 \times 10^{-5},$ $A_{44} = 1.136 \times 10^{-6}$ $B_{33} = 2.84 \times 10^{-7},$	$b_3 = 11.11863853$ $k_2 = 1.066666667,$ $R_2 = 83.77266973,$ $R_5 = -64.77134340,$ $e_0 = 1.27,$ $\omega_{11} = 0.45,$ $\omega_{44} = 0.59,$ $A_{22} = 1.231 \times 10^{-6},$ $B_{11} = 4.733 \times 10^{-7},$ $B_{44} = 2.840 \times 10^{-7}$
--	--	--

and 33 respectively, the time history and frequency response curve obtained using the modal equation and the direct numerical simulation presented above. It appears that two curves are closed meaning that our analytical investigation is quantitatively and qualitatively good. Also having a look on the frequency response curve leads us to the conclusion that the dynamics of the system exhibits resonance and antiresonance along with subharmonic oscillations.

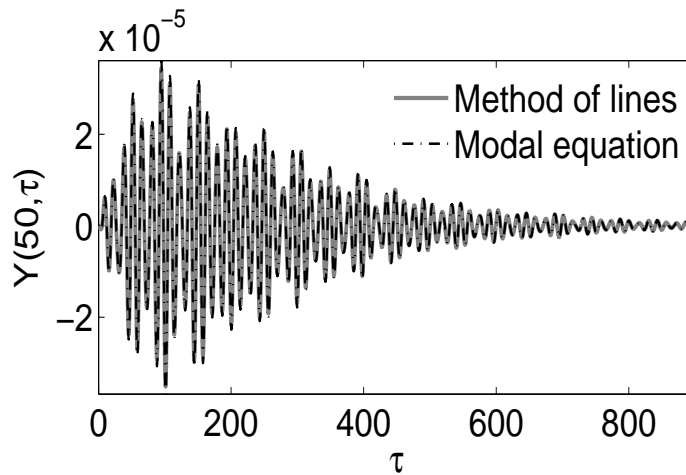


Figure 32: Time history response of the relative displacement

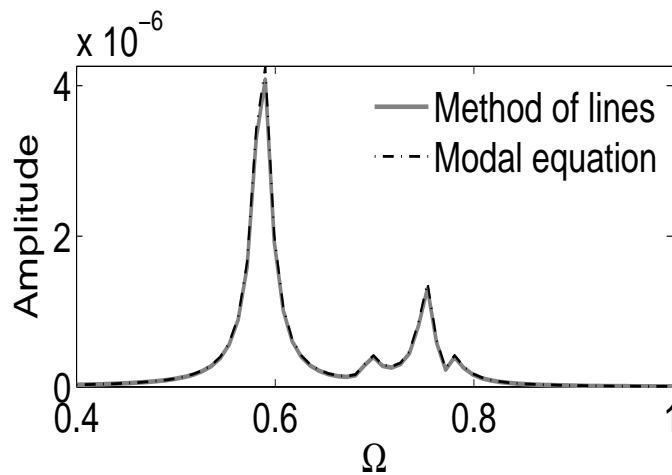


Figure 33: Frequency response curve

3.2.3 Semi-active control of the cantilever Timoshenko beam

The next step is to minimize the dynamic deflection of the structure. For that aim we define a set up so that the control of the beam is taken to be a transverse applied force or moment. A suitable way to reduce vibration in mechanical structures subjected to earthquake excitation is to use a semi active control technique named magneto rheological dampers [91, 114]. The ones are devices that are capable of generating the magnitude of forces necessary for full-scale application. Amongst these technics the modified Bouc Wen model plays a key role. Spencer et al [91] proposed a phenomenological model base on a Bouc Wen model, by which the dynamic behaviour of MR damper is described accurately (see Figure 34).

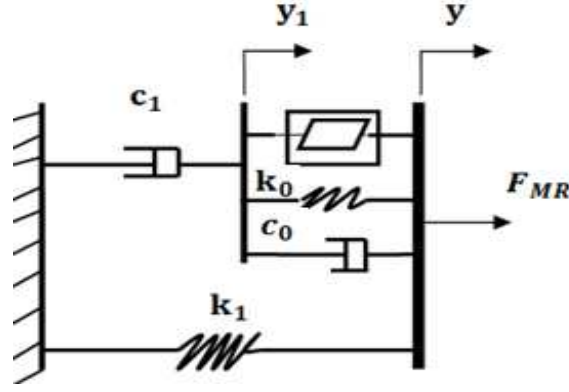


Figure 34: Modified Bouc-Wen model

The equations governing the force predicted by this model are

$$f_{MR}(t) = c_1 \dot{y}_1 + K_1(y - y_0) \quad (121)$$

$$\dot{y}_1 = \frac{1}{(c_0 + c_1)} \{c_0 \dot{y} + \alpha z + K_0(y - y_1)\} \quad (122)$$

$$\dot{z} = (\dot{y} - \dot{y}_1)[A - |z|^{n-1}(\beta + \gamma \operatorname{sgn}(z) \operatorname{sgn}(\dot{y} - \dot{y}_1))] \quad (123)$$

where

f_{MR} is the force generated by damper, y is the displacement of the damper, y_1 is the internal displacement of the damper; K_1 is the accumulator stiffness ; y_0 is the initial displacement of the spring K_1 ; z is the evolutionary variable that describes the hysteretic behaviour of the damper; α is the evolutionary coefficient; c_0 and c_1 control the viscous damping at large and low velocities, respectively.

γ , β , n and A are the shape parameters of the hysteresis loops, K_0 represent the stiffness at large velocity.

Le voltage dependent parameters are modelled by

$$\alpha = \alpha(u) = \alpha_a + \alpha_b u, \quad c_1 = c_1(u) = c_{1a} + c_{1b} u, \quad c_0 = c_0(u) = c_{0a} + c_{0b} u \quad (124)$$

The command voltage is accounted for through the first-order filter

$$\dot{u} = -\eta(u - v) \quad (125)$$

Where

v is the voltage applied to the damper and η is a positive number that reflects the delay time of the damper.

Erkus et al [109] gave the parameters of the model defined above based on

a prototype model of the MR damper. We define the suitable control parameters knowing that the objective here is to have the values leading to the efficiency of the control according to the position of damper on the structure (see Table 5)

Table 5: Modified MR damper parameters

Parameter	Value	Parameter	Value
A	301	$K_1(N/m)$	5 MF
$\beta(m^{-2})$	363	γm^{-2}	363
$c_{0a}(N.s/m)$	2100 MF	$\eta(s^{-1})$	190
$c_{0b}(N.s/mV)$	350 MF	$Y_0(m)$	0
$c_{1a}(N.s/m)$	28300 MF	n_1	2
$c_{1b}(N.s/mV)$	295000 MF	$K_0(N/m)$	46.90 MF
$\alpha_a(N/m)$	14000 MF	$\alpha_b(N/m.V)$	69500 MF

The parameters c_1 , c_0 and α depend the voltage

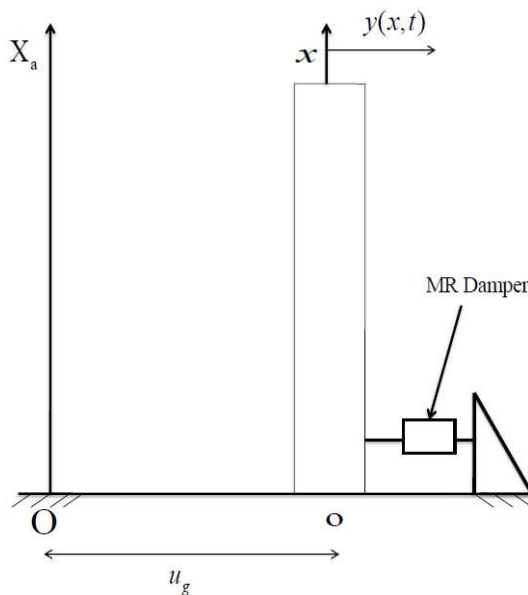


Figure 35: Simplified model structure under control

3.2.4 Effect of the control on the dynamics responses

The structure under control is shown in Figure 35, where the MR damper is fixed at a specific point of the cantilever beam, therefore the mathematical model of structure in presence of the magneto-rheological damper is de-

scribed by the following equations

$$\begin{aligned} \frac{\partial^4 Y}{\partial \tau^4} + 2\lambda \frac{\partial^3 Y}{\partial \tau^3} + (k_2 + \lambda^2) \frac{\partial^2 Y}{\partial \tau^2} - (1 + k_1) \frac{\partial^4 Y}{\partial X^2 \partial \tau^2} - \lambda(1 + k_1) \frac{\partial^3 Y}{\partial X^2 \partial \tau} + \\ \lambda k_2 \frac{\partial Y}{\partial \tau} + k_1 \frac{\partial^4 Y}{\partial X^4} + \varepsilon F_{MR}(\tau) \delta(X - X_1) = k_2 P_1(\tau) + \lambda \dot{P}_1(\tau) + \ddot{P}_1(\tau) \end{aligned} \quad (126)$$

with

$$F_{MR}(\tau) = \frac{kGT^4 f_{mr}(t)}{\rho^2 IL^2}$$

where

$F_{MR}(\tau)$ is the dimensionless force exerted by the damper on the structure and $\delta(X - X_1)$ is the Dirac delta function which indicates that the concentrated force is applied at the attachment point, $X = X_1$.

The parameter ε allow here to have general equation, ie for $\varepsilon = 0$, the structure is uncontrolled and $\varepsilon = 1$, the structure is controlled.

The equations at first mode vibration are

$$\begin{aligned} \ddot{\ddot{Q}}(\tau) + R_1 \ddot{\ddot{Q}}(\tau) + R_2 \ddot{\ddot{Q}}(\tau) + R_3 \dot{\ddot{Q}}(\tau) + R_4 \ddot{Q}(\tau) + \varepsilon_1 F_{MR}(\tau) = R_5 P_1(\tau) + R_6 \dot{P}_1(\tau) + \\ R_7 \ddot{P}_1(\tau) \end{aligned} \quad (127)$$

with

$$F_{MR} = a_1 \dot{Y}_1 + a_2 (\eta_2 - Y_0)$$

where Y_1 is governed by

$$\dot{Y}_1 = a_3 \dot{\eta}_2 + a_4 Z + a_5 (\eta_2 - Y_1) \quad (128)$$

$$\dot{Z} = (\dot{\eta}_2 - \dot{Y}_1) \left[A - |Z|^{n_1} \left(\beta_1 + \gamma_1 \text{sign}(Z) \text{sign}(\dot{\eta}_2 - \dot{Y}_1) \right) \right] \quad (129)$$

$$\dot{U} = -\xi(U - V) \quad (130)$$

with the dimensionless parameters defined by

$$Z = \frac{z}{L}, \quad Y_1 = \frac{y_1}{L}, \quad Y_0 = \frac{y_0}{L}, \quad U = \frac{u}{V_1}, \quad V = \frac{v}{V_1}, \quad \varepsilon_1 = \frac{\varepsilon \Phi(X_1)}{b_1}$$

where V_1 is the reference voltage ($V_1 = 50 \text{ Volt}$).

$$\eta_2 = Q(\tau) \Phi(X_1), \quad \dot{\eta}_2 = \dot{Q}(\tau) \Phi(X_1), \quad \gamma_1 = \gamma L^{n_1}, \quad \beta_1 = \beta L^{n_1}, \quad \xi = \eta T$$

$$a_1 = a_1(U) = \frac{kGT^3 c_1}{\rho^2 IL}, \quad a_2 = \frac{kGT^4 k_1}{\rho^2 IL}, \quad a_3 = a_3(U) = \frac{c_0}{c_0 + c_1}, \quad a_4 = a_4(U) = \frac{\alpha T}{c_0 + c_1},$$

$$a_5 = a_5(U) = \frac{k_0 T}{c_0 + c_1}$$

with

$$\alpha = \alpha(U) = \alpha_a + \alpha_{b1} U, \quad c_1 = c_1(U) = c_{1a} + c_{1b1} U, \quad c_0 = c_1(U) = c_{0a} + c_{0b1} U$$

$$\alpha_{b1} = \alpha_b V_1, \quad c_{1b1} = c_{1b} V_1, \quad c_{0b1} = c_{0b} V_1$$

the damper performance of the structure subjected to an earthquake deterministic through the computer simulation is analysed. The different values of the dimensionless parameters are

$$\beta_1 = 2323200, \quad \gamma_1 = 2323200, \quad \xi = 7.394556555, \quad \Phi(0.2) = -0.1741045662,$$

$$\Phi(0.25) = -0.2493107942, \quad \Phi(0.3) = -0.3349121633,$$

$$a_1 = \frac{(0.7832175921 \times 10^{-3} + .4082141160 U) MF}{2100 + 17500 U}, \quad a_2 = \frac{5.385481475 \times 10^{-9} MF}{546 + 135525 U},$$

$$a_3 = \frac{30400 + 14767500 U}{1.825287907}, \quad a_4 = \frac{30400 + 14767500 U}{30400 + 14767500 U},$$

$$a_5 = \frac{30400 + 14767500 U}{30400 + 14767500 U}$$

We have plotted in Figures 36 and 37 the time histories to see the effects of the voltage and position of the MR damper on the control process.

Figures 36a shows the reduction amplitude of vibration of the structure at point $X_1 = 0.2$, which indicates the place where the concentrated force magneto-rheological damper is applied. The dimensionless voltage is $U = 0.39$.

Figure 36b presents the effects the voltage on the control. We can notice that when the voltage amplitude is high the amplitude of vibration is more and more reduced. For example at $\tau = 240$ the amplitude in Figure 36a is 2.012×10^{-5} and in Figure 36b is 1.448×10^{-5}

From Figures 37a and 37b, we observe that the position of the attachment point of the damper is an important parameter for the optimization of the control process.

In fact Figure 37 shows us that the control is more and more efficient as the contact point between the control and the structure is far from the base. This means that the best implementation of the control design should locate the optimal point for the controller action.

3.2.5 Stability of semi-active structural control

One of the consequences when a device is added on a mechanical structural is that the fixed points position change.

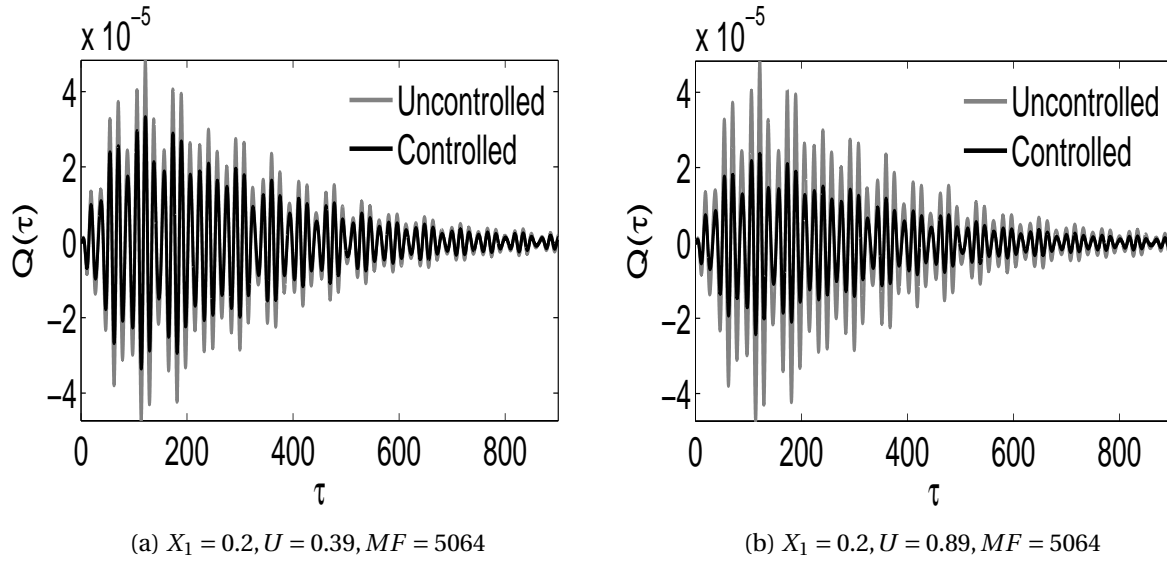


Figure 36: Time histories: Effects of the input voltage on the amplitude of vibration

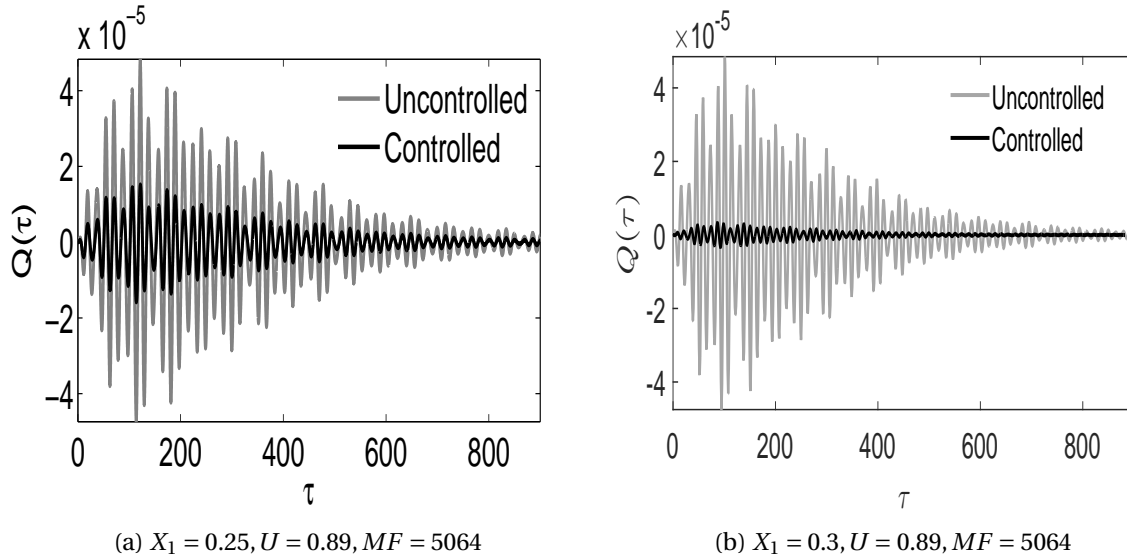


Figure 37: Time histories: effects of the position of contact between the controller and the structure

Thus instead of reinforcing the stability of the structure, it can destabilize the system leading to premature destruction of the system. Therefore, it is important to address the stability condition.

Introducing the new variables

$$\chi_1, \chi_2, \chi_3, \chi_4, \chi_5, \chi_6 \text{ and } \chi_7 \text{ such that}$$

$$\dot{Q} = \dot{\chi}_1 = \chi_2, \quad \ddot{Q} = \ddot{\chi}_1 = \dot{\chi}_2 = \chi_3, \quad \dddot{Q} = \dddot{\chi}_1 = \ddot{\chi}_2 = \dot{\chi}_3 = \chi_4, \quad Y_1 = \chi_5, \quad z = \chi_6, \\ U = \chi_7$$

Equations. (127), (128), (129) and (130) can then be rewritten as follows

$$\left\{ \begin{array}{l} \dot{\chi}_1 = \chi_2 \\ \dot{\chi}_2 = \chi_3 \\ \dot{\chi}_3 = \chi_4 \\ \dot{\chi}_4 = -R_1\chi_4 - R_2\chi_3 - (R_3 + \varepsilon_1\varepsilon_2 a_1 a_3)\chi_2 - (R_4 + \varepsilon_1\varepsilon_2(a_1 a_5 + a_2))\chi_1 + \\ \quad \varepsilon_1 a_1 a_5 \chi_5 - \varepsilon_1 a_1 a_4 \chi_6 + \varepsilon_1 a_2 Y_0 \\ \dot{\chi}_5 = a_3 \varepsilon_2 \chi_2 + a_4 \chi_6 + a_5 (\varepsilon_2 \chi_1 - \chi_5) \\ \dot{\chi}_6 = (\varepsilon_2 \chi_2 - a_3 \varepsilon_2 \chi_2 - a_4 \chi_6 - a_5 (\varepsilon_2 \chi_1 - \chi_5)) [A - \chi_6^{n_1} (\beta_1 + \gamma_1 \mu)] \\ \dot{\chi}_7 = -\xi (\chi_7 - V) \end{array} \right. \quad (131)$$

where

$$\varepsilon_2 = \Phi(X_1); \quad a_1 = a_1(\chi_7); \quad a_3 = a_3(\chi_7); \quad a_4 = a_4(\chi_7); \quad a_5 = a_5(\chi_7); \\ \mu = \text{sign}(\chi_6) \text{sign}(\varepsilon_2 \chi_2 - \dot{\chi}_5)$$

The general form of the equilibrium point is

$$P = \left(\begin{array}{l} \chi_1 = \frac{\varepsilon_1 a_2 Y_0}{R_4 + \varepsilon_1 \varepsilon_2 a_2}, \chi_2 = 0, \chi_3 = 0, \chi_4 = 0, \\ \chi_5 = \frac{\varepsilon_1 \varepsilon_2 a_2 Y_0}{R_4 + \varepsilon_1 \varepsilon_2 a_2} + \frac{a_4(V)}{a_5(V)} \chi_6, \chi_6 = \chi_6, \chi_7 = V \end{array} \right)$$

The characteristic equation is given as follows

$$\Lambda^7 + aa_1 \Lambda^6 + aa_2 \Lambda^5 + aa_3 \Lambda^4 + aa_4 \Lambda^3 + aa_5 \Lambda^2 + aa_6 \Lambda + aa_7 = 0 \quad (132)$$

In which

$$aa_1 = \xi + R_1 + h_1(\chi_6, V); \quad aa_2 = \xi R_1 + R_2 + (\xi + R_1) h_1(\chi_6, V)$$

$$aa_3 = (\xi R_1 + R_2) h_1(\chi_6, V) + h_2(V) + \xi R_2 + R_3$$

$$aa_4 = \xi h_2(V) + h_1(\chi_6, V) (\xi R_2 + \varepsilon_1 \varepsilon_2 a_1(V)) + R_1 + \varepsilon_1 \varepsilon_2 a_2 + \xi R_3 + R_3$$

$$aa_5 = \xi \varepsilon_1 \varepsilon_2 a_2 + h_1(\chi_6, V) (\varepsilon_1 \varepsilon_2 (a_2 + \xi a_1(V)) + (R_1 + \xi R_3)) + \xi R_1$$

$$aa_6 = \xi (R_1 + \varepsilon_1 \varepsilon_2 a_2) h_1(\chi_6, V); \quad aa_7 = 0$$

where $h_1(\chi_6, V) = T \frac{(\alpha(V)g(\chi_6) + K_0)}{c_0(V) + c_1(V)}$ and $h_2(V) = \frac{\varepsilon_1 \varepsilon_2 a_1(V) c_0(V)}{c_0(V) + c_1(V)}$

with

$$g(x_6) = \begin{cases} A - \chi_6^{n_1} (\beta_1 + \gamma_1) & \text{if } \mu > 0 \\ A - \chi_6^{n_1} (\beta_1 - \gamma_1) & \text{if } \mu < 0 \end{cases} \quad (133)$$

χ_6 is an evolutionary variable that influences the vibration of the structure

response. χ_6 has a finite ultimate value χ_{6max} , analytically this maximum can be found from of Equation (129), which leads to [104]

$$\chi_{6max} = \left[\frac{A}{\gamma_1 + \beta_1} \right]^{\frac{1}{n_1}}$$

thus

$$0 \leq \chi_6 \leq \left[\frac{A}{\gamma_1 + \beta_1} \right]^{\frac{1}{n_1}}$$

where n_1 is an even number

Assuming that

$$0 < \frac{A}{\gamma_1 + \beta_1} < 1$$

leads us to the following conclusion

$$0 \leq g(\chi_6) \leq A.$$

From the Equation (132), we have $\Lambda_1 = 0$ the solutions are all constant. Since we are interested in the dynamics response it remains to determine the others eigenvalues where the stability depends on the characteristic equation below

$$\Lambda^6 + aa_1\Lambda^5 + aa_2\Lambda^4 + aa_3\Lambda^3 + aa_4\Lambda^2 + aa_5\Lambda + aa_6 = 0 \quad (134)$$

Now, using the Routh-Hurwitz criterion, the equilibrium point P_f is stable if and only if the following analytic relations are satisfied.

$$\begin{aligned} aa_i &> 0 \quad (i = 1, 2, 3, 4, 5, 6) \\ \Delta_3 &> 0 \\ \Delta_5 &> 0 \end{aligned} \quad (135)$$

where

$$\Delta_3 = aa_1aa_2aa_3 - aa_3^2 - aa_1^2aa_4 + aa_1aa_5,$$

and

$$\begin{aligned} \Delta_5 = &aa_1aa_2aa_3aa_4aa_5 - aa_3^2aa_4aa_5 - aa_1^2aa_4^2aa_5 - aa_1aa_2^2aa_5^2 + \\ &aa_2aa_3aa_5^2 + 2aa_1aa_4aa_5^2 - aa_5^3 - aa_1aa_2aa_3^2aa_6 + aa_3^2aa_6^2 + \\ &aa_1^2aa_3aa_4aa_6 + 2aa_1^2aa_2aa_5aa_6 - 3aa_1aa_3aa_5aa_6 - aa_1^3aa_6^2 \end{aligned}$$

From the relation (135), we deduce that the equilibrium point P_f is stable

when the following condition is satisfied.

$$\chi_6^{n_1} < \frac{A}{\beta_1 + \gamma_1} + \frac{(c_0(V) + c_1(V))(\xi + R_1)}{\alpha(V)T(\beta_1 + \gamma_1)} + \frac{K_0}{\alpha(V)(\beta_1 + \gamma_1)} \quad (136)$$

The Figure 38 presents region in the control space parameters α , c_0 and c_1 . Note that, these can be adjusted since they depend on the applied voltage.

As a result, the shaded domains represent the regions of values of men-

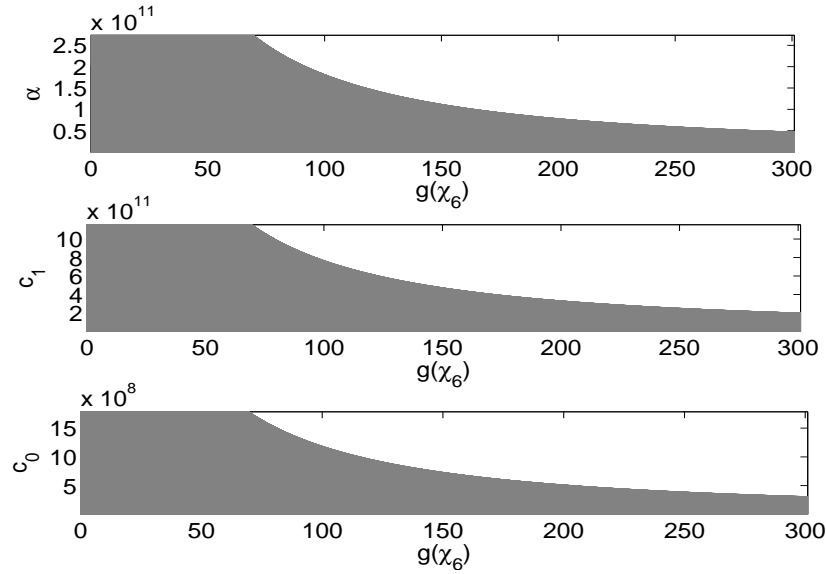


Figure 38: Stability diagram in the space parameters of control for $X_1 = 0.3$ and $U = 0.89$

tioned parameters, for which the structural control strategy is always stable. The boundary values of these parameters can be obtained from this Figure, because allow to have the optimal scale coefficient MF as in Table 5.

3.3 Quenching of vibration modes on two interconnected buildings subjected to seismic loads

In this section; we describe the statistical responses of the two buildings subjected to the repeated sequence of excitation. The nonstationary random approach is employed to simulate seismic events.

3.3.1 Description of the system

The structural system is constituted of two cantilever beams Bg_1 and Bg_2 , They are subjected to the same disturbance force denoted seismic load. At a located point of each tall building, is connected a semi-active controller dubbed MR damper, as illustrated in Figure 39.

This shock absorber generates the variable forces acting on the mechani-

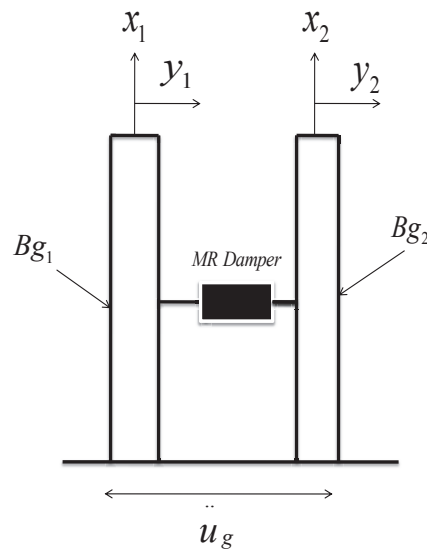


Figure 39: Simplified model

cal structures to safeguard them against undesirable vibrations. The control device is equipped of a moving piston head, which is fixed on the structure Bg_2 , another extremity of this device is embedded on the second structure Bg_1 , which not only is subjected to earthquake excitation and at the same time play the rule of support of the controller.

The mathematical modelling

Both buildings under investigation are modelled each like an continuum cantilever Timoshenko beam, where I_1 and I_2 are the moments of inertia of the cross-section ; G_1 and G_2 are the shear modulus of elasticity, E_1 and E_2 are

the Young's modulus; the mass per unit length are $m_1 = \rho_1 A_1$ and $m_2 = \rho_2 A_2$; k_s is the shear coefficient depending on the shape of the cross section of each beam and function of Young's modulus; $r_1 = (I_1/A_1)^2$ and $r_2 = (I_2/A_2)^2$ are the radius of gyration; $\delta(\bullet)$ denotes the Dirac function; c_a and c_b are the mechanical damping coefficients. The subscript 1 and 2 denoted the beams Bg_1 and Bg_2 , respectively.

Moreover the vibration amplitude of the structural system are described by $y_1 = y(x_1, t)$ and $y_2 = y(x_2, t)$, which depend on axial coordinate x_1 and x_2 and time, namely the relative transverse displacements.

In considering the Timoshenko model, which is governing by the differential partial equation. This implies that the equations of motion for both interconnected buildings by the magneto rheological damper under the earthquake excitation are given [97]

$$m_1 \frac{\partial^2 y_1}{\partial t^2} + c_a \frac{\partial y_1}{\partial t} + E_1 I_1 \frac{\partial^4 y_1}{\partial x_1^4} - m_1 r_1^2 \left(1 + \frac{E}{k_s G_1} \right) \frac{\partial^4 y_1}{\partial x_1^2 \partial t^2} = -m_1 \ddot{u}_g(t) + f_d(t) \delta(x_1 - x_3) \quad (137a)$$

$$m_2 \frac{\partial^2 y_2}{\partial t^2} + c_b \frac{\partial y_2}{\partial t} + E_2 I_2 \frac{\partial^4 y_2}{\partial x_2^4} - m_2 r_2^2 \left(1 + \frac{E_2}{k_s G_2} \right) \frac{\partial^4 y_2}{\partial x_2^2 \partial t^2} = -m_2 \ddot{u}_g(t) - f_d(t) \delta(x_2 - x_3) \quad (137b)$$

x_3 represents the located point of the MR device on Bg_1 and Bg_2 .

The nonstationary ground acceleration $\ddot{u}_g(t)$ adopted here, is the form of n sequences [92]. This random function is assume to take the form of a filtered Gaussian stationary white noise modulated by a deterministic envelope function. This mentioned form describes the real earthquake that has the time-variation of both the intensity and frequency content. Expression of this term is defined in section 2.3.6.

The equations governing the force f_d generated by the MR damper at the attachment point x_3 is expressed as follows

$$f_d = c_1(\dot{y} - \dot{y}_1(x_3, t)) + k_1 [(y_2(x_3, t) - y_1(x_3, t)) - y_0] \quad (138)$$

y is an internal displacement, governed by

$$\dot{y} = \frac{1}{c_0 + c_1} [\alpha z + c_0 \dot{y}_2(x_3, t) + c_1 \dot{y}_1(x_3, t) + k_0 (y_2(x_3, t) - y)] \quad (139)$$

$$\dot{z} = -\gamma |\dot{y}_2(x_3, t) - \dot{y}| z |z|^{n-1} - \beta (\dot{y}_2(x_3, t) - \dot{y}) |z|^n + \delta_a (\dot{y}_2(x_3, t) - \dot{y}) \quad (140)$$

where

c_0 and c_1 are the viscous damping at larger velocities and low velocities respectively; k_1 is the accumulator stiffness; k_0 represents the stiffness at large velocity; γ , β and δ_a are the shape parameters of the hysteresis loops.

In equation (139), some parameters depend on the command voltage u are given by

$$c_0 = c_{0a} + c_{0b}u, \quad c_1 = c_{1a} + c_{1b}u \quad \text{and} \quad \alpha = \alpha_a + \alpha_b u \quad (141)$$

where the command voltage u is accounted for through the first order filter

$$\dot{u} = \eta_p(u - v_c) \quad (142)$$

v_c is the voltage applied to current driver

Introducing the dimensionless variables, these lead to following expressions.

$$Y_1 = \frac{y_1}{L}, \quad Y_2 = \frac{y_1}{L}, \quad Z = z, \quad Y = \frac{y}{L}, \quad \tau = \frac{t}{T}, \quad \kappa_1 = \frac{c_a T}{m_1}, \quad \kappa_2 = \frac{c_b T}{m_2}, \quad a_1 = \frac{E_1 l_1 T^2}{L^4 m_1}, \quad a_2 = \frac{E_2 l_2 T^2}{L^4 m_2}, \quad a_3 = \frac{r_1^2}{L^2}, \quad a_5 = \frac{E_1}{k_s G_1}, \quad a_4 = \frac{r_2^2}{L^2}, \quad a_6 = \frac{E_2}{k_s G_2}, \quad \ddot{y}_g(\tau) = \frac{\ddot{u}_g(t) T^2}{L}, \quad F_d = \frac{f_d(t) T^2}{m_1 L^2}, \quad \mu = \frac{m_1}{m_2}, \quad \alpha_b = \frac{\alpha T}{(c_0 + c_1)}, \quad C_0 = \frac{c_0}{c_0 + c_1}, \quad C_1 = \frac{c_1}{c_0 + c_1}, \quad K_0 = \frac{k_0 T}{c_0 + c_1}, \quad c_l = \frac{c_1 T}{m_1 L}, \quad K_1 = \frac{k_1 T^2}{m_1 L}, \quad \gamma_l = \gamma L^2, \quad \delta_l = \delta_a, \quad \beta_l = \beta L^2, \quad s_{01} = \frac{s_0}{S_0}, \quad \Omega = \omega T, \quad \Omega_g = \omega_g T, \quad T = L \sqrt{\frac{\rho}{k_s G_1}}, \quad \eta_T = \eta T, \quad U = \frac{u}{V_1}, \quad V_c = \frac{v_c}{V_1}$$

By considering the above new parameters, multiplying by the different spatial expression the set of equation (137) and integrating from 0 to 1.

One can obtain the modal forms of above equations as follows

$$\ddot{\xi}_i(\tau) + \zeta_1^i \dot{\xi}_i(\tau) + \varsigma_1^i \xi_i(\tau) = -\sigma_1^i \ddot{y}_g(\tau) + \varepsilon_1^i F_d(\tau) \quad (143a)$$

$$\ddot{\chi}_i(\tau) + \zeta_2^i \dot{\chi}_i(\tau) + \varsigma_2^i \chi_i(\tau) = -\sigma_2^i \ddot{y}_g(\tau) - \varepsilon_2^i F_d(\tau) \quad (143b)$$

The dimensionless voltage U is given as

$$\dot{U} = -\eta_T(U - V_c) \quad (144)$$

Introducing the new variable, this leads us to yield the set of equations that are now be written as

$$\ddot{z}_1(\tau) + \zeta_1^i \dot{z}_1(\tau) + \varsigma_1^i z_1(\tau) = -\sigma_{11}^i \ddot{y}_g(\tau) + \varepsilon_{11}^i F_d(\tau) \quad (145a)$$

$$\ddot{z}_2(\tau) + \zeta_2^i \dot{z}_2(\tau) + \varsigma_2^i z_2(\tau) = -\sigma_{22}^i \ddot{y}_g(\tau) - \varepsilon_{22}^i F_d(\tau) \quad (145b)$$

with

$$F_d(\tau) = c_l(\dot{z}_2 - \dot{Y}_h - \dot{z}_1) + K_1(z_2 - z_1 - Y_0) \quad (146)$$

where Y

$$\dot{Y}_h(\tau) = -\alpha_b Z + (1 - C_0)\dot{z}_2 - C_1\dot{z}_1 - K_0 Y_h \quad (147)$$

and Z is governed by

$$\dot{Z}(\tau) = \dot{Y}_h [\delta_a - |Z|^n (\beta_l + \gamma_l \text{sgn}(\dot{Y}_h) \text{sgn}(Z))] \quad (148)$$

This made transformation allows us now to rewrite the set of equations (143) under the form of the state space equation, therefore expression is given as

$$\dot{\mathbf{W}}(\tau) = \Sigma \mathbf{W}(\tau) + \mathbf{B} \ddot{y}_g(\tau) + \mathbf{B}_1 F_d(\tau) \quad (149)$$

$$\mathbf{W} = \begin{bmatrix} z_1 \\ z_2 \\ \dot{z}_1 \\ \dot{z}_2 \end{bmatrix}, \quad \Sigma = \begin{bmatrix} 0 & 0 & 1 & 0 \\ 0 & 0 & 0 & 1 \\ -\zeta_1^i & 0 & -\zeta_1^i & 0 \\ 0 & -\zeta_2^i & 0 & -\zeta_2^i \end{bmatrix}, \quad \mathbf{B} = \begin{bmatrix} 0 \\ 0 \\ -\sigma_{11}^i \\ -\sigma_{22}^i \end{bmatrix}, \quad \mathbf{B}_1 = \begin{bmatrix} 0 \\ 0 \\ \varepsilon_{11}^i \\ -\varepsilon_{22}^i \end{bmatrix}$$

From the above equations, an independence of different modes exhibit by the mechanical structures.

The geometric and material properties of beams Bg_1 and Bg_2 are defined in Table 6

and these lead to the dimensionless values: $T = 0.03$, $X_3 = 0.3$

Table 6: Geometric and material properties

$E_1 = E_2 = 2.1 \times 10^{11} \text{ N/m}^2$ $L = 80 \text{ m},$	$A_1 = 25 \times 20 \text{ m}^2;$ $\rho_1 = 7850 \text{ kg/m}^3$	$I_1 = 16666.7 \text{ m}^4;$ $\rho_2 = 7850 \text{ kg/m}^3; \nu = 0.3$	$I_2 = 1250 \text{ m}^4;$ $A_1 = 15 \times 10 \text{ m}^2;.$
---	---	---	---

The parameter values listed in Table 8 are those used in Ref.[105]. These parameters depend on the coefficient MF , also allowing to modify the properties of the damper, in order to have the parameter values for a large scale MR damper, enable to control the mechanical structure in the optimal condition.

3.3.2 Numerical results of the controlled mechanical system

With a view to obtain the optimal input voltage corresponding to the desired damper force, the control algorithm used in semi-active control based on the Lyapunov stability theory [113] is employed.

Table 7: Model parameters of the MR damper.

First mode			
$\delta_1^1 = 1.86459029946901$	$\epsilon_1^1 = 1.79961176980009$	$\zeta_1^1 = 0.1794505064$	$\epsilon_1^1 = -0.292553544$
$\delta_2^1 = 1.87234598422580$	$\epsilon_2^1 = 1.85523372531123$	$\zeta_2^1 = 0.0480761492$	$\epsilon_2^1 = -1.00458791$
$\sigma_1^1 = -0.7823279832$		$\sigma_2^1 = -0.7604937075$	
Second mode			
$\delta_1^2 = 4.63405503453255$	$\epsilon_1^2 = 3.76159351295218$	$\zeta_1^2 = 5.597669667$	$\epsilon_1^2 = -0.712027715$
$\delta_2^2 = 4.49341259217513$	$\epsilon_2^2 = 4.39148518126663$	$\zeta_2^2 = 2.028598833$	$\epsilon_2^2 = -3.188313916$
$\sigma_1^2 = -0.2915422860$		$\sigma_2^2 = -0.2283758422$	
Third mode			
$\delta_1^3 = 7.50656628630713$	$\epsilon_1^3 = 5.07068861723638$	$\zeta_1^3 = 28.38752152$	$\epsilon_1^3 = -0.444999427$
$\delta_2^3 = 7.72105209323756$	$\epsilon_2^3 = 6.73269253778025$	$\zeta_2^3 = 13.2367535$	$\epsilon_2^3 = -3.44782732$
$\sigma_1^3 = -0.08394819892$		$\sigma_2^3 = -0.05571034952$	

Table 8: Model parameters of the MR damper.

$\delta_a = 301$	$n_1 = 2$
$\gamma(m^{-2}) = 363$	$\eta_p(s^{-1}) = 190$
$\beta(m^{-2}) = 363$	$k_1(N/m) = 617.31MF$
$k_0(N/m) = 46.90MF$	$y_0(m) = 0.0$
$\alpha_a(N/m) = 14,000MF$	$\alpha_b(N/mV) = 69,500MF$
$c_{0a}(Ns/m) = 2,100MF$	$c_{0b}(Ns/mV) = 350MF$
$c_{1a}(Ns/m) = 28,300MF$	$c_{1b}(Ns/mV) = 295,000MF$

The Lyapunov function, denoted $L_y(\mathbf{W})$ must be a positive function of the state of the system, \mathbf{W} . According to the Lyapunov stability theory, if the rate of change of lyapunov function, $\dot{L}_y(\mathbf{W})$, is negative semi-definite, the origin is stable. Lyapunov function is chosen of the form

$$L_y = \frac{1}{2} \|\mathbf{W}\|_p^2 \quad (150)$$

where $\|\Sigma\|_p = P$ -norm of the states defined by

$$\|\Sigma\|_p = [\Sigma' \mathbf{P}_L \Sigma]^{1/2} \quad (151)$$

where \mathbf{P}_L is real, symmetric, positive definite matrix. \mathbf{P}_L is found by using Lyapunov equation.

$$\Sigma' \mathbf{P}_L + \mathbf{P}_L \Sigma = -\mathbf{Q}_p \quad (152)$$

\mathbf{Q}_p is a positive definite matrix. The derivative of the Lyapunov function for a solution of the state-space equation is

$$\dot{L}_y = -\frac{1}{2} \mathbf{W}' \mathbf{Q}_p \mathbf{W} + \mathbf{W}' \mathbf{P}_L \mathbf{B}_1 F_d + \mathbf{W}' \mathbf{P}_L \mathbf{B} \ddot{y}_g \quad (153)$$

the control law which minimize \dot{L}_y is

$$V_c = V_{max}H(-\mathbf{W}'\mathbf{P}_L\mathbf{B}_1F_d) \quad (154)$$

Where

V_{max} is the maximum voltage and $H(\cdot)$ is Heaviside step function. When this function is greater than zero, the voltage (V_c) applied to the damper should be maximum (V_{max}), otherwise, the command voltage is set to zero.

By considering all defined parameters in the dimensionless form of mechanical structures, with those of controller, which are associated with an appropriated algorithm to display in Figures 40a, 40b and 40c.

In what follows, these figures show a considerable reduction of vibration of the amplitude of buildings Bg_1 and Bg_2 at a interconnected point $X_3 = 0.25$ of the MR device. They also show that the MR damper it is a element that reduces the excessive energy bring by the external disturbances.

To observe the efficiency of MR damper on the structures, root mean square displacement of each building is presented.

Figures 41a, 41b and 41c display root mean square of Bg_1 and Bg_2 controlled and uncontrolled at different modes of vibration and different localized points of the MR device, in order to have the optimal location.

In Figure 41a shows that the good attachment points where the controller can offer a best performance are $X_p = 0.7$ and $X_p = 0.25$ for Bg_1 and Bg_2 , respectively.

It is also observed that at the point $X_3 = 0.25$, the controller reduces even better the vibration than the points $X_3 = 0.5$ and $X_3 = 0.75$ in Figure 41b.

As regards, in Figure 41c at the localized point $X_p = 0.5$, it is seen that there is no exist a difference between controlled and uncontrolled cases. This proves that the controller is not able to reduce the excessive vibrations on the two buildings. While the located points $X_p = 0.25$ and $X_p = 0.7$, the shock absorber performs a considerable effort to attenuate the vibration.

One can clearly see in these figures illustrating the root mean square for all the modes show that the optimal position of the dynamic controller on the buildings is the point $X_p = 0.25$. In this location, the MR device reduces better the excessive vibrations.

By resuming all the mentioned details, one can note that the MR device is a good candidate that also able to minimize disturbances. As further information that one can have from these figures, the time that the controller will launch to act on the structures, which can be computed through the follow-

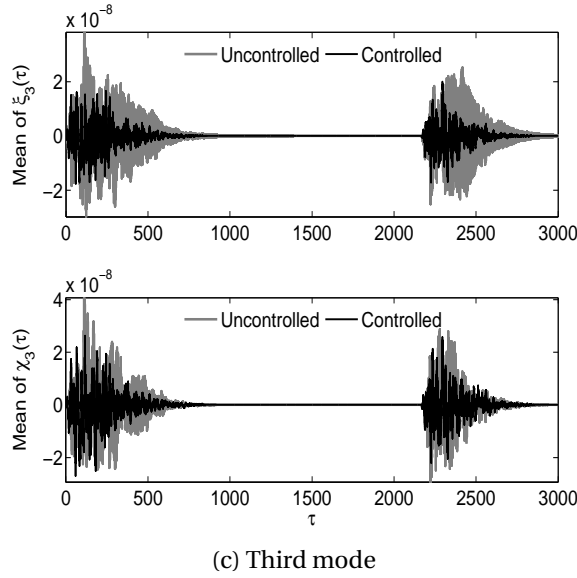
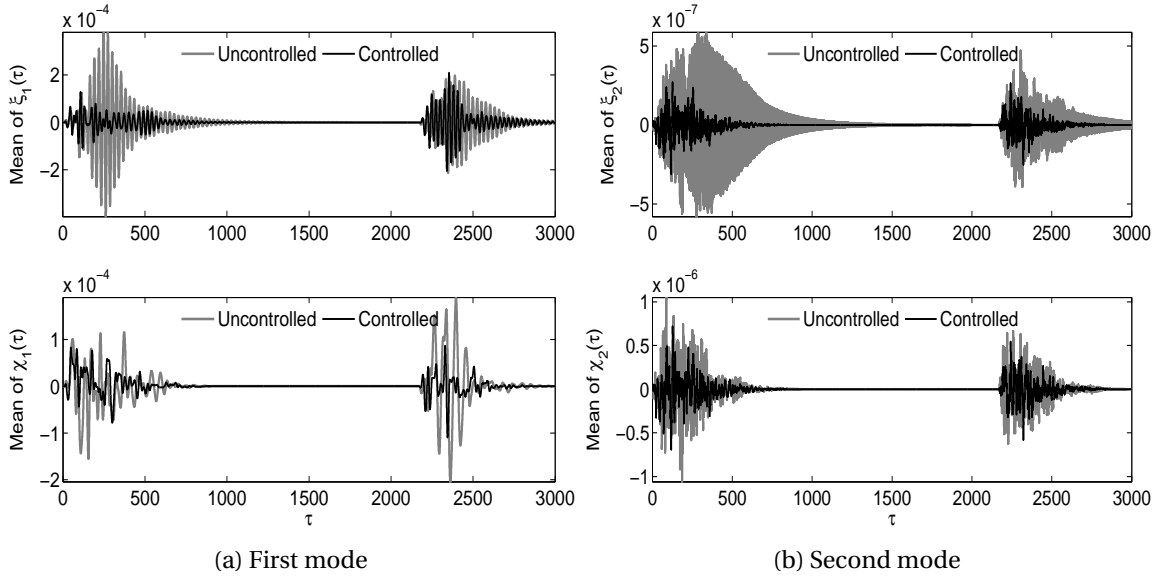


Figure 40: Time history of buildings Bg_1 and Bg_2 (third mode), $V_{max} = 2.0$, $MF=12090$, $X_3 = 0.25$

ing expression given by

$$\epsilon_{1i} = \frac{E[\xi_i^2]_{uncontrolled}^{1/2} - E[\xi_i^2]_{controlled}^{1/2}}{\max(E[\xi_i^2]_{uncontrolled}^{1/2} - E[\xi_i^2]_{controlled}^{1/2})} \quad (155)$$

$$\epsilon_{2i} = \frac{E[\chi_i^2]_{uncontrolled}^{1/2} - E[\chi_i^2]_{controlled}^{1/2}}{\max(E[\chi_i^2]_{uncontrolled}^{1/2} - E[\chi_i^2]_{controlled}^{1/2})}$$

The time where the controller begin to attenuate the vibration on buildings Bg_1 and Bg_2 is got if $\epsilon_{1i} < h_1$ and $\epsilon_{2i} < h_1$, respectively.

For instance at a fixed position $X_3 = 0.25$ with the chosen precision $h_1 = 10^{-2}$,

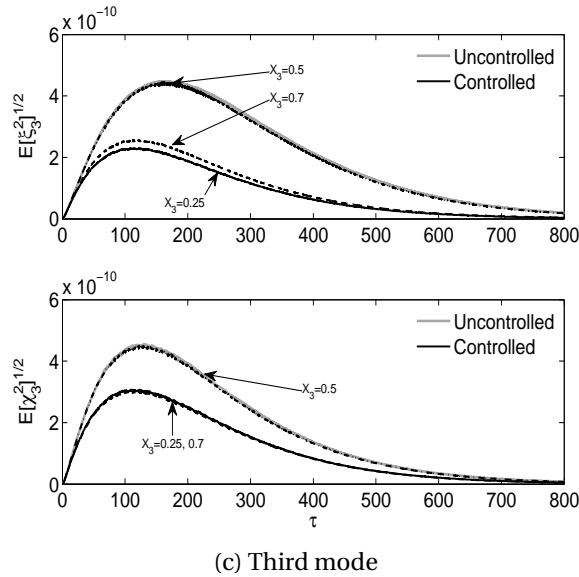
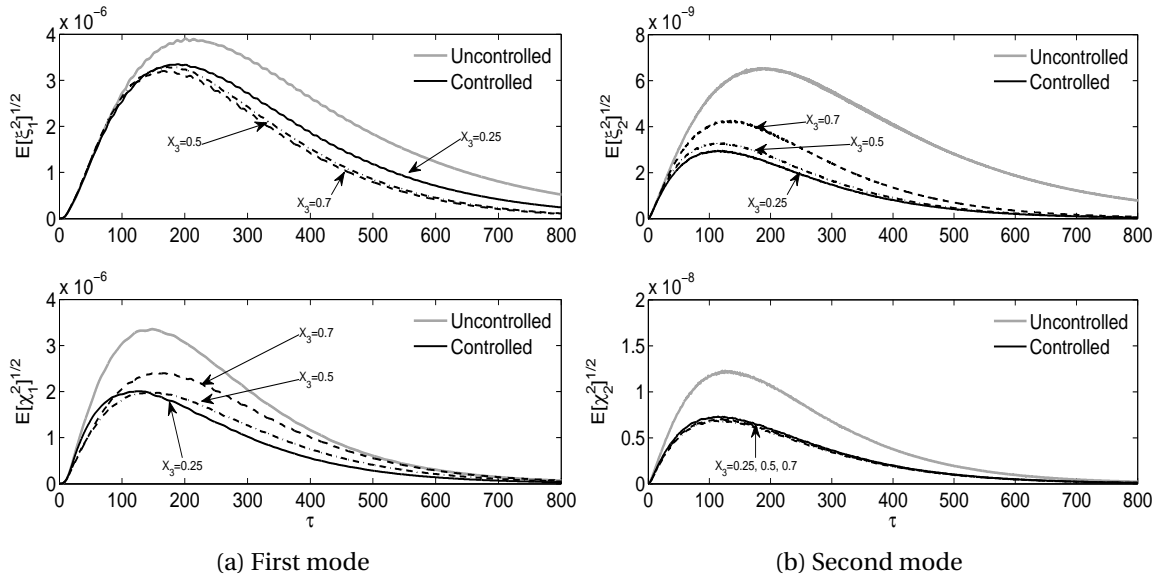


Figure 41: Root square response Bg_1 and Bg_2 , $V_{max} = 2.0$, MF=12090

the time that the MR damper launch to reduce the excessive vibration is, at the first mode $\tau = 45.42$ for Bg_1 and $\tau = 18.48$ for Bg_2 , at the second mode $\tau = 13.59$ for Bg_1 and $\tau = 4.2$ for Bg_2 , at the third mode $\tau = 11.49$ for Bg_1 and $\tau = 7.05$ for Bg_2 .

It should be noted that the employed root mean square displacement approach also allows to assess the percentage reduction of excessive vibrations from the external loads by the controller.

3.4 Fuzzy MR Device Vibration Control of two Cantilever Timoshenko Beams interconnected under Earthquake Excitation

This part of the thesis deals with the nonstationary random response of two cantilevers structures connected via a MR damper. The cantilever Timoshenko beam approach is used to model each of structures. An analytical procedure is detailed to obtain the modal equations of the set of structural system.

A Fuzzy logic strategic is used to foresee the appropriate voltage leading to a good control of earthquake-induced vibrations. Since the applied voltage to control device is the only parameter that can be adjusted to modify the control force.

3.4.1 Description of the physical model

The structural system is constituted of the two continuum cantilever structures (Bg_1) and (Bg_2) of different heights. The buildings are subjected to the same environmental dynamic force in the horizontal direction denoted ground excitation, which is considered to simulate a seismic motion. At location fixed point of each structure; a semi active device dubbed MR damper (D) is installed, consequently this control device rigidly interconnects the two buildings between them such manner that they work together, as illustrated in Figure 42. The control device is equipped of a moving piston head

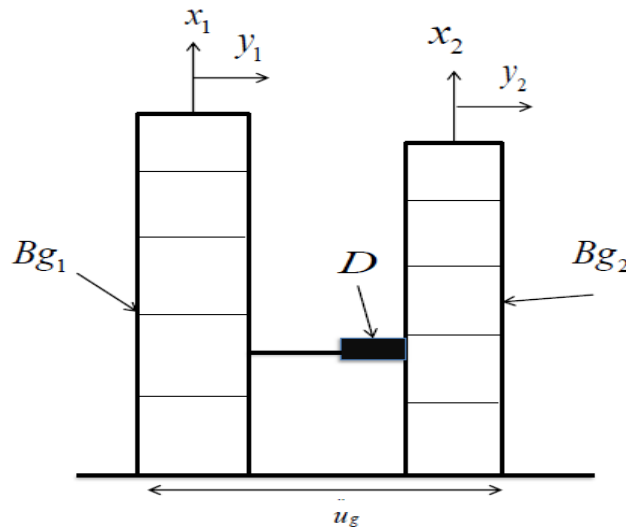


Figure 42: The simplified model of the interconnected buildings

fixed on Bg_1 and another of their extremities is linked on Bg_2 . It also plays the support role of this damper which, generates the damping forces acting

on both mechanical structures in order to safeguard them against undesirable vibrations.

Considering the Timoshenko model which is governing by the differential partial equation, the dynamics of both buildings interconnected by a magneto rheological damper under the earthquake excitation is given as follows[97]

$$m_1 \frac{\partial^2 y_1}{\partial t^2} + c_1 \frac{\partial y_1}{\partial t} + E_1 I_1 \frac{\partial^4 y_1}{\partial x_1^4} - m_1 r_1^2 \left(1 + \frac{E_1}{k_s G_1} \right) \frac{\partial^4 y_1}{\partial x_1^2 \partial t^2} = -m_1 \ddot{u}_g(t) - f_D(t) \delta(x_1 - x_a) \quad (156a)$$

$$m_2 \frac{\partial^2 y_2}{\partial t^2} + c_2 \frac{\partial y_2}{\partial t} + E_2 I_2 \frac{\partial^4 y_2}{\partial x_2^4} - m_2 r_2^2 \left(1 + \frac{E_2}{k_s G_2} \right) \frac{\partial^4 y_2}{\partial x_2^2 \partial t^2} = -m_2 \ddot{u}_g(t) + f_D(t) \delta(x_2 - x_c) \quad (156b)$$

In this formulation, the fourth term represents the correction for rotary inertia plus the shear deformation effect. The joint action of rotary inertia and shear deformation effects are neglected [29].

The above set of equations shows the MR damper is at origin of the connection of two structures. This means that the two buildings act independently when they do not connect with the control device. Its presence is to increase the safety and reliability of buildings, and offering the full advantage to modify their response dynamics.

To describe the dynamics of the MR device, Spencer *et al.*[91] have proposed a phenomenological model which is described as the Bouc Wen modified version. Based on the obtained results, the authors concluded that the approach numerically tractable and effectively portrays the behaviour of a MR damper.

The equations governing force f_D generated by the MR damper D , at the attachment points x_a , of Bg_1 and x_c of Bg_2 , respectively, can be expressed as follows

$$f_D = c_1 (\dot{y}_b - \dot{y}_2(x_c, t)) + k_1 [(y_1(x_a, t) - y_2(x_c, t)) - y_0] \quad (157)$$

The internal displacement y_b is illustrated

$$\dot{y}_b = \frac{1}{c_0 + c_1} [\alpha_i z_b + c_0 \dot{y}_1(x_a, t) + c_1 \dot{y}_2(x_c, t) + k_0 (y_1(x_a, t) - y_b)] \quad (158)$$

and z_b is given by

$$\dot{z}_b = -\gamma |\dot{y}_1(x_a, t) - \dot{y}_2(x_c, t)| |z_b|^{n-1} + (\delta_a - \beta |z_b|^n) (\dot{y}_2(x_c, t) - \dot{y}_b) \quad (159)$$

where c_0 and c_1 are the viscous damping at larger velocities and low veloci-

ties respectively; k_1 is the accumulator stiffness; k_0 represents the stiffness at large velocity; γ , β and δ_a are the shape parameters of the hysteresis loops In (158), some parameters depend on the command voltage u_1 which are illustrated as follows

$$c_0 = c_{0a} + c_{0b}u_1, c_1 = c_{1a} + c_{1b}u_1, \alpha = \alpha_{a1} + \alpha_{b1}u_1 \quad (160)$$

where the command voltage u_1 is accounted for through the first order filter

$$\dot{u}_1 = \eta_{p1}(u_1 - v_{c1}) \quad (161)$$

v_{c1} is the maximum applied voltage associated with the saturation of the magnetic field in the MR damper [9].

Introducing the dimensionless variables, these result in to following expressions.

$$\begin{aligned} Y_1 &= \frac{y_1}{L_1}, Y_2 = \frac{y_2}{L_2}, Z_b = \frac{z_b}{L_1}, Y_b = \frac{y_b}{L_2}, \tau = \frac{t}{T}, \kappa_1 = \frac{c_m T}{m_1}, a_1 = \frac{E_1 I_1 T^2}{L_1^4 m_1}, a_2 = \frac{E_2 I_2 T^2}{L_2^4 m_2}, \\ a_3 &= \frac{r_1^2}{L_1^2}, a_5 = \frac{E_1}{k_s G_1}, a_4 = \frac{r_2^2}{L_2^2}, a_6 = \frac{E_2}{k_s G_2}, \ddot{y}_g(\tau) = \frac{\ddot{y}_g(t) T^2}{L_1}, \mu_m = \frac{m_2}{m_1}, \mu_l = \frac{L_2}{L_1}, \\ \alpha_b &= \frac{\alpha_i T}{(c_0 + c_1)}, C_0 = \frac{c_0}{c_0 + c_1}, C_1 = \frac{c_1}{c_0 + c_1}, \gamma_l = \gamma_i L_1^2, \delta_{li} = \delta_a, \beta_l = \beta_i L_1^2, \kappa_2 = \frac{c_n T}{m_2}, \\ K_0 &= \frac{k_0 T}{c_0 + c_1}, c_l = \frac{c_l T}{m_1 L_1}, K_1 = \frac{k_1 T^2}{m_1 L_1}, T = L_1 \sqrt{\frac{\rho}{k_s G_1}}, U_i = \frac{u_i}{V_1}, V_c = \frac{v_c}{V_1}, \eta_T = \eta_p T \end{aligned}$$

By Taking into account the above new parameters, the resulting relationships lead us to the dimensionless mathematical models which are represented by the below equations

$$\frac{\partial^2 Y_1}{\partial \tau^2} + \kappa_1 \frac{\partial Y_1}{\partial \tau} + a_1 \frac{\partial^4 Y_1}{\partial X_1^4} - a_3 (1 + a_5) \frac{\partial^4 Y_1}{\partial X_1^2 \partial \tau^2} = -\ddot{y}_g(\tau) - F_D(\tau) \delta(X_1 - X_a) \quad (162a)$$

$$\frac{\partial^2 Y_2}{\partial \tau^2} + \kappa_2 \frac{\partial Y_2}{\partial \tau} + a_2 \frac{\partial^4 Y_2}{\partial X_2^4} - a_4 (1 + a_6) \frac{\partial^4 Y_2}{\partial X_2^2 \partial \tau^2} = -\frac{1}{\mu_l} \ddot{y}_g(\tau) + \frac{1}{(\mu_m \mu_l^2)} F_D(\tau) \delta(X_2 - X_c) \quad (162b)$$

the dimensionless equation of the MR damper force is illustrated as follows

$$F_D(\tau) = c_l (\dot{Y}_b - \dot{Y}_2(X_c, \tau)) + K_1 (Y_1(\mu_l X_c, \tau) - \mu_l Y_2(X_c, \tau) - Y_0) \quad (163)$$

Y_b and Z_b are governed by the below equations

$$\dot{Y}_b(\tau) = \alpha_b Z_b + C_0 \dot{Y}_1(\mu_l X_c, \tau) + C_1 \mu_l \dot{Y}_2(X_c, \tau) + K_0 (Y_1(\mu_l X_c, \tau) - Y_b) \quad (164)$$

$$\dot{Z}_b(\tau) = -\gamma_l |\dot{Y}_1(\mu_l X_c, \tau) - \dot{Y}_b| Z_b |Z_b|^{n-1} + (\delta_l - \beta_l |Z_b|^n) (\dot{Y}_1(\mu_l X_c, \tau) - \dot{Y}_b) \quad (165)$$

Where, X_a and X_c are the dimensionless variables of x_a and x_c , which characterize the attachment points of the control device on the building Bg_1 and Bg_2 , respectively; V_1 is the reference voltage, μ_l and μ_m are the length and mass ratios, respectively.

To reduce the partial differential equations to a set of ordinary differential equations. The mentioned relative displacements Y_1 and Y_2 are considered each one, as the product of a spatial expression multiplied by a function of time and by considering the above new parameters. We have the following expressions

$$Y_1(X_1, t) = \sum_{j=1}^{n_m} \Phi_1^j(X_1) \xi_j(\tau), \quad Y_2(X_2, t) = \sum_{j=1}^{n_m} \Phi_2^j(X_2) \chi_j(\tau) \quad (166)$$

$\xi_j(\tau)$ and $\chi_j(\tau)$ are the time dependent displacement of Bg_1 and Bg_2 for the j^{th} vibration mode, n_m is the total number of modes, $\Phi_1^j(X_1)$ and $\Phi_2^j(X_1)$ are the spatial forms.

By using the mode decomposition of expressions of the equation (166) and substituting them into the dimensionless form of (156), multiplying by different spatial expressions and performing the integration from 0 to 1; we get the modal forms of above equations, defined as follows

$$\ddot{\xi}_j(\tau) + \zeta_1^j \dot{\xi}_j(\tau) + \varsigma_1^j \xi_j(\tau) = -\sigma_1^j \ddot{y}_g(\tau) - \varepsilon_3^j F_D(\tau) \quad (167a)$$

$$\ddot{\chi}_j(\tau) + \zeta_2^j \dot{\chi}_j(\tau) + \varsigma_2^j \chi_j(\tau) = -\frac{1}{\mu_l} \sigma_2^j \ddot{y}_g(\tau) + \frac{1}{\mu_m \mu_l^2} \varepsilon_3^j F_D(\tau) \quad (167b)$$

The dimensionless equation of the force generated by the MR device is satisfied by the expressions illustrated as follows

$$F_D(\tau) = c_l \left(\dot{\xi}_j \Phi_1^j(\mu_l X_c) - \dot{Y}_h - \dot{\chi}_j \Phi_2^j(X_c) \right) + K_1 \left(\xi_j \Phi_1^j(\mu_l X_c) - \mu_l \chi_j \Phi_2^j(X_c) - Y_0 \right) \quad (168)$$

where Y_h and Z_b can be rewritten as

$$\dot{Y}_h(\tau) = -\alpha_b Z_b + (1 - C_0) \dot{\xi}_j \Phi_1^j(\mu_l X_c) - C_1 \mu_l \dot{\chi}_j \Phi_2^j(X_c) - K_0 Y_h \quad (169)$$

$$\dot{Z}_b(\tau) = -\gamma_l |\dot{Y}_h| Z_b |Z_b|^{n-1} + (\delta_a - \beta_l |Z_b|^n) \dot{Y}_h \quad (170)$$

with

$$Y_h = \xi_j \Phi_1^j(\mu_l X_c) - Y_b \quad (171)$$

The applied voltage to the control device is defined by the dimensionless expression which is given by

$$\dot{U} = \eta_T (U_1 - V_{c1}) \quad (172)$$

Equations (167)-(172) describe the time evolution of buildings Bg_1 and Bg_2 interconnected at the attachment point by the shock absorber. Afterwards, it is seen that, the parameter of equations varied at each mode of vibration and the force generated by MR device depend on its location point on both buildings. All of these indicated that the optimal connection point of the controller is necessary.

Table 9: parameter values of Bg_1 and Bg_2 .

Parameters	δ_1^j	ε_1^j	d_{11}^j	d_{33}^j	ζ_1^j
First	1.8748	1.8729	-0.7350	-0.7336	0.0052
Second	4.6872	4.6582	-1.0315	-1.0191	0.2000
Parameters	δ_2^j	ε_2^j	d_{11}^j	d_{33}^j	ζ_2^j
First	1.8734	1.8629	-0.7397	-0.7316	0.0288
Second	4.6567	4.5031	-1.0918	-1.0224	1.0407

3.4.2 Passive on control

Although the attachment point of the control device can significantly affect the dynamic response of buildings. It is also important to define the saturation capacity of the damping force produced by the control device. Because it is always appropriate to enhance the structural safety. For illustrating this underlying phenomenon in the reasonable context, the passive on control will be employed.

Thus, Mean and root mean square of the relative transverse displacements at the first and second modes are displayed through Figures 43 and 44, respectively. The selected control device position $X_c = 0.3$ for Bg_2 , referring to position $X_a = 0.27$ for Bg_1 .

In Figures 43a and 43b, the difference between the controlled and uncontrolled amplitudes during the interval time $\tau \in [0, 100]$ is observed. One can see that the control device has modified the response of structures by adding

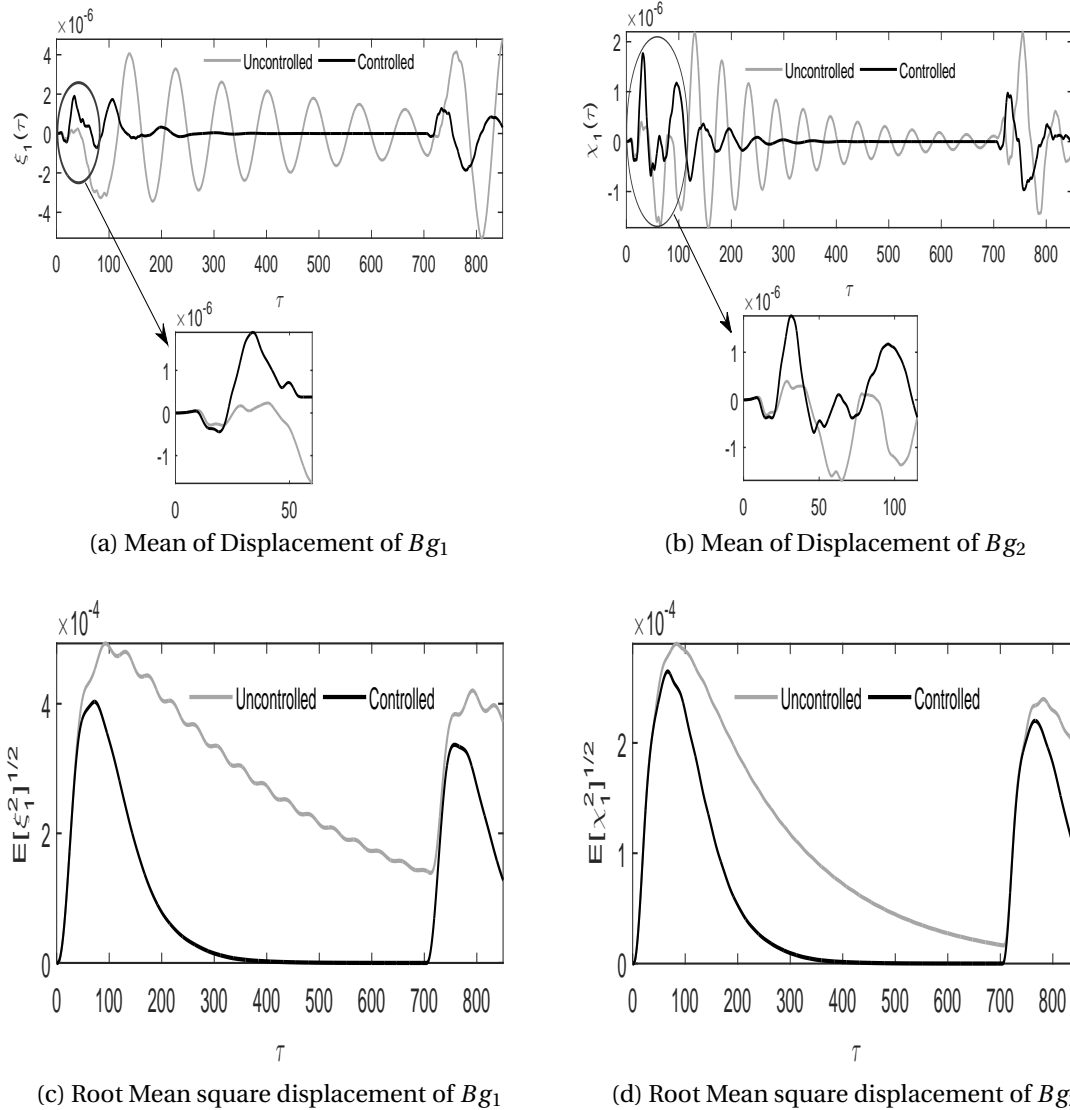


Figure 43: First mode $X_c = 0.3$, MF= 1000

the mechanical energy into Bg_1 and Bg_2 instead of reducing. In this configuration, the device does not presently show its capacity to protect the two buildings at the same time; this can be due to its intrinsic nonlinear characteristic.

To overcome this shortcoming, it will be crucial to associate with device control an appropriated algorithm that can be dynamically modify its response by improving the response of buildings subjected to earthquake. All these figures are displayed at the dimensionless voltage $V_c = 0.4$.

It is well-known that the MR damper is characterized by a limited capacity to control the vibration-induced the external excitation. As the control device can change the properties through the modification of the parameter MF. The variation of this automatically affects the force generated by the control device. It will be convenient to have the best MF value leading to good

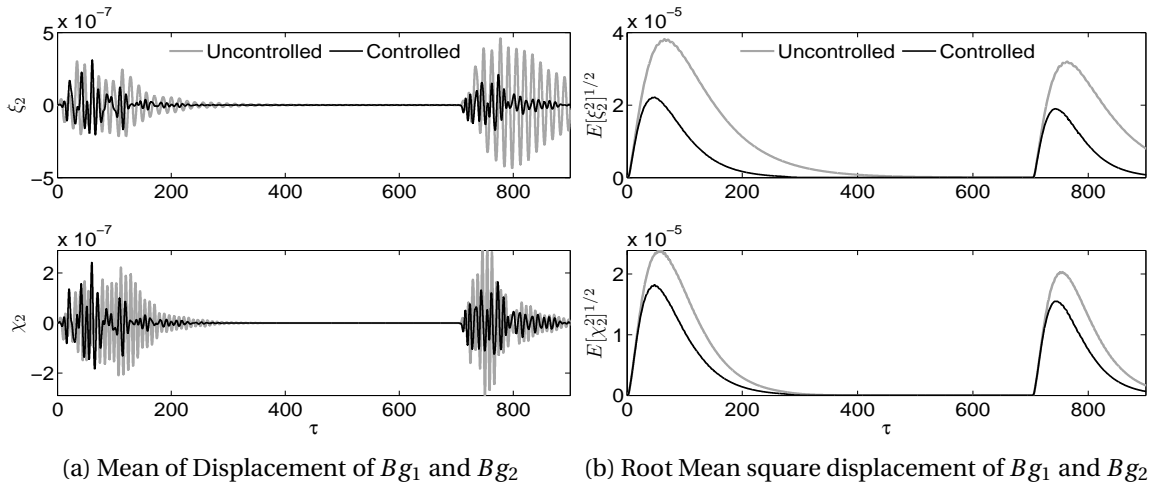


Figure 44: Second mode $X_c = 0.3, MF = 1000$

control and maintaining stable the structural system.

The analyse for finding the optimal mentioned parameter is illustrated in Figures 45a and 45b at first and second vibration modes, respectively. These display the peak root mean square displacement versus MF.

Figure 45 shows that the best value of MF guiding to better reduction for first the two modes is 1000.

In addition, one can notice that beyond of this value, the amplitude vibration of structures increase significantly, what is a catastrophic consequence for the buildings. Since the further energy can destabilize the structural system leading to premature destruction.

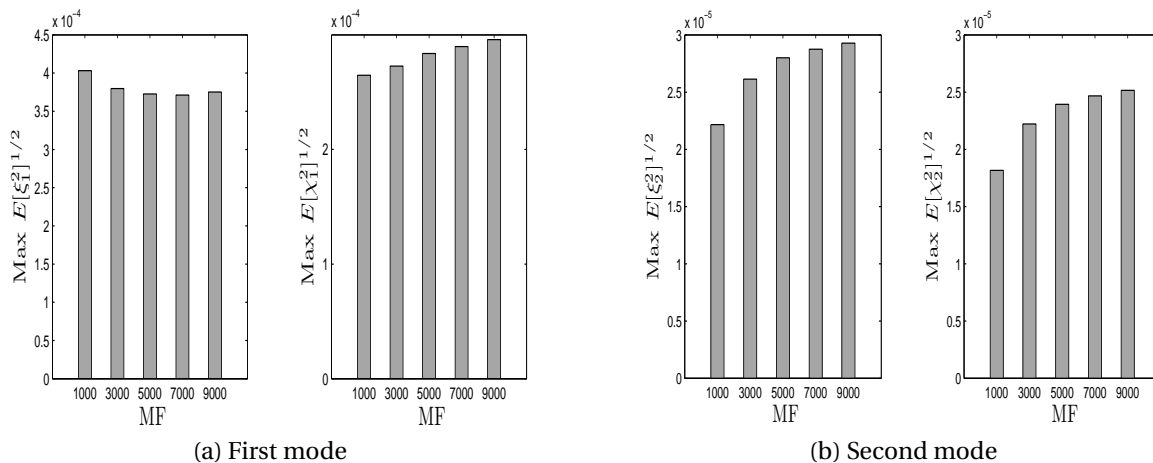


Figure 45: Limit value of the MR damper

As showed earlier by equations (167)-(172) of the influence of the location control device on the dynamic response of structures.

Figure 45 shows that the location points versus the maximal of Root mean

square displacement of structures Bg_1 and Bg_2 at each vibration mode. It is important to note the location of the MR damper on the structures Bg_1 and Bg_2 is indicated by the couple of coordinates (X_a, X_c) where $X_a = \mu_l X_c$, since the two structures defined in the context of our study do not have the same length.

Thus, with regard the first mode (Figure 46a), one can clearly see that the values 0.27, 0.45, 0.63 and 0.1, 0.3, 0.5 are best location points of the control device on Bg_1 and Bg_2 ; respectively. The analyse of these results leading to define only the two couples (0.27,0.3), (0.45,0.5) as the optimal positions of the control device. All these positions presented here,are associated with maximal root means square displacement (see table 10).

For the case second mode as shown in Figure 46b, there are the values 0.27, 0.45, 0.63 and 0.3, 0.9 defined as the best position of vibration control

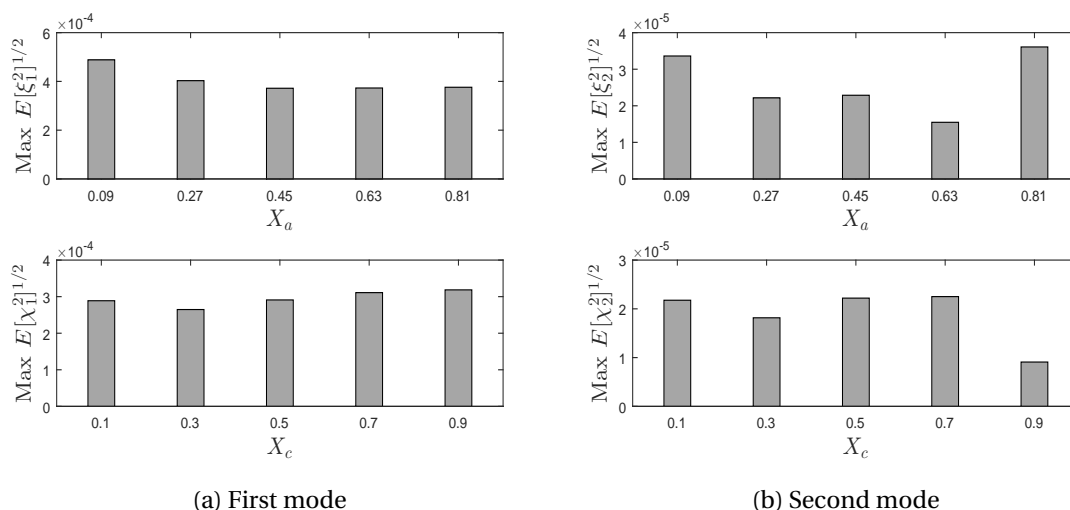


Figure 46: Location point of the MR device

Table 10: Max RMS Bg_1 and Bg_2 versus location points.

Location points	Bg_1					Bg_2				
	0.09	0.27	0.45	0.63	0.81	0.1	0.3	0.5	0.7	0.9
First mode ($\times 10^{-4}$)	4.88	4.03	3.72	3.73	3.76	2.88	2.65	2.91	3.11	3.19
Second mode ($\times 10^{-5}$)	3.36	2.22	2.29	1.54	3.61	2.18	1.82	2.22	2.25	0.91

on Bg_1 and Bg_2 ; respectively. The analyse only gives one couple (0.27, 0.3) as the optimal position.

Note in passing that it is impossible to change the location control device at each vibration mode. As a consequence from first and second modes, one can see that the couple (0.27, 0.3) appears as the best position adapted for the

two vibration modes leading to better attenuation excessive vibration without adding mechanical energy to any structure.

3.4.3 Fuzzy Logic Control

Due to the inherent nonlinear nature of the MR damper, the appropriated control strategies were developed, in order to allow the controller to achieve high level of performance [86]. The MR damper-based the strategy control offer the reliability of passive control device but also maintain adaptability of fully active control systems [110]. In this view, the Fuzzy algorithm will be adopted to perform the response dynamics of the MR damper during the control process by guaranteeing the safety and the stability of structures. As a consequence of underlying fact, it will be necessary to define an algorithm that allows to avoid the increase of the energy in the structures during the control process (as observed in Figure 43), since the presence of the supplementary energy can drive at the destabilisation or destruction of the structure.

It is important to note that the mentioned correction is necessary in order to adjust the voltage that commands the MR damper.

In what follows, the relative displacement ($X_r = \xi_j - \chi_j$) and relative velocity ($V_r = \dot{\xi}_j - \dot{\chi}_j$) of the two buildings will be used like input variables.

Each of these is divided to a total of seven fuzzy variables, which are defined as NL (Negative Large), NM (Negative Medium), NS (Negative Small), ZE (Zeros), PS (Positive Small), PM (Positive Medium), PL (Positive Large). The considered output information is the voltage applied to the MR damper. The fuzzy variables for this output is separated of 6 membership functions: Z (Zeros), P (Small), M (Medium), L (Large), VL (Very Large) and EL (Extreme Large).

The triangular membership functions for input and output variable are plotted in Figure 47, where the input and output universe are $[0, 1]$ and $[-1, 1]$, respectively. Note that the universe of output variables is obtained by normalizing.

Fuzzy control rules employed in this paper to command the voltage are listed in Table 11.

Figure 48 shows that the time histories of displacements uncontrolled and controlled of structures Bg_1 and Bg_2 at the first and second modes of vibrations. We can clearly see that controller has achieved the performance.

The behaviour of the force generated by MR damper at the first (Figure 49a) and second (Figure 49b) modes is illustrated in Figure 49. By focusing much attention on this figure, it is noticed that the nonstationary random excita-

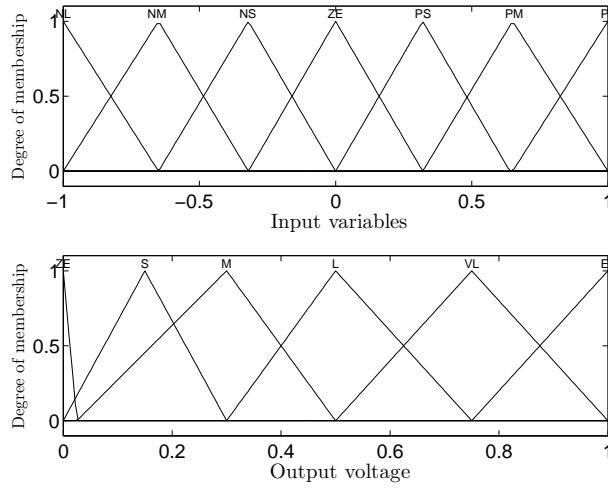


Figure 47: Membership functions for Input and Output

Table 11: Fuzzy control rules

X_r / V_r	NL	NM	NS	ZE	PS	PM	PL
NL	EL	M	VL	ZE	VL	S	PL
NM	L	VL	L	M	S	VL	ZE
NS	L	L	M	L	EL	L	S
ZE	ZE	ZE	ZE	ZE	ZE	M	L
PS	S	L	M	L	ZE	L	EL
PM	L	EL	M	S	M	VL	EL
PL	L	M	EL	EL	L	L	L

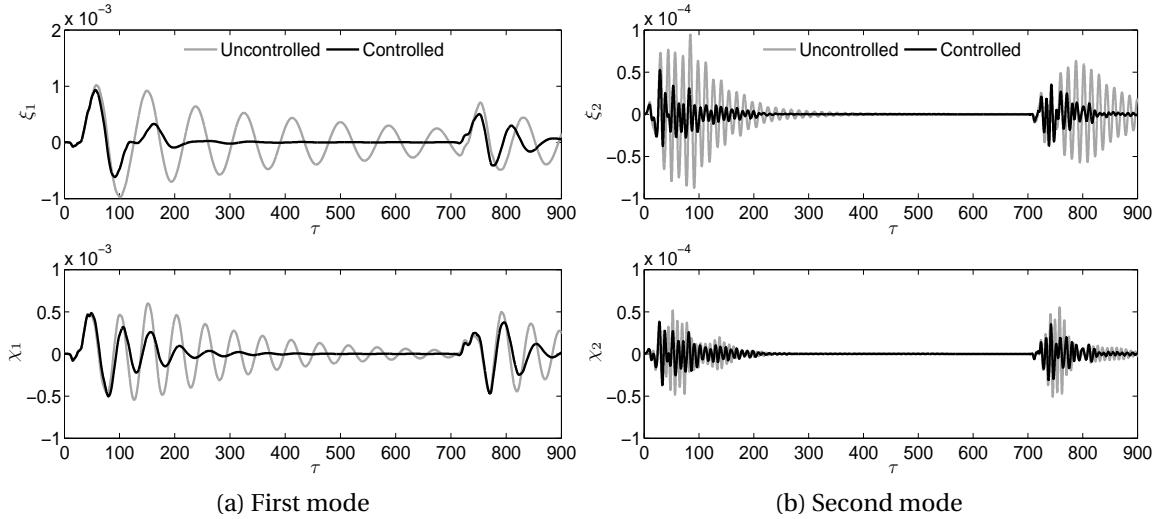


Figure 48: Time histories of structures Bg_1 and Bg_2

tion impose almost the same dynamics to the control device force.

The control input to the MR damper at the first and second modes is presented in Figure 50. One can observe that, the time response of the applied

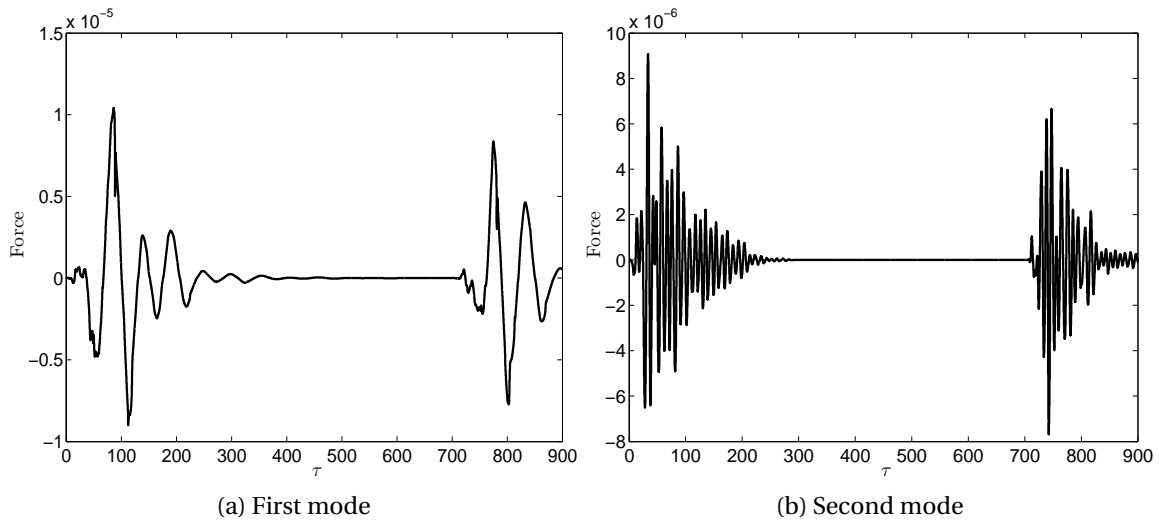


Figure 49: Force generated by the MR damper

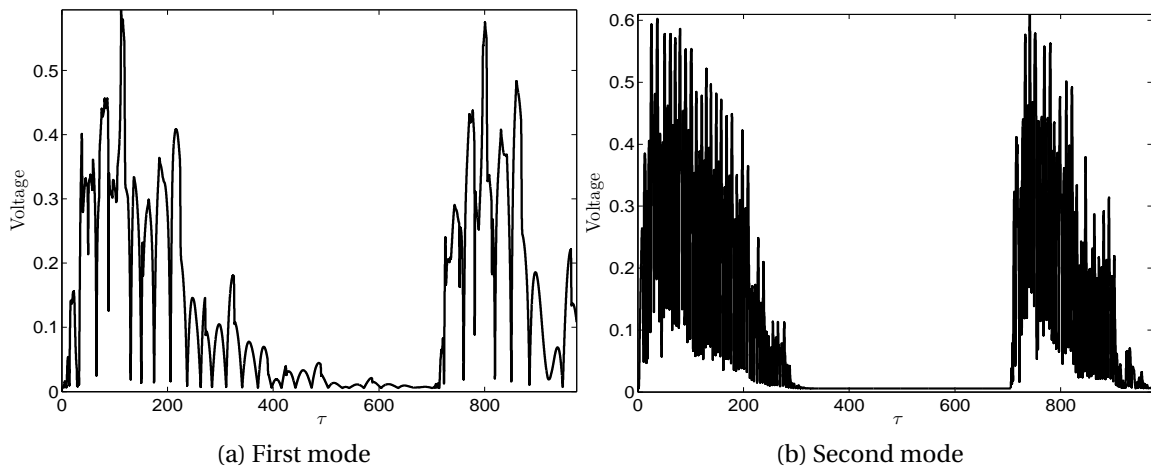


Figure 50: Applied voltage to the MR damper

voltage to the damper have tendency to follow the sequential dynamic of the ground acceleration.

3.5 Reduction of vibration on a Cantilever Timoshenko beam subjected to repeated sequence of excitation with MR Outriggers

We deal with the statistical effects of an outrigger system on a cantilever beam under seismic excitation. The Timoshenko beam approach is used to model the frame-core tube linked at a point of its length by the damped outriggers, therefore are connected vertically to two magneto-rheological (MR) damper devices.

3.5.1 Description of Physical system and Dynamic model formulation

The physical model represented in Figure 51 is a structural system which is constituted of a uniform cantilever beam and one outrigger truss. The set of the system is subjected to the same environmental dynamic force in the horizontal direction denoted ground excitation, which is considered to simulate a seismic motion. The outriggers and the exterior columns have commonly a high stiffness. In this context they are assumed to be infinitely rigid. As a result, the outrigger behaves as a rigid body and is attached at a point a from the end of the core tube.

In view of increasing the capacity of the dynamic response of the structural system to resist against the non stationary excitation. Two semi active devices dubbed MR dampers (D) are installed vertically and symmetrically, therefore the generated forces are applied to the core tube through the outriggers.

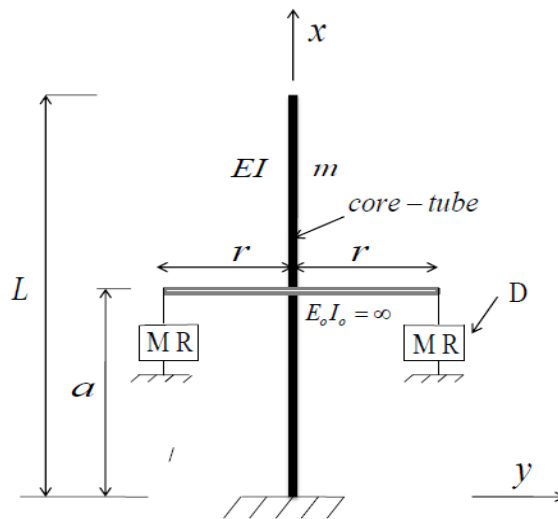


Figure 51: Cantilever beam with MR outriggers

The mass per unit length is m_1 ; I is the moment of inertia of the cross-section

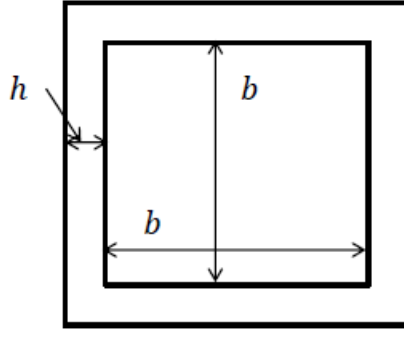


Figure 52: Cross-section of the core tube

about the neutral axis, E is the Young's modulus; G is the shear modulus of elasticity; r_a is the radius of gyration. These geometrical characteristic are assumed constant. The lateral displacement is defined by $y(x, t) = y$, which varies with the coordinate along the beam x and with time t .

The control device f_d is generated by a MR damper. The influence of the perimeter columns on the dynamics of the core is not taken into consideration.

The governing equations describing the dynamics of the cantilever Timoshenko beam with one damped outrigger under the earthquake loadings can be written as

$$m_1 \frac{\partial^2 y}{\partial t^2} + EI \frac{\partial^4 y}{\partial x^4} - m_1 r_a^2 \left(1 + \frac{E}{k_s G} \right) \frac{\partial^4 y}{\partial x^2 \partial t^2} = -m_1 \ddot{x}_g(t) + \frac{\partial M_a}{\partial x} \quad (173)$$

where the distributed moment generated by the MR dampers is

$$M_a = 2\delta(x - a) r f_d(t) \quad (174)$$

in which

$\delta(x - a)$ denotes the Dirac function, it indicates that the point a is the place where the damped outriggers is installed.

The distance from the control devices to the centre of the core is denoted r . The dimensionless quantity k_s , is the shear coefficient depending on the geometric of the cross section of the beam and depend on as well as of the Poisson's ratio.

It is assumed that the dimensional ratio of the width on the area to the thickness is very small, reason why the core tube is considered such a beam being the cross section at the small thickness. This analysis lead us to adopt that, the expression of the mentioned coefficient associated with the cross-

section of the core tube is given by [36]

$$k_s = \frac{20(1 + \nu)}{48 + 39\nu} \quad (175)$$

ν is the Poisson's ratio coefficient, it is clearly seen that k_s depends solely on the material property.

In what follows, the moment of inertia and area of the cross-section can be formulated as

$$A = (b + 2h)^2 - b^2; \quad I = \frac{(b + 2h)^4}{12} - \frac{b^4}{12}$$

For convenience in the present study, the joint action of rotary inertia and shear deformation effects is neglected. Thereafter the bending stiffness for the outriggers is assumed to be infinite [21].

$$Y = \frac{y}{L}, \tau = \frac{t}{T}, \delta_a = \delta_1 L, \gamma_L = \gamma L, \zeta_a = \frac{2r}{L}, \ddot{y}_g(\tau) = \frac{T^2}{L} \ddot{x}_g(t);$$

$$a_1 = \frac{EIT^2}{mL^4}, a_2 = \frac{r_a^2}{L^2} \left(1 + \frac{E}{k_s G}\right), C_0 = \frac{c_0}{c_0 + c_1}, K_0 = \frac{k_0 T}{c_0 + c_1}, \alpha_b = \frac{\alpha T}{(c_0 + c_1)L},$$

$$C_1 = \frac{c_1 T}{mL}, K_1 = \frac{k_1 T^2}{mL}, T = L \sqrt{\frac{\rho}{k_s G}}, Y_0 = \frac{y_0}{L}$$

One gets the modal forms of above equations, that can be expressed as follows

$$\ddot{\chi}_j(\tau) + \zeta_j \dot{\chi}_j(\tau) + \varsigma_j \chi_j(\tau) = -\sigma_j \ddot{y}_g(\tau) - \zeta_a \eta_j F_d(\tau) \quad (176)$$

The dimensionless equation of the force generated by the MR device is satisfied by the illustrated expressions as follows

$$F_d(\tau) = C_1 \dot{Y}_1 + K_1 (\chi_j(\tau) \Phi_j(X_0) - Y_0) \quad (177)$$

where Y_h and Z can be rewritten as

$$\dot{Y}_1 = \alpha_b Z + C_0 \dot{\chi}_j(\tau) \Phi_j(X_0) + K_0 (\chi_j(\tau) \Phi_j(X_0) - Y_1) \quad (178)$$

$$\dot{Z} = -\gamma_L |\dot{\chi}_j(\tau) \Phi_j(X_0) - \dot{Y}_1| |Z| |Z|^{n-1} + (\delta_L - \beta_L |Z|^n) (\dot{\chi}_j(\tau) \Phi_j(X_0) - \dot{Y}_1) \quad (179)$$

The applied voltage to the control device is defined by the dimensionless expression which is given by

$$U = \eta_T (U - Vc) \quad (180)$$

with

$$\varsigma_j = \frac{a_1 b_3}{b_1 + a_2 b_2}, \eta_j = \frac{\Phi_j'(X_0)}{b_1 + a_2 b_2}, \sigma_j = \frac{b_4}{b_1 + a_2 b_2}$$

in which

$$b_1 = \int_0^1 \Phi_j(X)^2 dX, \quad b_2 = \int_0^1 \Phi_j''(X)\Phi_j(X) dX,$$

$$b_3 = \int_0^1 \Phi_j''''(X)\Phi_j(X) dX, \quad b_4 = \int_0^1 \Phi_j(X) dX$$

Equations (176)-(180) describe the time evolution of the concrete core tube which is fixed at the point X_0 by the damped outriggers. It is useful to observe that the parameter of the Equation (176) varied at each mode of vibration and that the force generated by MR device depends on the attachment point of the damped outriggers on core tube.

All these results indicate that outrigger locations could modify the structural response at the different mode of the vibration and can provide a better understanding of the outrigger design.

3.5.2 Semi-active controller

With a view to obtain the optimal input voltage corresponding to the desired damper force and to assess the performance of control system.

The control algorithm as an effective mean used in semi-active control based on the Lyapunov stability theory [113] is employed. Because the control device is not directly controllable and that only applied voltage can be adjusted. Also the mentioned control algorithm is developed for characterizing adequately the damper's intrinsic non-linear behaviour [91].

Thus, Lyapunov function, denoted $L_y(\mathbf{W})$ must be a positive function of the state of the system, \mathbf{W} . According to the Lyapunov stability theory, if the rate of change of Lyapunov function, $\dot{L}_y(\mathbf{W})$, is negative semi-definite, the origin is stable. Lyapunov function is chosen of the form

$$L_y = \frac{1}{2} \|\mathbf{W}\|_p^2 \quad (181)$$

where $\|\Sigma\|_p = P$ -norm of the states defined by

$$\|\Sigma\|_p = [\Sigma' \mathbf{P}_L \Sigma]^{1/2} \quad (182)$$

where \mathbf{P}_L is real, symmetric, positive definite matrix. \mathbf{P}_L is found using Lyapunov equation.

$$\Sigma' \mathbf{P}_L + \mathbf{P}_L \Sigma = -\mathbf{Q}_p \quad (183)$$

\mathbf{Q}_p is a positive definite matrix. The derivative of the Lyapunov function for a solution of the state-space equation is

$$\dot{L}_y = -\frac{1}{2}\mathbf{W}'\mathbf{Q}_p\mathbf{W} + \mathbf{W}'\mathbf{P}_L\mathbf{B}_1F_d + \mathbf{W}'\mathbf{P}_L\mathbf{B}\ddot{y}_g \quad (184)$$

The above parameters are defined as follows

$$\mathbf{W} = \begin{bmatrix} \chi_j \\ \dot{\chi}_j \end{bmatrix}, \quad \Sigma = \begin{bmatrix} 0 & 1 \\ -\zeta_j & -\zeta_j \end{bmatrix}, \quad \mathbf{B} = \begin{bmatrix} 0 \\ -\sigma_j \end{bmatrix}, \quad \mathbf{B}_1 = \begin{bmatrix} 0 \\ -\zeta_a\eta_j \end{bmatrix}$$

The control law which minimize \dot{L}_y

$$V_c = V_{max}H(-\mathbf{W}'\mathbf{P}_L\mathbf{B}_1F_d) \quad (185)$$

Where V_{max} is the maximum voltage and $H(\cdot)$ is Heaviside step function. When this function is greater than zero, the voltage (V_c) applied to the damper should be maximum (V_{max}), otherwise, the command voltage is set to zero.

To investigate efficiency of the simplified model, the building is considered, such as the concrete core of the geometric $12\text{ m} \times 12\text{ m}$ with a 0.5 m thickness, and with the height of 210 m [63], The mass per unit length is $m_1 = 62500\text{ Kg/m}$.

The eigenvalues are obtained through the Newton-Raphson numerical. The results obtained through this method are illustrated in Table 12. The listed

Table 12: parameters of the structural system.

Paramter	First	Second	Third
δ_1^j	1.873	4.649	7.752
ϵ_1^j	1.860	4.465	6.979
d_1^j	-0.743	-1.127	-1.283
d_3^j	-0.731	-1.023	-0.998
ζ_1^j	0.039	1.579	13.918

parameter values in Table 13, are those obtained from the analysis of experimental data and theoretical results by [112].

As it is difficult to have a MR damper with the obtained parameters experimentally, that will lead to the optimal minimization of excessive vibration of mechanical structures. To avoid this drawback, some parameters in Table 13 depend on MF named the scaled coefficient. The objective here is to modify the properties of the damper, in view of having the parameter values for a large scale MR damper, enable to control the mechanical structure. [109]. To assess the optimal position of outriggers on the core tube, the passive-on strategy of the controller is employed. Thus Figures 53 and 54 display the peak RMS versus locations of outriggers on the structure.

Table 13: Model parameters of the MR damper.

Parameter	Value	Parameter	Value
δ_a	1107.2	n_1	2
$\gamma(m^{-2})$	164.0×10000	$\eta_p(s^{-1})$	190
$\beta(m^{-2})$	164.0×10000	$k_1(N/m)$	9.7 MF
$k_0(N/m)$	2 MF	$y_0(m)$	0.0
$\alpha_a(N/m)$	46200 MF	$\alpha_b(N/mV)$	41200' MF
$c_{0a}(Ns/m)$	110000 MF	$c_{0b}(Ns/mV)$	114300 MF
$c_{1a}(Ns/m)$	8359200 MF	$c_{1b}(Ns/mV)$	7482900 MF

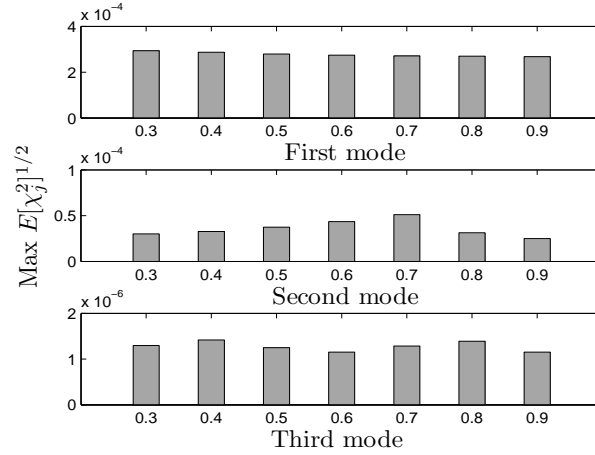


Figure 53: Optimal position of damped outriggers, $\zeta_a = 0.762$ and MF=1.0

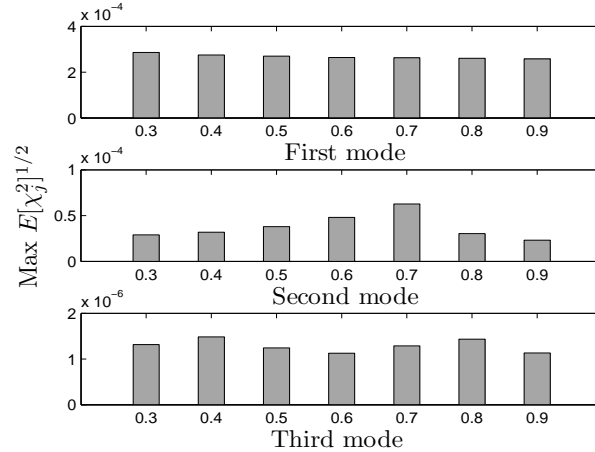


Figure 54: Optimal position of damped outriggers, $\zeta_a = 0.095$ and MF=1.0

Figure 53 presents at the first mode, a slight variation between the amplitude at the different position of outriggers on the core tube. We can realize that the positions 0.7, 0.8 and 0.9 at this quoted mode, are the location points of damped outriggers where the displacement of the structural system is reduced slightly in relation to other positions.

The second mode exhibits only one best position of outriggers on the core

tube which is 0.9.

It is well-seen that at this point the amplitude of vibration is reduced dramatically. As regards the third mode, the optimal positions are 0.6 and 0.9. In these points the peak amplitude of vibration of the structure are reduced than other positions. The global analysis of different observations from Figure 53 lead us to mention that the optimal attachment point of outriggers benefits for the three modes of vibration is 0.9.

The same observation from Figure 53 is illustrated in Figure 54, That is to say the point 0.9 stay only the best position of outriggers on the frame core tube.

Analysing these figures, as can be seen, the point 0.9 is better attachment point of damped outriggers on the frame-core tube favourable for the three first modes of vibration. Thus, the variation of the length of each outrigger do not affect the value of its optimal attachment point on the beam.

As mentioned before, it is not easy to get the best parameters from experi-

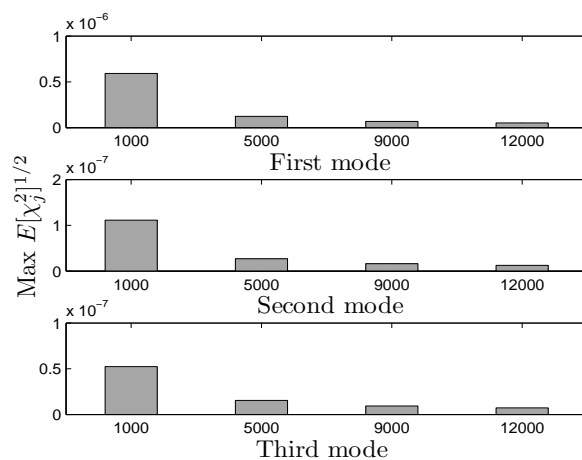
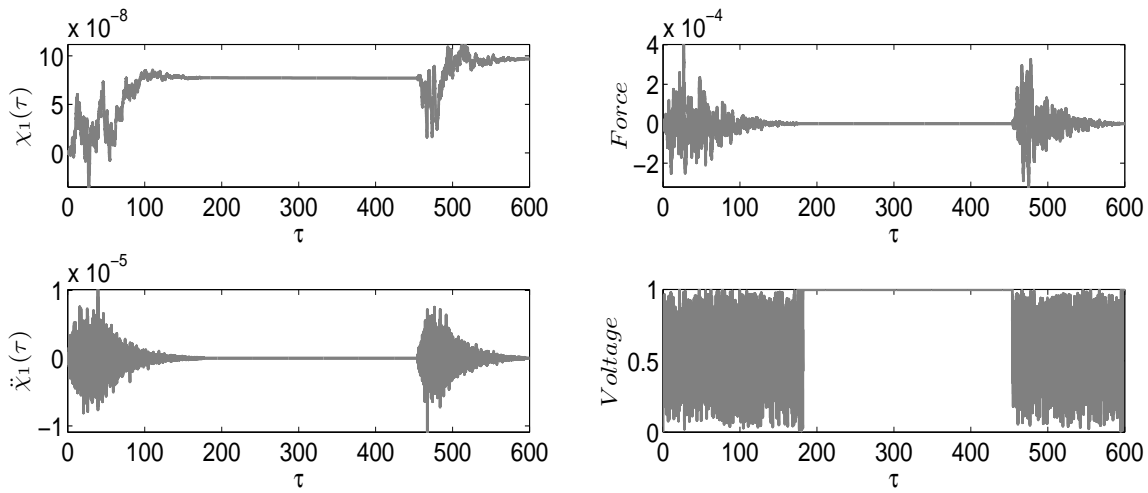


Figure 55: Optimal scale coefficient MF

mental results of the MR damper which incorporated into the structure that lead to efficient control.

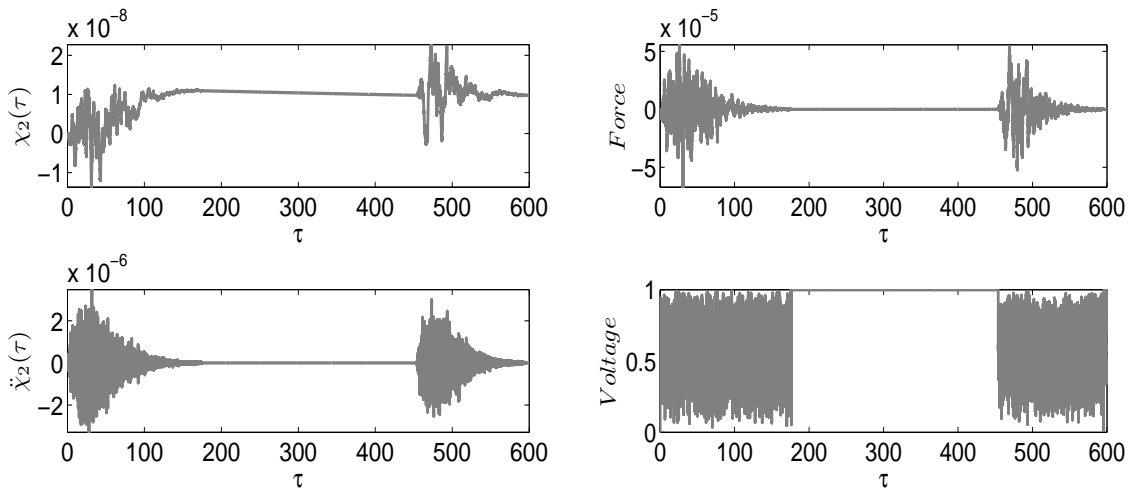
Figure 55 displays the peak RMS versus the scale coefficient MF at the first three modes of vibration. It is observed that the increasing of this quoted coefficient affects the performance of damped outrigger in reducing the seismic response of the structure.

It is important to note that the choice of MF is done such as the control device cannot increase the mechanical energy in the structural system. In other words the control device should reinforce the stability of the structure in order to avoid their premature destruction.



(a) Displacement and acceleration of the outrigger system (b) Control force and applied voltage to MR damper

Figure 56: Time histories at the first mode of the vibration.

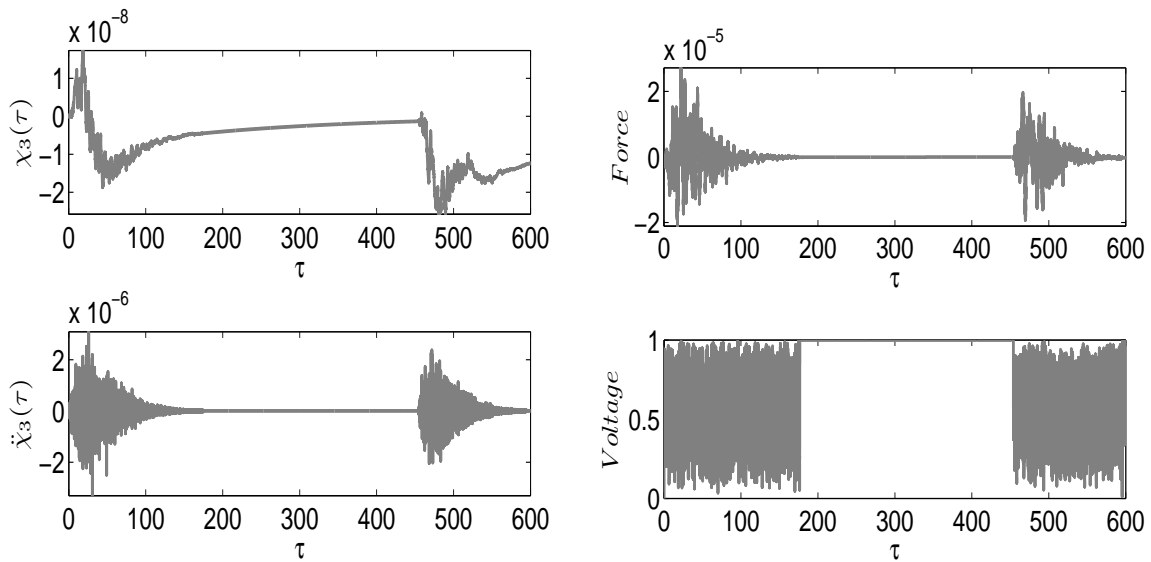


(a) Displacement and acceleration of the outrigger system (b) Control force and applied voltage to MR damper

Figure 57: Time histories at the second mode of the vibration.

By taking into account of optimal position of the damped outriggers and scale coefficient, one results in Figures 56, 57 and 58 which display the time histories of transverse displacement, acceleration, control force and applied voltage to MR damper at the first, second and third modes of the vibration for $MF=9000$.

The structural response of the outrigger system at the three first modes of vibration is shown in Figures 56a, 57a and 58a. One can see that the structural response shows two sequences of the vibration.



(a) Displacement and acceleration of the outrigger system (b) Control force and applied voltage to MR damper

Figure 58: Time histories at the third mode of the vibration .

The command signal V_c is selected through the control algorithm based on Lyapunov stability illustrated in Equation (185). The numerical result of this adopted strategy allows of having Figures 56b, 57b and 58b at the first second and third modes of vibration.

The observed separating time interval between $\tau = 170$ and $\tau = 460$ indicates that the controller is in passive-off mode. Since in this relaxation time, the structure did not receive the input produced by earthquake, as a result the system cease to exhibit the vibration.

3.6 Conclusion

The present chapter has shown the results obtained in this work. In general, Timoshenko beam approach was employed to model the dynamical state of buildings under earthquake loadings. Two approaches of modelling of buildings were presented.

The first approach, the joint action of rotary inertia and shear deformation effects was considered. In this case. In section 3.2, the dynamic response of the structure under deterministic earthquake loads was investigated. These ones were expanded in term of a Fourier series, of unknown coefficients, that is modulated by an enveloping function. The methods of lines were then used to solve the basic equations using direct numerical simulation and also to confirm our analytical predictions.

Afterwards, the second approach of modelling of buildings, the joint action of rotary inertia and shear deformation effects was neglected. In this configuration, the dynamic response of buildings under the nonstationary stochastic ground motion was investigated in section 3.3, section 3.4 and section 3.5. The action of earthquake excitation on the structural system were extended in two sequences. The specificities of these two sequences are the separating time intervals and the frequency contents. The non-stationary random process were used to simulate the seismic events. It was shown that the control device is not efficient at all located position on the mechanical structures. To reduce undesirable vibration by increasing the structural safety, the MR damper was employed. The results obtained through statistical analysis have shown that the MR damper is a good candidate to suppress the vibration in a mechanical structure subjected to earthquake loads.

General Conclusion

The aim of the present thesis was the study of the dynamics response of tall buildings excited by the nonstationary ground motion. The control device was employed to attenuate the excessive vibration, in order to stabilize the structural health. Because these structures under the disturbances sometimes induced a premature destruction.

Summary of the main results

The first chapter was devoted to the literature review on the generalities on beam models and on the vibration control of the mechanical structure. By combining of shear-type deformation and rotary inertia effects, the Timoshenko theory beam was presented. Since the mentioned theory combined all other model detailed in the literature. Furthermore the mathematical modelling of the magneto-rheological device, combines the best feature by offering the reliability of passive devices, yet maintaining the versatility and adaptability of fully active systems was given.

In the second chapter, various mathematical models of the nonstationary earthquake, the analytical and numerical tools used for development and analysis were presented. Thus, method of lines defined as a method to approximate were then used to solve the based equation using direct numerical simulation. Routh-Hurwitz stability of a system were also detailed. The algorithm of fourth order Runge-Kutta of deterministic and stochastic versions described by Kasdin was given in the numerical section. We have also presented the same section the Newton-Raphon method for solving of equations. Finally, we have closed this chapter with the presentation well-detailed of fuzzy logic architecture.

The third chapter, is devoted to the results obtained in the thesis. The action of earthquake excitation extended in on the structural system was analysed. The value of Modified Factor (MF), which can define the maximum force capacity generated by the control device was obtained. It appears that for a good choice of parameters of the control device, the structural system can remain stable by guaranteeing the safety and the stability of structures without leading to premature destruction. The investigation of the study at different modes of vibration, was really necessary to obtain the optimal location of the MR device on of structures. Since its attachment point fully influences the response of structures.

In order to reduce, the excessive vibration of structures during the earth-

quake without adding supplementary mechanical energy, the control algorithm such that the Lyapunov stability theory, in the first case and fuzzy logic in second step were used as supplementary means to select the suitable voltage that operates MR damper. Since the voltage can directly be modified by the control algorithm during the control process. As a result, it was shown that, the application of the algorithm control refines dynamically of the MR damper by improving the control process at different mode of vibration.

Future work

In this thesis, some interesting results were obtained and this work leads to some prospective works for future investigations. In this sense, it will be interesting to analyse the effects of the time delay of the control device on the dynamic response of the structural system. It will also be important to analytically obtain the time when the controller begins to attenuate the vibration of structures.

Bibliography

- [1] **Soong T**, "State-of-the-art review: Active structural control in civil engineering", *Engineering Structures* 1988; 10: 74-84.
- [2] **Sandoval ME, Ugarte LB, Spencer BF**, "Study of structural control in coupled buildings" *Proceeding of the 15th World Conference on Earthquake Engineering, Lisbon, Portugal* 2012.
- [3] **Bigdeli K, Hareb W, Tesfamariama S**, "Configuration optimization of dampers for adjacent buildings under seismic excitations" *Engineering Optimization* 2012; 44: 1491-1509.
- [4] **Bigdeli K, Hare W, Nutini J, Tesfamariam S**, "Optimizing damper connectors for adjacent buildings" *Optimization and Engineering* 2016; 17: 47-75.
- [5] **Cimellaro GP, Reinhorn AM**, "Algorithm for optimal design of adjacent buildings connected by fluid viscous devices." *In Proceedings of Structures Congress* 2008; 24-26.
- [6] **Ni YQ, Ko JM, Ying ZG**, "Random seismic response analysis of adjacent buildings coupled with non-linear hysteresis dampers", *Journal of Sound and Vibration* 2001; 246 :403-417
- [7] **Ni YQ, Liu HJ, Ko JM**, "Experimental investigation on seismic response control of adjacent buildings using semi-active MR dampers." *In SPIE's 9th Annual International Symposium* 2002: 334-344.
- [8] **Bharti SD, Dumne SM, Shrimali MK**, "Seismic response analysis of adjacent buildings connected with MR dampers", *Engineering Structures* 2010; 32: 2122-2133.

- [9] **Mehmet E, Muhammad NS**, "Optimal design of semi-active control for adjacent buildings connected by MR damper based on integrated fuzzy logic and multi-objective genetic algorithm", *Engineering structures* 2014; 69: 135-148.
- [10] **Patel C, Jangid R**, "Dynamic response of identical adjacent structures connected by viscous damper" *Structural Control Health Monitoring* 2014; 21: 205-224.
- [11] **Yang ZD, Lam SS**, "Dynamic responses of two buildings connected by viscoelastic dampers under bidirectional earthquake excitations", *Earthquake Engineering and Engineering Vibration* 2014; 13: 137-150.
- [12] **Yang G**, "Large-scale Magneto-rheological Fluid Damper for vibration mitigation: Modeling, Testing and Control", *Thesis, University of Notre Dame* 2001.
- [13] **Christenson RE, Spencer BF, Hori N, Seto K**, "Coupled building control using acceleration feedback ", *Computer aided Civil and infrastructure Engineering* 2003; 18: 4-18.
- [14] **Smith RJ, Willford MR**, "The damped outrigger concept for tall buildings", *The Structural Design of Tall Special Buildings* 2007; 16: 501-517.
- [15] **Asai T, Chang CM, Phillips BM, Spencer BF**, "Real-time hybrid simulation of a smart outrigger damping system for high-rise buildings", *Engineering Structures* 2013; 57: 177-188.
- [16] **Cheng MH, Muhammad NS**, " Simulating building motions using the ratios of its natural frequencies and a Timoshenko beam model", *Earthquake Spectra* 2015; 31: 403-420.
- [17] **Hong H, Zhang SE**, "Spatial ground motion effect on relative displacement of adjacent building structures", *Earthquake Engineering and Structural Dynamics* 1999; 28: 333-349.

- [18] **Seto K, Toba Y, Matsumoto Y**, "Reduced order modeling and vibration control methods for flexible structures arranged in parallel", *American Control Conference, Proceeding of the 1995. IEEE* :2344-2348.
- [19] **Richardson A, Walsh KK, Abdullah MM**, "Closed form equations for coupling linear structures using stiffness and damping elements", *Structural Control and Health Monitoring* 2013; 20: 259-281.
- [20] **Ping T, Chuangjie F, Fulin Z**, "Dynamic characteristics of a novel damped outrigger system. *Earthquake Engineering and Engineering Vibration* 2014; 13: 293-304.
- [21] **Chen Y, McFarland DM, Wang Z, Spencer BE, Bergman LA**, " Analysis of Tall Buildings with Damped Outriggers", *Journal of Structural Engineering* 2010; 136: 1435-1443.
- [22] **Deng K, Pan P, Lom A**, "A simplified model for analysis of high rise buildings equipped with hysteresis damped outrigger", *The Structural Design of tall and Special Buildings* 2013.
- [23] **Lee J, Bang M, Kim JY**, "An analytical Model for high-rise wall-frame structures with outriggers." *The Structural Design of Tall and Special Buildings*. 2008; 17: 839-851.
- [24] **Seon MH, Haym B, Timothy W** , "Dynamics of Transversely Vibrating Beams Using four Engineering Theories", *Journal of Sound and vibration* 1999;225: 935-988.
- [25] **Nana BR** "Amplitude control on hinged-hinged beam using piezoelectric absorber: Analytical and numerical explanation", *International Journal of Non-Linear Mechanics* 2009; 44: 704-708.
- [26] **Nana BR, Wofo P**, "Modeling and Optimal Active Control with Delay of the Dynamics of a Strongly Nonlinear Beam " *Journal of Advanced Research in Dynamical and Control Systems* 2009: 57-74.

- [27] **Kitio CA, Nana BR, Wofo P**, " Optimization of electromechanical control of beam dynamics: Analytical method and finite differences simulation" *Journal of Sound and Vibration* 2006 298: 180-193.
- [28] **Bhashyam G.R, Prathap G**, "The second frequency spectrum of Timoshenko beams", *Journal of Sound and Vibration* 1981; 76: 407-420.
- [29] **Mosaad AF**, "Influence of shear deformation and rotary inertia on non-linear free vibration of a beam with pinned ends", *Computers and Structures* 1999;71: 663-670.
- [30] **Han MS, Benaroya H, Wei T**, "Dynamics of transversely vibrating beams using four engineering theories." *Journal of Sound and Vibration* 1999; 225: 935-988.
- [31] **Kausel E**, "Nonclassical Modes of Unrestrained Shear Beams" *Journal of Engineering Mechanics* 2002; 128:663-667.
- [32] **Challamel N**, "On the Comparison of Timoshenko and Shear Models in Beam Dynamics" *Journal of Engineering Mechanics* 2006;132:1141-1145.
- [33] **Timoshenko SP**, "On the correction factor for shear of the differential equation for transverse vibrations of bars of uniform cross section" *Philosophical Magazine* 1921;41: 744-746.
- [34] **Hutchinson JR**, "Shear Coefficients for Timoshenko Beam Theory", *Journal of Applied Mechanics* 2001; 68:87-92
- [35] **Bruch JC, Mitchell TP**, "Vibrations of a Mass-Loaded Clamped-Free Timoshenko Beam ", *Journal of Sound and Vibration* 1987; 114: 341-345.
- [36] **Cowper**, "The Shear Coefficient in Timoshenko's Beam Theory", *Journal of Applied Mechanics* 1966; 33: 335-340
- [37] **Xie J, Wen Z**, "A measure of drift demand for earthquake ground motions based on Timoshenko beam model", *In the 14th world conference on earthquake engineering, Beijing* 2008.

- [38] **Aly AM**, "Vibration control of buildings using magnetorheological damper: a new control algorithm", *Journal of Engineering* 2013.
- [39] **Preumont A, Seto K**, "Active control of structures" *John Wiley and Sons,Ltd* 2008.
- [40] **Soong TT, Spencer BF** "Active, Semi-Active and Hybrid Control of Structures" *Conference 12WCEE*, 2000.
- [41] **Michalopoulos A, Stavroulakis GE, Zacharenakiss EC, Panagiotopoulos PD**, "A prestressed tendon based passive control system for bridges", *Computers and Structures* 1997; 63: 1165-1175.
- [42] **Saaed TE, George Nikolakopoulos G, Jonasson JE, Hedlund H**, "A state-of-the-art review of structural control systems" *Journal of Vibration and Control* 2013.
- [43] <https://pubs.usgs.gov/fs/2005/3052/>.
- [44] <https://underamexicansky.com/2013/05/23/cultural-event-part-1-tour-of-parliament-and-the-beehive/>
- [45] **Aldemir U, Yanik A, Bakioglu M** "Control of Structural Response Under Earthquake Excitation", *Computer-Aided Civil and Infrastructure Engineering* 2012; 27: 620-638.
- [46] **Mrabet E** "Optimisation de la fiabilité des structures contrôlées", *These Ecole Centrale de lyon* 2016.
- [47] <https://buildcivil.wordpress.com/2013/11/25/passive-energy-dissipation-devices/>
- [48] **Boore M**, "Stochastic simulation of high-frequency ground motions based on Seismological models of the radiated spectra ", *Bulletin of the Seismological Society of America* 1983; 73: 1865-1894.
- [49] **Saragoni R and HART G**, "Simulation of artificial earthquakes", *Earthquake Engineering and Structural Dynamics* 1974; 2: 249-267

- [50] <https://www.boredpanda.com/italy-earthquake-before-after/>
- [51] <http://www.rtmd.lehigh.edu/projects/advanced-damping-systems>.
- [52] **Housner GW, Bergman LA, Caughey TK, Chassiakos AG, Claus RO, Masri SF, Skelton RE, Soong TT, B.F Spencer BF, Yao JT** "Structural Control: Past, Present, and Future", *Journal of Engineering Mechnaics* 1997; 123: 897-971.
- [53] **Nguyen SD, Choi SB** "A new neuro-fuzzy training algorithm for identifying dynamic characteristics of smart dampers" *Smart Materials and Structures* 21 (2012).
- [54] **Tan P, Fang CJ, Tu WR, Zhou FL, Wang Y, Jiang M**, "Experimental study on the outrigger damping system for high-rise building", *Proceeding of the 15th World Conference on Earthquake Engineering* 2012.
- [55] **Christenson ER, Spencer BF, Johnson EA, Seto K**, "Coupled building control considering the effects of building/connector configuration", *Journal of Structural Engineering* 2006; 132:853-863.
- [56] **Cimellaro GP, Lopez GD**, "Algorithm for design of controlled motion of adjacent structures." *Structural Control and Health Monitoring* 2011; 18: 140-148.
- [57] **Roh H, Cimellaro GP, Lopez GD**, "Seismic response of adjacent steel structures connected by passive device", *Advances in Structural Engineering* 2011; 4: 499-517.
- [58] **Zhang WS, XU YL**, "Dynamic characteristics and seismic response of adjacent buildings linked by discrete dampers", *Earthquake Engineering and Structural Dynamics* 1999; 28: 1163-1185.
- [59] **Matsagar VA, Jangid RS**, "Viscoelastic damper connected to adjacent structures involving seismic isolation" *Journal of Civil Engineering and Management* 2005; 11: 309-322.

- [60] **Tubaldi E, Barbato M, Dall'Asta A,** " Stochastic seismic response analysis of adjacent buildings coupled by nonlinear viscous dampers", *Proceedings of the 9th International Conference on Structural Dynamics, EURO-DYN* 2014.
- [61] **Park HS, Lee'S, Choi SW, Kwan B, Cho T, Kim Y,** "Genetic-algorithm-based minimum weight design of an outrigger system." *Engineering structure* 2016; 117: 496-505.
- [62] **Chen WF, Scawthorn** "Earthquake Engineering" *Handbook*
- [63] Chang CM, Wang Z, Spencer BF, Chen Z, "Semi-active damped outriggers for seismic protection of high-rise buildings", *Smart Structures and Systems* 2013; 11: 435-451.
- [64] **Basili M, Angelis M,** "Optimal passive control of adjacent structures interconnected with nonlinear hysteretic devices", *Journal of Sound and Vibration* 2007;301: 106-125.
- [65] **Zhu H, Wen Y, Iemura H,** "A study on interaction control for seismic response of parallel structures", *Computers and Structures* 2001; 79: 231-242.
- [66] **Bharti SD, Dumne SM, Shrimali MK,** "Earthquake response of asymmetric building with MR damper", *Earthquake Engineering and Engineering Vibration* 2014; 13: 305-316.
- [67] **Chang CM., Asai T, Wang Z, Spencer BF, Chen Z,** " Smart outriggers for seismic protection of high-rise buildings." *Proceedings of the 15th WCEE* 2012.
- [68] **Kappos A,** "Dynamic loading and design of structures". *CRC Press* 2001.
- [69] www.yourarticlelibrary.com/earthquake/earthquakes-definition-causes-measures-and-other-details-with-diagram/31854
- [70] **K. Kumar,** "Basic Geotechnical Earthquake Engineering", *New Age International*.

- [71] **Chang TP**, "Deterministic and random vibration of an axially loaded Timoshenko beam resting on an elastic foundation", *Journal of Sound and Vibration* 1994; 178: 55-66.
- [72] **Basili M, M. Angelis M**, "Optimal passive control of adjacent structures interconnected with nonlinear hysteretic devices", *Journal of Sound and Vibration* 2007; 301: 106-125.
- [73] **Bhaskararao A, Jangid R**, "Seismic Analysis of structures connected with friction dampers", *Engineering Structures* 2006; 28 : 690-703.
- [74] **Sivanandam SN, Sumathi S, Deepa SN**, "Introduction to Fuzzy Logic using MATLAB", *Springer* 2006
- [75] **Choi YT, Wereley NM**, "Comparative analysis of the time response of electrorheological and magnetorheological dampers using nondimensional parameters" *Journal of Intelligent Material Systems and Structures* 2002; 13(7-8): 443-451.
- [76] **Nazmul S, Hojjat A**, "Computational Intelligence Synergies of Fuzzy Logic, Neural Networks and Evolutionary Computing" *Wiley* 2013.
- [77] **RJ, Jyh-Shing** "ANFIS: Adaptive-Network-Based Fuzzy Inference System" *IEEE Transactions ON Systems, Man, AND Cybernetics*(1993) 23:665-685.
- [78] '<http://www.vibrationdata.com/elcentro.htm>'
- [79] '<http://instruct.uwo.ca/earth-sci/240a/D4.JPG>'
- [80] **Kasdin NJ**, "Runge-Kutta Algorithm for the Numerical Integration of Stochastic Differential Equations", *Journal of Guidance Control and Dynamics* 1995; 18: 114-120.
- [81] **Ahmadi G**, "Earthquake Response of Linear Continuous Systems", *Nuclear Engineering and Design* 1978; 50: 327-345.

- [82] **Jung HJ, Spencer BF, Lee IW**, "Control of seismically excited cable-stayed bridge employing magnetorheological fluid dampers", *Journal of Structural Engineering* 2003; 129: 873-883.
- [83] **Spencer BF, Nagarajaiah S**, "State of the Art of Structural Control", *Journal of Structural Engineering* 2003; 129: 845-856.
- [84] **Kahan MM**, "Approches Stochastiques pour le Calcul des Ponts aux Seisme", *These de Doctorat de l'Ecole Nationale des ponts et Chaussées*.
- [85] **Dorka UE**, "Introduction to Earthquake Engineering" *Univeristy of Kas-sel* October 2014.
- [86] **Jansen LM, Dyke SJ**, "Semiactive Control Strategies for MR dampers: Comparative study", *Journal of Engineering Mechanics* 2000; 126:795-803.
- [87] **Jennings PC, Housner GW, Tsai NC**, "Simulated earthquake motions", 1968.
- [88] **Graney L, Richardson AA**, "The numerical solution of non-linear partial differential equations by the method of lines", *Journal of Computational and Applied Mathematics* 1981; 7: 229-236.
- [89] **Rofooei FR, Mobarake A, Ahmadi G**, "Generation of artificial earthquake records with a nonstationary Kanai-Tajimi model", *Engineering Structures* 2001; 33: 827-837.
- [90] **Abbas AM**, "Critical seismic load inputs for simple inelastic structures", *Journal of Sound and Vibration* (2006) ;296: 949-967.
- [91] **Spencer BF, Dyke SJ, Sain MK, Carlson JD**, "Phenomenological model for magnetorheological dampers." *Journal of Engineering Mechanics* 1997; 123:230-238.
- [92] **Abbas AM, Takewaki I**, " Response of nonlinear single-degree-of-freedom structures to random acceleration sequences", *Engineering Structures* 2011; 33: 1251-1258.

- [93] **Kung SY, Pecknold DA**, "Effect of ground motion characteristics on the seismic response of torsionally coupled elastic systems", *Thesis, University of Illinois at Urbana-Champaign Urbana, Illinois* (1982).
- [94] **Ahmadi G, Fan FG**, "Nonstationary Kanai-Tajimi models for El Centro 1940 and Mexico City 1985 earthquake", *Probabilistic Engineering Mechanics* 1990; 5: 171-81.
- [95] **Capra A, Davidovici V**, "Calcul Dynamique des Structures en Zone Sismique", *Eyrolle* 1980.
- [96] **Bhushan PB**, "Advanced Soil Dynamics and Earthquake Engineering", PHI Learning Pvt. Ltd (2011).
- [97] **Abramovieh HH, Elishakoff I**, "Application of the Krein's Method for Determination of Natural Frequencies of Periodically Supported Beam Based on Simplified Bresse-Timoshenko Equations" *Acta Mechanica* 1987; 66: 39-59.
- [98] **Amirouche FML, Tajiri GC, Valco MJ**, "Mathematical model of a time and position variant external load on a gear tooth using the modified Timoshenko beam equation", *International Journal for Numerical Methods in Engineering* 1996; 39: 2073-2094.
- [99] **Hijmissen JW, Van Horssen WT**, "On transverse vibrations of a vertical Timoshenko beam", *Journal of Sound and Vibration* 2008; 314: 161-179.
- [100] **Lee S., Koo J., Choi J**, "Variational formulation for Timoshenko beam element by separation of deformation mode", *International Journal for Numerical Methods in Biomedical Engineering* 1994; 10: 599-610.
- [101] **Kloedon PE, Platen E., Schurz H**, "Numerical Solution of SDE through computer experiments", Springer.
- [102] **Christenson ER, Spencer BF, Johnson EA**, "Semiactive connected control method for adjacent multidegree-of-freedom buildings", *Journal of Engineering Mechanics* 2007; 133: 290-298.

- [103] **Cundumi O**, "Numerical investigation of a variable damping semiactive device for the mitigation of the seismic response of Adjacent Structures", *Computer-Aided Civil Infrastructure Engineering* 2008; 23: 291-308.
- [104] **Ikhouane F, Manosa V, Rodellar J**, "Adaptive control of hysteretic structural system", *Automatica* 2005; 41: 225-231.
- [105] **Ndemanou BP, Metsebo J, Nana NBR, Wofo P** "Dynamics and magneto-rheological control of vibration of cantilever Timoshenko beam under earthquake loads", *Nonlinear Dynamics* 2014; 78: 163-171.
- [106] **Luco JE, Barros CP**, "Optimal damping between two adjacent elastic structures", *Earthquake Engineering and Structural Dynamics* 1998; 27: 649-659.
- [107] **Tubaldi E**, "Dynamic behavior of adjacent buildings connected by linear viscous/viscoelastic dampers", *Structural Control and Health Monitoring* 2015.
- [108] **Tse KT, Song J**, "Modal analysis of a linked cantilever flexible building system", *Journal of Structural Engineering* 2015; 141.
- [109] **Erkus B, Abe M, Fujino Y**. "Investigation of semi-active control for seismic protection of elevated highway bridges", *Engineering Structures* 2002; 24: 281-293.
- [110] **Jung HJ, Spencer BF, Lee IW**, "Control of Seismically Excited Cable-Stayed Bridge Employing Magnetorheological Fluid Dampers", *Journal of Structural Engineering* 2003; 129: 873-883.
- [111] **Miranda E**, "Approximate seismic lateral deformation demands in multistory buildings", *Journal of Structural Engineering* 1999; 125:417-425.

- [112] **Jung HJ, Spencer BF, Lee IW**, "Control of Seismically Excited Cable-Stayed Bridge Employing Magnetorheological Fluid Dampers", *Journal of Structural Engineering* 2003; 129: 873-883.
- [113] **Laura M, Dyke SJ**, "Semiactive control strategies for MR dampers: comparative study", *Journal of Engineering Mechanics* 2000; 126: 795-803.
- [114] **Dyke S., Spencer BF, Sain M., Carlson J**, " Modeling and control of magneto rheological dampers for seismic response reduction", *Smart Materials and Structures* 1996; 5: 565-575
- [115] **Lin YK, Yong Y**, "Evolutionary kanai-tajimi earthquake models", *Journal of engineering mechanics* 1987; 113: 1119-1137.
- [116] **Wanga Z, Chang CM, Spencer BF, Chen Z**, "Controllable outrigger damping system for high rise building with MR dampers", *Proceeding of SPIE* 2010; 7647.

List of Publications

Published in international journals

1. **B. P. Ndemanou**, J. Metsebo B. R. Nana Nbandjo P. Wofo, "Dynamics and magneto-rheological control of vibration of cantilever Timoshenko beam under earthquake loads", *Nonlinear Dynamics*. (2014) 78:163-171.
2. **B. P. Ndemanou**, B. R. Nana Nbandjo, U. Dorka , "Quenching of vibration modes on two interconnected buildings subjected to seismic loads using magneto rheological device", *Mechanics Research Communications*. (2016) 78: 6-12.
3. **B. P. Ndemanou**, E.R. Fankem, B. R. Nana Nbandjo "Reduction of vibration on a Cantilever Timoshenko beam subjected to repeated sequence of excitation with Magnetorheological Outriggers", *The Structural Design of Tall and Special Buildings*. (2017); e1393.

Dynamics and magneto-rheological control of vibration of cantilever Timoshenko beam under earthquake loads

B. P. Ndemanou · J. Metsebo ·
B. R. Nana Nbandjo · P. Wofo

Received: 29 January 2014 / Accepted: 23 April 2014 / Published online: 16 May 2014
© Springer Science+Business Media Dordrecht 2014

Abstract The problem of minimizing the dynamics response of a damped cantilever Timoshenko beam subjected to earthquake excitation is investigated in this paper. The ground acceleration is expressed in terms of a Fourier series that is modulated by an enveloping function. The method of lines and modal approach are developed for analyzing the eigenvalues and the flexural vibrations. A magneto rheological damper is proposed to reduce the vibration of the structure. The device is localized at a specific point of the beam. A modal shape which characterizes the vibration of the uncontrolled and controlled system is obtained. The condition of stability of the controlled system is derived using the Routh–Hurwitz criterion.

Keywords Cantilever Timoshenko beam · MR damper · Earthquake excitation · Method of lines · Routh–Hurwitz criterion

1 Introduction

In the early of the 20th century, the importance of shear deformation and rotational inertia effects in the dynamics of elastic beams was first demonstrated by Timoshenko [15]. The model is suitable for describing the behavior of short beams, sandwich composite beams, or beams subject to high-frequency excitation when the wavelength approaches the thickness of the beam. Therefore, much attention has been devoted to their dynamic behavior under various excitations [4, 8, 17]. The case of interest in this work is the beam where one boundary is clamped, while the other is free generally called cantilever beam subjected to earthquake loads. The dynamics of mechanical structures under earthquake excitation has focused the attention of several researchers [10, 12, 13]. Due to the complexity of earthquake ground excitation, these works are purely numerical and in some cases experimental and generally do not take into account the influence of shear deformation or rotational inertia.

In this paper, the mathematical model of earthquake loads presented by Abbas et al. [1, 2] is the case of study. He demonstrated that the earthquake loads can be modeled as a deterministic time history which is expressed in terms of Fourier series that is modulated by an enveloping function. With this approach, we were able to present some analytical manipulations in the aim of foreseeing or predicting some dynamic behaviors appearing in the structure due to earthquake. In view of protecting these mechanical structures, a magneto-

B. P. Ndemanou · J. Metsebo · B. R. N. Nbandjo (✉) ·
P. Wofo

Laboratory of Modelling and Simulation in Engineering
and Biomimetics and Prototypes, University of Yaoundé I,
P. O. Box 812, Yaoundé, Cameroon

Present Address:

B. R. N. Nbandjo
Max-Planck-Institut für Physik Komplexer Systeme,
Nöthnitzer Str. 38, 01187 Dresden, Germany
e-mail: nananbandjo@yahoo.com

rheological (MR) damper is used to control the vibration of the mentioned structure. In fact the MR damper is a device that is capable of generating forces necessary for control applications. The effectiveness of MR dampers for seismic protection of base-isolated structures has been shown in Refs. [5, 6, 14, 16, 18].

The organization of the paper will be the following: In sect. 2, an analytical and numerical solution is proposed to predict the dynamic response of the cantilever beam under earthquake loads. Section 3 deals with the application of MR dampers as control design on the previous mechanical structure, and then comes up with the condition for which the vibration is reduced along with the condition of stability of the controlled system. Section 4 is devoted to the conclusion.

2 General mathematical formalism

Consider a Timoshenko beam of length L , with density ρ . The bending vibration can be described by two variables depending on axial coordinate x and time t , namely, transverse displacement $y = y(x, t)$ and $\theta = \theta(x, t)$, the transverse rotation of the beam cross-section due to the bending moment.

The governing equations for the vibration of Timoshenko beam thus involve a system of two partial differential equations given by [3, 4, 8, 11]

$$\rho I \frac{\partial^2 \theta}{\partial t^2} + \alpha_2 \rho A \frac{\partial \theta}{\partial t} = EI \frac{\partial^2 \theta}{\partial x^2} + kGA \left(\frac{\partial y}{\partial x} - \theta \right) \tag{1a}$$

$$\rho A \frac{\partial^2 y}{\partial t^2} + \alpha_1 \rho A \frac{\partial y}{\partial t} = kGA \left(\frac{\partial^2 y}{\partial x^2} - \frac{\partial \theta}{\partial x} \right) + P(t), \tag{1b}$$

where E is the Young's modulus of elasticity of beam material, G is the shear modulus of the beam material, α_1 and α_2 are the linear viscous damping coefficients, A is the cross-sectional area of the beam, k is the effective area coefficient in shear, I is the area moment of inertia, and $P(t)$ is the external force.

Taking into account the following dimensionless variables

$$\begin{aligned} \theta^* &= \theta, & Y &= \frac{y}{L}, & X &= \frac{x}{L}, & \tau &= \frac{t}{T}, & T &= L \sqrt{\frac{\rho}{Gk}} \\ \alpha_2 &= \frac{I}{A} \alpha_1, & \lambda &= \alpha_1 T, & k_1 &= \frac{E}{kG}, \\ k_2 &= \frac{AL^2}{I}, & P_1(\tau) &= \frac{LP(t)}{kGA} \end{aligned}$$

Eqs.(1a)–(1b) are reduced to these sets of non-dimensional differential equations

$$\frac{\partial^2 \theta^*}{\partial \tau^2} + \lambda \frac{\partial \theta^*}{\partial \tau} = k_1 \frac{\partial^2 \theta^*}{\partial X^2} + k_2 \left(\frac{\partial Y}{\partial X} - \theta^* \right) \tag{2a}$$

$$\frac{\partial^2 Y}{\partial \tau^2} + \lambda \frac{\partial Y}{\partial \tau} = \left(\frac{\partial^2 Y}{\partial X^2} - \frac{\partial \theta^*}{\partial X} \right) + P_1(\tau) \tag{2b}$$

with the boundary conditions

$$\begin{aligned} Y(0, \tau) &= 0, & \theta^*(0, \tau) &= 0, \\ \frac{\partial \theta^*}{\partial X}(1, \tau) &= 0, & \frac{\partial Y}{\partial X}(1, \tau) - \theta^*(1, \tau) &= 0 \end{aligned}$$

The two expressions of Eq. (2) of motion for a Timoshenko beam are combined to formulate an equation for transverse deflection Y , in the form

$$\begin{aligned} \frac{\partial^4 Y}{\partial \tau^4} + 2\lambda \frac{\partial^3 Y}{\partial \tau^3} + (k_2 + \lambda^2) \frac{\partial^2 Y}{\partial \tau^2} - (1 + k_1) \frac{\partial^4 Y}{\partial X^2 \partial \tau^2} \\ - \lambda(1 + k_1) \frac{\partial^3 Y}{\partial X^2 \partial \tau} + \lambda k_2 \frac{\partial Y}{\partial \tau} + k_1 \frac{\partial^4 Y}{\partial X^4} \\ = k_2 P_1(\tau) + \lambda \dot{P}_1(\tau) + \ddot{P}_1(\tau) \end{aligned} \tag{3}$$

Eq. (3) is the general equation governing the transversal displacement of the damped Timoshenko beam

2.1 Derivation of the modal equation

To deal with the analytical analysis, we resort to an assumed mode expansion. Specifically, it is assumed that Y can be written as the finite sums

$$Y(X, \tau) = \sum_{n=1}^N \Phi_n(X) Q_n(\tau), \tag{4}$$

where $Q_n(\tau)$ is the unknown function of time at n th mode and $\Phi_n(X)$ is the solution of the eigenvalue problem obtained by solving Eqs. (1a) and (1b) without damping and excitation, and $\Phi_n(X)$ is given by

$$\begin{aligned} \Phi_n(X) &= (C_{1n} \cos(\delta_n X) + C_{2n} \sin(\delta_n X) \\ &+ C_{3n} \sinh(\varepsilon_n X) + C_{4n} \cosh(\varepsilon_n X)), \end{aligned} \tag{5}$$

where

C_{1n}, C_{2n}, C_{3n} , and C_{4n} are obtained as (using the beam boundary condition) [19]

$$C_{1n} = \frac{\cos(\delta_n) + \frac{(\varepsilon_n^2 + \mu \delta_n^2)}{(\delta_n^2 + \mu \varepsilon_n^2)} \cosh(\varepsilon_n)}{-\left(\sin(\delta_n) + \frac{\varepsilon_n}{\delta_n} \sinh(\varepsilon_n) \right)}; \quad C_{2n} = 1;$$

$$C_{3n} = -C_{1n} \frac{\left(\delta_n + \mu \frac{\varepsilon_n^2}{\delta_n}\right)}{\left(\varepsilon_n + \mu \frac{\delta_n^2}{\varepsilon_n}\right)}; \quad C_{4n} = -C_{2n}$$

The eigenvalues δ_n and ε_n of the n th mode are obtained from Eq. (6) and (7), using an appropriate algorithm

$$\left[\left(\delta_n^2 + \mu \varepsilon_n^2\right)^2 + \left(\mu \delta_n^2 + \varepsilon_n^2\right)^2 \right] \cos \delta_n \cosh \varepsilon_n - \left(\delta_n^2 + \mu \varepsilon_n^2\right) \left(\mu \delta_n^2 + \varepsilon_n^2\right) \left(-2 + \frac{\delta_n^2 - \varepsilon_n^2}{\delta_n \varepsilon_n} \sin \delta_n \sinh \varepsilon_n\right) = 0 \tag{6}$$

$$\left(\delta_n^2 - \varepsilon_n^2\right) \left[\eta^2 - \frac{1}{\mu + 1} \left(\delta_n^2 - \varepsilon_n^2\right)\right] - \left(1 + \frac{1}{\mu}\right) \delta_n^2 \varepsilon_n^2 = 0 \tag{7}$$

with

$$\eta = \sqrt{\frac{k_2}{k_1}}, \quad \mu = k_1.$$

Substituting Eq.(4) into Eq.(3), multiplying Eq.(3) by $\Phi_n(X)$ and integrating from 0 to 1, for the first mode of vibration ($n = 1$), we obtain the following modal equation

$$\ddot{Q}(\tau) + R_1 \ddot{Q}(\tau) + R_2 \dot{Q}(\tau) + R_3 Q(\tau) + R_4 Q(\tau) = R_5 P_1(\tau) + R_6 \dot{P}_1(\tau) + R_7 \ddot{P}_1(\tau) \tag{8}$$

with

$$R_1 = 2\lambda, \quad R_2 = k_2 + \lambda^2 - \frac{b_2}{b_1}(1 + k_1),$$

$$R_3 = \lambda k_2 - \lambda \frac{b_2}{b_1}(1 + k_1), \quad R_4 = \frac{b_3}{b_1} k_1,$$

$$R_5 = \frac{b_4}{b_1} k_2, \quad R_6 = \frac{b_4}{b_1} \lambda, \quad R_7 = \frac{b_4}{b_1}$$

and

$$b_1 = \int_0^1 \Phi^2(X) dX; \quad b_2 = \int_0^1 \Phi''(X) \Phi(X) dX;$$

$$b_3 = \int_0^1 \Phi'''(X) \Phi(X) dX; \quad b_4 = \int_0^1 \Phi(X) dX$$

The description of the transverse displacement of the mechanical structure can thus be derived by solving the differential Eq. (8).

2.2 Direct numerical simulation of the partial differential equation

To validate the analytical investigation, a direct numerical simulation of the partial differential Eq. (2) is explored. The method of lines [7] or semi-discretization is applied.

We set $\Delta X = 1/N$, $\tau = j \Delta \tau$, where ΔX and $\Delta \tau$ are the spatial and temporal steps, respectively, i and j are integer numbers relative to position and time, and N is the number of discrete points considered along the beam length.

The semi-discretization form of Eq. (2a) is

$$\begin{cases} \frac{d\theta_{i,j}^*}{dt} = F_1(\theta_{i,j}^1) \\ \frac{d\theta_{i,j}^1}{dt} = F_2(\theta_{i,j}^1, \theta_{i+1,j}^*, \theta_{i,j}, \theta_{i-1,j}^*, y_{i+1,j}, y_{i-1,j}) \end{cases} \tag{9}$$

and Eq. (2b) is

$$\begin{cases} \frac{dY_{i,j}}{dt} = F_3(Y_{i,j}^1) \\ \frac{dY_{i,j}^1}{dt} = F_4(Y_{i,j}^1, Y_{i+1,j}, Y_{i,j}, Y_{i-1,j}, \theta_{i+1,j}^*, \theta_{i-1,j}^*) + P_1(\tau_j). \end{cases} \tag{10}$$

The discretization of the boundary conditions leads to $\theta_{0,j}^* = 0$, $Y_{0,j} = 0$, $\theta_{n+1,j}^* = \theta_{n-1,j}^*$, $Y_{n+1,j} = Y_{n-1,j} + 2\Delta X \theta_{n,j}^*$

The excitation force is taken under the form

$$P(t) = -\rho A \ddot{u}_g(t) \tag{11}$$

According to [2], the ground acceleration $\ddot{u}_g(t)$ is assumed to be represented by

$$\ddot{u}_g(t) = e_0 \left(e^{-\beta_1 t} - e^{-\beta_2 t} \right) \sum_{n=1}^{N_f} (A_n \cos(\omega_n t) + B_n \sin(\omega_n t)) \tag{12}$$

This model is expressed in terms of a Fourier series that is modulated by an enveloping function. A_n and B_n are constants, ω_n is selected such that they span satisfactorily the frequency range (0.2, 25) Hz. β_1 and β_2 ($\beta_2 > \beta_1 > 0$) are parameters that impart the observed transient trends in the recorded ground motion. In our study, we assume that A_n and B_n are known. The function $P_1(\tau)$ can thus be given as

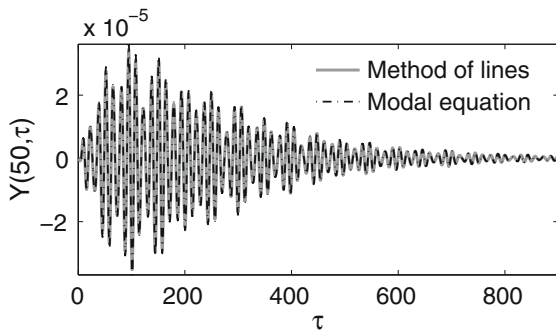


Fig. 1 Time history response of the relative displacement

$$P_1(\tau) = -e_0(e^{-\beta_{11}\tau} - e^{-\beta_{22}\tau}) \sum_{n=1}^{N_f} (A_{1n} \cos(\omega_{1n}\tau) + B_{1n} \sin(\omega_{1n}\tau)) \quad (13)$$

with

$$A_{1n} = \frac{\rho L}{kG} A_n, \quad B_{1n} = \frac{\rho L}{kG} B_n, \\ \beta_{11} = \beta_1 T, \quad \beta_{22} = \beta_2 T, \quad \omega_{1n} = \omega_n T$$

The geometric and material properties of the beam are $E = 3 \times 10^{10}$ Pa, $G = 1.25 \times 10^{10}$ Pa, $\rho = 2,500$ kgm⁻³, $A = 600$ m², $k = 0.8450704225$, $L = 80$ m, $I = 45 \times 10^3$ m⁴, $\nu = 0.2$, and this leads to $\delta_1 = 1.854172414231125$, $\varepsilon_1 = 1.725031549472968$ (we remind the reader that δ_1 and ε_1 have been obtained after solving the system of Eqs. (6) and (7) using Newton Raphson algorithm). Using the relation between the dimensional and the non-dimensional parameters which we obtained before, we derive the following dimensionless values for the parameters of Eq. (8)

$$b_1 = 1.111690369, \quad b_2 = 0.5504788466, \quad b_3 = 11.11863853, \quad b_4 = -0.8438165466, \quad k_1 = 2.84, \quad k_2 = 1.066666667, \quad \lambda = 0.5837807806, \quad R_1 = 1.167561561, \quad R_2 = 83.77266973, \quad R_3 = 48.70592206, \quad R_4 = 28.40443194, \quad R_5 = -64.77134340, \quad R_6 = -0.4431124853, \quad R_7 = -0.7590391804, \quad e_0 = 1.27, \quad \beta_{11} = 0.00507, \quad \beta_{22} = 0.0195, \quad \omega_{11} = 0.45, \quad \omega_{12} = 0.53, \quad \omega_{13} = 0.60 \text{ Hz}, \quad \omega_{14} = 0.59, \quad N_f = 4, \quad A_{11} = 1.344 \times 10^{-5}, \quad A_{12} = 1.231 \times 10^{-6}, \quad A_{13} = 4.733 \times 10^{-6}, \quad A_{14} = 1.136 \times 10^{-6}, \quad B_{11} = 4.733 \times 10^{-7}, \quad B_{12} = 1.041 \times 10^{-6}, \quad B_{13} = 2.84 \times 10^{-7}, \quad B_{14} = 2.840 \times 10^{-7}.$$

Setting ourself at a point $X = 0.5$ of the beam, we display in Figs. 1 and 2, respectively, the time history and frequency response curve obtained using the modal equation and the direct numerical simulation presented above. It appears that the two curves are closed mean-

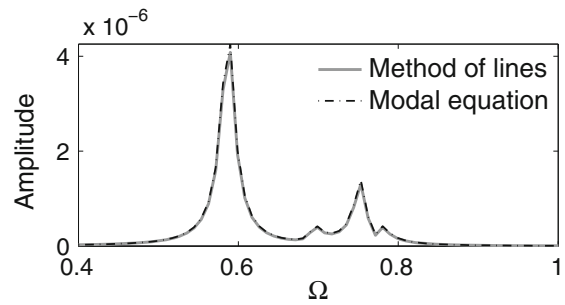


Fig. 2 Frequency response curve

ing that our analytical investigation is quantitatively and qualitatively good. Also having a look on the frequency response curve leads us to the conclusion that the dynamics of the system exhibits resonance and antiresonance along with subharmonic oscillations.

3 Semi-active control of the cantilever Timoshenko beam

3.1 Description of the control model

Since the vibration of the structure is fully predicted as shown in part 2, the next step is to minimize the dynamic deflection of the structure. For that aim, we define a set up so that the control of the beam is taken to be a transverse applied force or moment. A suitable way to reduce vibration in mechanical structures subjected to earthquake excitation is to use a semi-active control technique named magneto-rheological dampers (MR damper) [5,14]. The MR dampers are devices that are capable of generating the magnitude of forces necessary for full-scale application. Among these techniques, the modified Bouc–Wen model plays a key role. Spencer et al. [14] proposed a phenomenological model base on a Bouc–Wen model, by which the dynamic behavior of MR damper is described accurately (see Fig. 3). The equations governing the force predicted by this model are

$$f_{MR}(t) = c_1 \dot{y}_1 + K_1(y - y_0) \quad (14)$$

$$\dot{y}_1 = \frac{1}{(c_0 + c_1)} \{c_0 \dot{y} + \alpha z + K_0(y - y_1)\} \quad (15)$$

$$\dot{z} = (\dot{y} - \dot{y}_1)[A - |z|^m(\beta + \gamma \text{sgn}(z)\text{sgn}(\dot{y} - \dot{y}_1))], \quad (16)$$

where f_{MR} is the force generated by damper, y is the displacement of the damper, and y_1 is the internal dis-

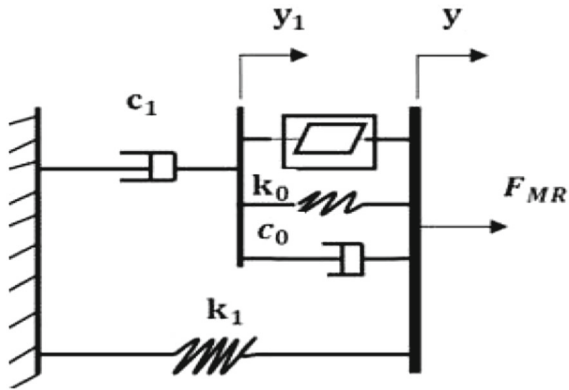


Fig. 3 Modified Bouc–Wen model

placement of the damper; K_1 is the accumulator stiffness ; y_0 is the initial displacement of the spring K_1 ; z is the evolutionary variable that describes the hysteretic behavior of the damper; α is the evolutionary coefficient; c_0 and c_1 control the viscous damping at large and low velocities, respectively; γ , β , n , and A are the shape parameters of the hysteresis loops, and K_0 represents the stiffness at large velocity.

The voltage-dependent parameters are modeled by

$$\alpha = \alpha(u) = \alpha_a + \alpha_b u, \quad c_1 = c_1(u) = c_{1a} + c_{1b} u, \quad c_0 = c_0(u) = c_{0a} + c_{0b} u \tag{17}$$

The command voltage is accounted for through the first-order filter

$$\dot{u} = -\eta(u - v), \tag{18}$$

where v is the voltage applied to the damper and η is a positive number that reflects the delay time of the damper.

Erkus et al. [6] gave the parameter of the model defined above based on a prototype model of the MR damper. We define the suitable control parameters knowing that the objective here is to have the values leading to the efficiency of the control according to the position of damper on the structure (see Table 1).

The parameters c_1 , c_0 , and α depend on the voltage.

3.2 Effect of the control on the dynamics responses

The structure under control is shown in Fig. 4, where the MR damper is fixed at a specific point of the cantilever beam. Therefore, the mathematical model of structure in the presence of the magneto-rheological damper is described by the following equations

Table 1 MR damper parameters

Parameter	Value	Parameter	Value
A	301	K_1 (N/m)	5 MF
β (m ⁻²)	363	γ (m ⁻²)	363
c_{0a} (N s/m)	2,100 MF	η (s ⁻¹)	190
c_{0b} (N s/mV)	350 MF	y_0 (m)	0
c_{1a} (N s/m)	28,300 MF	n_1	2
c_{1b} (N s/mV)	295,000 MF	K_0 (N/m)	46.90 MF
α_a (N/m)	14,000 MF	α_b (N/mV)	69,500 MF

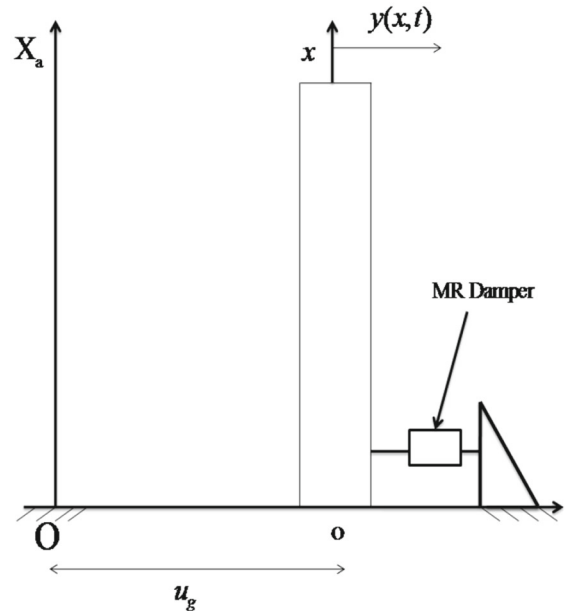


Fig. 4 Simplified model of the structure under control

$$\begin{aligned} \frac{\partial^4 Y}{\partial \tau^4} + 2\lambda \frac{\partial^3 Y}{\partial \tau^3} + (k_2 + \lambda^2) \frac{\partial^2 Y}{\partial \tau^2} - (1 + k_1) \frac{\partial^4 Y}{\partial X^2 \partial \tau^2} \\ - \lambda(1 + k_1) \frac{\partial^3 Y}{\partial X^2 \partial \tau} + \lambda k_2 \frac{\partial Y}{\partial \tau} \\ + k_1 \frac{\partial^4 Y}{\partial X^4} + \varepsilon F_{MR}(\tau) \delta(X - X_1) \\ = k_2 P_1(\tau) + \lambda \dot{P}_1(\tau) + \ddot{P}_1(\tau) \end{aligned} \tag{19}$$

with

$$F_{MR}(\tau) = \frac{kGT^4 f_{mr}(t)}{\rho^2 IL^2},$$

where $F_{MR}(\tau)$ is the dimensionless force exerted by the damper on the structure and $\delta(X - X_1)$ is the Dirac delta

function which indicates that the concentrated force is applied at the attachment point, $X = X_1$. The parameter ε allows here to have a general equation, i.e., for $\varepsilon = 0$, the structure is uncontrolled and for $\varepsilon = 1$, the structure is controlled.

The equations at first mode vibration are

$$\begin{aligned} \ddot{Q}(\tau) + R_1 \ddot{Q}(\tau) + R_2 \dot{Q}(\tau) + R_3 Q(\tau) + R_4 \dot{Q}(\tau) \\ + \varepsilon_1 F_{MR}(\tau) = R_5 P_1(\tau) + R_6 \dot{P}_1(\tau) + R_7 \ddot{P}_1(\tau) \end{aligned} \tag{20}$$

$$F_{MR} = a_1 \dot{Y}_1 + a_2 (\eta_2 - Y_0),$$

where Y_1 is governed by

$$\dot{Y}_1 = a_3 \dot{\eta}_2 + a_4 Z + a_5 (\eta_2 - Y_1) \tag{21}$$

$$\begin{aligned} \dot{Z} = \left(\dot{\eta}_2 - \dot{Y}_1 \right) \left[A - |Z|^{n_1} \right. \\ \left. \times \left(\beta_1 + \gamma_1 \text{sign}(Z) \text{sign}(\dot{\eta}_2 - \dot{Y}_1) \right) \right] \end{aligned} \tag{22}$$

$$\dot{U} = -\xi(U - V) \tag{23}$$

with the dimensionless parameters defined by

$$\begin{aligned} Z = \frac{z}{L}, \quad Y_1 = \frac{y_1}{L}, \quad Y_0 = \frac{y_0}{L}, \\ U = \frac{u}{V_1}, \quad V = \frac{v}{V_1}, \quad \varepsilon_1 = \frac{\varepsilon \Phi(X_1)}{b_1}, \end{aligned}$$

where V_1 is the reference voltage ($V_1 = 50$ Volt).

$$\begin{aligned} \eta_2 = Q(\tau) \Phi(X_1), \quad \dot{\eta}_2 = \dot{Q}(\tau) \Phi(X_1), \quad \gamma_1 = \gamma L^{n_1}, \\ \beta_1 = \beta L^{n_1}, \quad \xi = \eta T \end{aligned}$$

$$\begin{aligned} a_1 = a_1(U) = \frac{kGT^3 c_1}{\rho^2 IL}, \quad a_2 = \frac{kGT^4 K_1}{\rho^2 IL}, \\ a_3 = a_3(U) = \frac{c_0}{c_0 + c_1}, \quad a_4 = a_4(U) = \frac{\alpha T}{c_0 + c_1}, \\ a_5 = a_5(U) = \frac{K_0 T}{c_0 + c_1} \end{aligned}$$

with

$$\begin{aligned} \alpha = \alpha(U) = \alpha_a + \alpha_{b1} U, \quad c_1 = c_1(U) = c_{1a} + c_{1b1} U, \\ c_0 = c_0(U) = c_{0a} + c_{0b1} U \\ \alpha_{b1} = \alpha_b V_1, \quad c_{1b1} = c_{1b} V_1, \quad c_{0b1} = c_{0b} V_1 \end{aligned}$$

The damper performance of the structure subjected to a deterministic earthquake through the computer simulation is analyzed. The different values of the dimensionless parameters are

$$\begin{aligned} \beta_1 = 2323200, \quad \gamma_1 = 2323200, \quad \xi = 7.394556555, \\ \Phi(0.2) = -0.1741045662, \quad \Phi(0.25) = -0.2493107942, \\ \Phi(0.3) = -0.3349121633, \quad a_1 = (0.7832175921 \times 10^{-3} \\ + 0.4082141160 U) \text{MF}, \quad a_2 = 5.385481475 \times 10^{-9} \text{MF}, \\ a_3 = \frac{2100 + 17500 U}{30400 + 14767500 U}, \quad a_4 = \frac{546 + 135525 U}{30400 + 14767500 U}, \\ a_5 = \frac{1.825287907}{30400 + 14767500 U}. \end{aligned}$$

We have plotted in Figs. 5 and 6 the time histories to see the effects of voltage and position of the MR damper on the control process. Figure 5a shows the reduction of the amplitude of vibration of the structure at point $X_1 = 0.2$, which indicates the place where the concentrated force magneto-rheological damper is applied. The dimensionless voltage is $U = 0.39$. Figure 5b presents the effects the voltage on the control. We can notice that when the voltage amplitude is high, the amplitude of vibration is more and more reduced. For example, at $\tau = 240$, the amplitude in Fig. 5a is 2.012×10^{-5} and in Fig. 5b is 1.448×10^{-5} .

From Fig. 6a, b, we observe that the position of the attachment point of the damper is an important parameter for the optimization of the control process. In fact, Fig 6 shows us that the control is more and more efficient as the contact point between the control and the structure is far from the base. This means that the best implementation of the control design should locate the optimal point for the controller action.

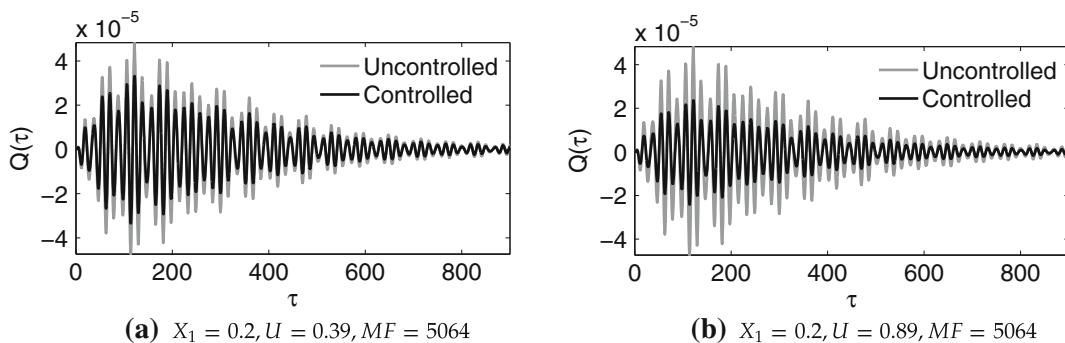


Fig. 5 Times histories: effects of the input voltage on the amplitude of vibration

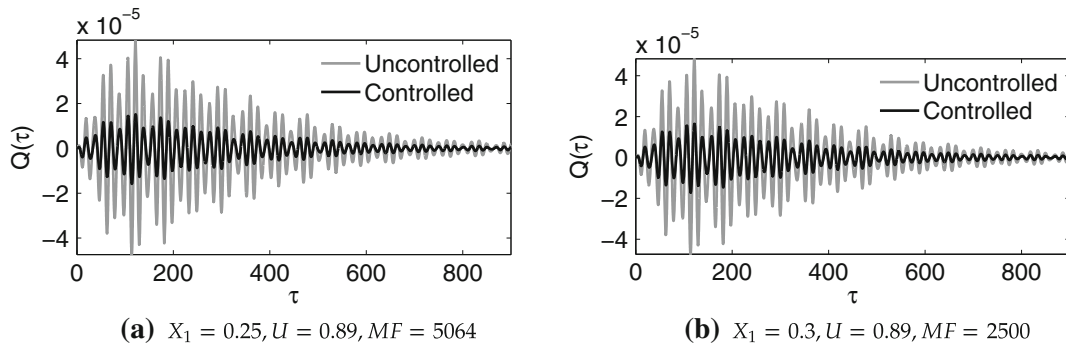


Fig. 6 Times histories: effect of the position of contact between the controller and the structure

3.3 Stability of semi-active structural control

One of the consequences when a device is added on a mechanical structure is that the fixed points position change. Thus, instead of reinforcing the stability of the structure, it can destabilize the system leading to premature destruction of the system. Therefore, it is important to address the stability condition when the system is perturbed by a control design. For that aim

Introducing the new variables $\chi_1, \chi_2, \chi_3, \chi_4, \chi_5, \chi_6,$ and χ_7 such that $\dot{Q} = \dot{\chi}_1 = \chi_2, \ddot{Q} = \ddot{\chi}_1 = \dot{\chi}_2 = \chi_3, \dddot{Q} = \dddot{\chi}_1 = \ddot{\chi}_2 = \dot{\chi}_3 = \chi_4, Y_1 = \chi_5, Z = \chi_6, U = \chi_7$

Eqs. (20, 21, 22, and 23) can then be rewritten as follows

$$\begin{cases} \dot{\chi}_1 = \chi_2 \\ \dot{\chi}_2 = \chi_3 \\ \dot{\chi}_3 = \chi_4 \\ \dot{\chi}_4 = -R_1\chi_4 - R_2\chi_3 - (R_3 + \varepsilon_1\varepsilon_2a_1a_3)\chi_2 \\ \quad - (R_4 + \varepsilon_1\varepsilon_2(a_1a_5 + a_2))\chi_1 + \varepsilon_1a_1a_5\chi_5 \\ \quad - \varepsilon_1a_1a_4\chi_6 + \varepsilon_1a_2Y_0 \\ \dot{\chi}_5 = a_3\varepsilon_2\chi_2 + a_4\chi_6 + a_5(\varepsilon_2\chi_1 - \chi_5) \\ \dot{\chi}_6 = (\varepsilon_2\chi_2 - a_3\varepsilon_2\chi_2 - a_4\chi_6 - a_5(\varepsilon_2\chi_1 - \chi_5)) \\ \quad [A - \chi_6^{n_1}(\beta_1 + \gamma_1\mu)] \\ \dot{\chi}_7 = -\xi(\chi_7 - V) \end{cases} \quad (24)$$

where $\varepsilon_2 = \Phi(X_1); a_1 = a_1(\chi_7); a_3 = a_3(\chi_7); a_4 = a_4(\chi_7); a_5 = a_5(\chi_7); \mu = \text{sign}(\chi_6) \text{sign}(\varepsilon_2\chi_2 - \chi_5)$

The general form of the equilibrium point is

$$P_f = \left(\chi_1 = \frac{\varepsilon_1a_2Y_0}{R_4 + \varepsilon_1\varepsilon_2a_2}, \chi_2 = 0, \chi_3 = 0, \chi_4 = 0, \chi_5 = \frac{\varepsilon_1\varepsilon_2a_2Y_0}{R_4 + \varepsilon_1\varepsilon_2a_2} + \frac{a_4(V)}{a_5(V)}\chi_6, \chi_6 = \chi_6, \chi_7 = V \right)$$

The characteristic equation is given as follows

$$\Lambda^7 + aa_1\Lambda^6 + aa_2\Lambda^5 + aa_3\Lambda^4 + aa_4\Lambda^3 + aa_5\Lambda^2 + aa_6\Lambda + aa_7 = 0 \quad (25)$$

In which

$$\begin{aligned} aa_1 &= \xi + R_1 + h_1(\chi_6, V); \\ aa_2 &= \xi R_1 + R_2 + (\xi + R_1) h_1(\chi_6, V) \\ aa_3 &= (\xi R_1 + R_2)h_1(\chi_6, V) + h_2(V) + \xi R_2 + R_3 \\ aa_4 &= \xi h_2(V) + h_1(\chi_6, V) (\xi R_2 + \varepsilon_1\varepsilon_2a_1(V)) \\ &\quad + R_1 + \varepsilon_1\varepsilon_2a_2 + \xi R_3 + R_3 \\ aa_5 &= \xi\varepsilon_1\varepsilon_2a_2 + h_1(\chi_6, V) \\ &\quad (\varepsilon_1\varepsilon_2(a_2 + \xi a_1(V)) + (R_1 + \xi R_3)) + \xi R_1 \\ aa_6 &= \xi(R_1 + \varepsilon_1\varepsilon_2a_2)h_1(\chi_6, V); \quad aa_7 = 0 \end{aligned}$$

where $h_1(\chi_6, V) = T \frac{(\alpha(V)g(\chi_6)+K_0)}{c_0(V)+c_1(V)}$ and $h_2(V) = \frac{\varepsilon_1\varepsilon_2a_1(V)c_0(V)}{c_0(V)+c_1(V)}$ with

$$g(\chi_6) = \begin{cases} A - \chi_6^{n_1}(\beta_1 + \gamma_1) & \text{if } \mu > 0 \\ A - \chi_6^{n_1}(\beta_1 - \gamma_1) & \text{if } \mu < 0 \end{cases} \quad (26)$$

χ_6 is an evolutionary variable that influences the vibration of the structure response. χ_6 has a finite ultimate value $\chi_{6\max}$, analytically this maximum can be found from Eq. (22), which leads to [9]

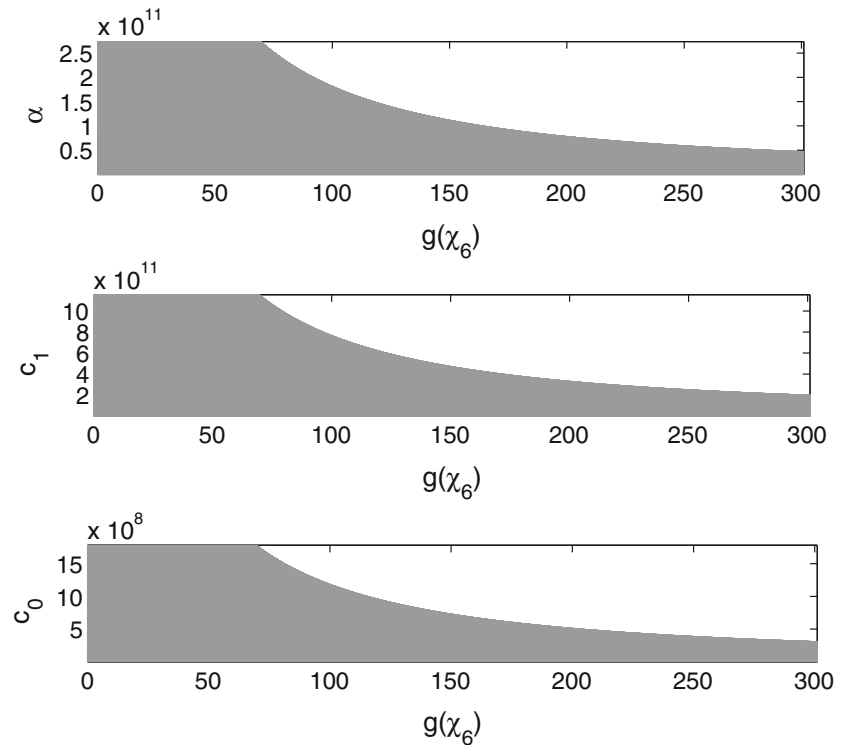
$$\chi_{6\max} = \left[\frac{A}{\gamma_1 + \beta_1} \right]^{\frac{1}{n_1}} \text{ thus } 0 \leq \chi_6 \leq \left[\frac{A}{\gamma_1 + \beta_1} \right]^{\frac{1}{n_1}},$$

(where n_1 is an even number).

Assuming that $0 < \frac{A}{\gamma_1 + \beta_1} < 1$, leads us to the following conclusion $0 \leq g(\chi_6) \leq A$.

From Eq. (25), we have $\Lambda_1 = 0$ the solutions are all constant. Since we are interested in the dynamics response, its remains to determine the other eigenvalues where the stability depends on the characteristic

Fig. 7 Stability diagram in the space parameters of control for $X_1 = 0.3$ and $U = 0.89$



equation below

$$\Lambda^6 + aa_1\Lambda^5 + aa_2\Lambda^4 + aa_3\Lambda^3 + aa_4\Lambda^2 + aa_5\Lambda + aa_6 = 0 \tag{27}$$

Now, using the Routh–Hurwitz criterion, the equilibrium point P_f is stable if and only if the following analytic relations are satisfied.

$$\begin{aligned} aa_i &> 0 \quad (i = 1, 2, 3, 4, 5, 6) \\ \Delta_3 &> 0 \\ \Delta_5 &> 0, \end{aligned} \tag{28}$$

where

$$\begin{aligned} \Delta_3 &= aa_1aa_2aa_3 - aa_3^2 - aa_1^2aa_4 + aa_1aa_5, \text{ and} \\ \Delta_5 &= aa_1aa_2aa_3aa_4aa_5 - aa_3^2aa_4aa_5 - aa_1^2aa_4^2aa_5 \\ &\quad - aa_1aa_2aa_3^2aa_5 + aa_2aa_3aa_4aa_5^2 + 2aa_1aa_4aa_5^2 - aa_3^3 \\ &\quad - aa_1aa_2aa_3^2aa_6 + aa_3^2aa_6^2 + aa_1^2aa_3aa_4aa_6 \\ &\quad + 2aa_1^2aa_2aa_5aa_6 - 3aa_1aa_3aa_5aa_6 - aa_1^3aa_6^2 \end{aligned}$$

From the relation (28), we deduce that the equilibrium point P_f is stable when the following condition is satisfied.

$$\begin{aligned} \chi_6^{n_1} &< \frac{A}{\beta_1 + \gamma_1} + \frac{(c_0(V) + c_1(V))(\xi + R_1)}{\alpha(V)T(\beta_1 + \gamma_1)} \\ &\quad + \frac{K_0}{\alpha(V)(\beta_1 + \gamma_1)} \end{aligned} \tag{29}$$

Figure 7 presents the region in the control space parameters. The shaded domains represent the regions for which the structural control strategy is always stable.

4 Conclusion

The dynamics response of a cantilever Timoshenko beam excited by earthquake loads has been investigated. By considering that the earthquake acceleration is expanded in term of a Fourier series, of unknown coefficients, that is modulated by an enveloping function; we were able to seek for the analytical solution using modal approach. The methods of lines were then used to solve the based equation using direct numerical simulation and also to confirm our analytical prediction. The magneto-rheological fluid damper appears to be a good candidate to suppress the vibration in a mechanical structure subjected to earthquake loads. The mathematical modeling of the structure under control has been presented along with the condition in the

space parameters of the system for which the vibration is reduced. Focusing on the stability, it appears that for a good choice of control gain parameters, the structures can remain stable even if the ground acceleration is high.

Acknowledgments Part of this work was completed during a research visit of Dr Nana Nbandjo at the Max Planck Institute for the Physics of Complex Systems (MPIPKS) at Dresden, Germany. I am grateful to Prof. Dr. Ing. Uwe Dorka from Kassel University for proposing this problem. The Humboldt foundation is thanked for financial support.

References

1. Abbas, A.M., Manohar, C.: Investigations into critical earthquake load models within deterministic and probabilistic frameworks. *Earthq. Eng. Str. Dyn.* **31**, 813–832 (2002)
2. Abbas, A.M.: Critical seismic load inputs for simple inelastic structures. *J. Sound Vib.* **296**, 949–967 (2006)
3. Amirouche, F.M.L., Tajiri, G.C., Valco, M.J.: Mathematical model of a time and position variant external load on a gear tooth using the modified Timoshenko beam equation. *Int. J. Numer. Methods Eng.* **39**, 2073–2094 (1996)
4. Chang, T.P.: Deterministic and random vibration of an axially loaded Timoshenko beam resting on an elastic foundation. *J. Sound Vib.* **178**, 55–66 (1994)
5. Dyke, S., Spencer, B., Sain, M., Carlson, J.: Modeling and control of magneto rheological dampers for seismic response reduction. *Smart Mater. Str.* **5**, 565–575 (1996)
6. Erkus, B., Abe, M., Fujino, Y.: Investigation of semi-active control for seismic protection of elevated highway bridges. *Eng. Str.* **24**, 281–293 (2002)
7. Graney, L., Richardson, A.A.: The numerical solution of non-linear partial differential equations by the method of lines. *J. Comput. Appl. Math.* **229**, 229–236 (1981)
8. Hijmissen, J.W., Van Horssen, W.T.: On transverse vibrations of a vertical Timoshenko beam. *J. Sound Vib.* **314**, 161–179 (2008)
9. Ikhouane, F., Manosa, V., Rodellar, J.: Adaptive control of hysteretic structural system. *Automatica* **41**, 225–231 (2005)
10. Iyengar, R.N., Shinozuka, M.: Effect of self-weight and vertical acceleration on the behaviour of tall structures during Earthquake. *Earthq. Eng. Str. Dyn.* **1**, 69–78 (1972)
11. Lee, S., Koo, J., Choi, J.: Variational formulation for Timoshenko beam element by separation of deformation mode. *Commun. Numer. Methods Eng.* **10**, 599–610 (1994)
12. Mostaghel, N.: Stability of columns subjected to earthquake support motion. *Earthq. Eng. Str. Dyn.* **3**, 347–352 (1975)
13. Saha, S., Manohar, C.: Inverse reliability based structural design for system dependent critical earthquake loads. *Probab. Eng. Mech.* **20**, 19–31 (2005)
14. Spencer, B., Dyke, S., Sain, M., Carlson, J.: Phenomenological model for magneto-rheological dampers. *J. Eng. Mech.* **123**, 230–238 (1997)
15. Timoshenko, S.P.: On the correction factor for shear of the differential equation for transverse vibrations of bars of uniform cross section. *Philos. Mag.* **41**, 744–746 (1921)
16. Tsang, H., Su, R., Chandler, A.: Simplified inverse dynamics models for MR fluid dampers. *Eng. Str.* **28**, 327–341 (2006)
17. Van Rensburg, N.F.J.: Natural frequencies and modes of a Timoshenko beam. *Wave Motion* **44**, 58–69 (2006)
18. Wang, D.H., Liao, W.H.: Semiactive controllers for magneto-rheological fluid dampers. *J. Intell. Mater. Sys. Str.* **16**, 983–993 (2005)
19. Xie, J., Wen, Z.: A measure of drift demand for earthquake ground motions based on Timoshenko beam model. In the 14th World conference on earthquake engineering. Beijing, 12–17 October, 2008



Quenching of vibration modes on two interconnected buildings subjected to seismic loads using magneto rheological device



B.P. Ndemanou^a, B.R. Nana Nbandjo^{a,b,*}, U. Dorka^b

^a *Laboratory of Modelling and Simulation in Engineering, Biomimetism and Prototypes, Department of Physics, Faculty of Science, University of Yaoundé I, Cameroon*

^b *Steel and Composite Structures, University of Kassel, Germany*

ARTICLE INFO

Article history:

Received 22 July 2016

Received in revised form

27 September 2016

Accepted 4 October 2016

Available online 12 October 2016

Keywords:

Cantilever Timoshenko beam

MR damper

Lyapunov theory

Root mean square method

ABSTRACT

In this paper, we describe the statistical responses of two buildings subjected to the repeated sequence of excitation. The nonstationary random approach is employed to simulate seismic events. The cantilever Timoshenko beam approach is used to model each of buildings and therefore are connected via a magneto-rheological (MR) damper device. The Lyapunov approach is adopted to seek for a voltage leading to a good control. Root mean square value is considered to foresee the effect of the control device along with the position on the effectiveness of the strategy. The starting times for which the shock absorber become efficient is obtained numerically and presented at each mode.

© 2016 Elsevier Ltd. All rights reserved.

1. Introduction

Nowadays, excitation seismic in relation to those from strong winds and large waves, stays the one of most powerful and severe disturbances and has never ceased to create the damages on the engineering structures. The recent events that hit multiple countries such as Haiti in 2010, Japan in 2011, China in 2014 and in 2016, Nepal in 2015, and Equator in 2016, destroying human lives and leaving behind a weak economy. All of these testified the devastating look of that disaster. Exciting by those seismic loads, the mechanical structures such as tall buildings vibrate at the different modes, which can create some damages and to drive these ones to their destruction. In order to overcome those issues and strengthen the safety of such structures, many techniques have been performed by the researchers on that topic to mitigate the undesirable effects from that disaster [1–3]. The controlling devices employing these mitigation vibration methods are of varied nature, passives, actives and semi-actives. These ones, have been employed to control the seismic response of adjacent buildings. Zhu et al. [8] used controlled interactions between a primary structure and

an auxiliary structure to reduce the seismic response of the primary structure during earthquake excitation. In the same view [9,12,25,28,31,32] used the passive control strategies to reduce the dynamic response of adjacent buildings. To increase the performance, that is to say to suppress better the induced-vibration on the same type of mechanical structures [16,21] have employed the semi-active control approach. The studies on the adjacent buildings do not only limit within the academic framework, the application of coupling buildings well-known in the world are Petronas Towers in Malaysia, also known as the Petronas twin tower and the Triton square office complex in Japan. These structures are three buildings 155, 175, 195 m tall and are coupled by two 35 t active control actuators for wind and seismic protection [14].

Interest for this semi-active devices, is due by the way that these ones combine the best features of both passive as well as actives and require a low voltage that changes the system's physical properties. Christenson et al. [15] examined the effects of relative building height and coupling link location on the semi-active performance. Moreover the authors showed that semi-active control is able to achieve performance similar to the optimal passive control at a fraction of the required control device force.

Integrating the semi-active nature, the MR damper has the ability to change its properties to generate the variable force and require a low power to operate [26]. Considerable attention has been given to the MR damper by many authors to control buildings. Bharti et al. [10] studied the effectiveness of various seismic control devices for interconnecting two adjacent buildings for earthquake

* Corresponding author at: University of Yaoundé I, Faculty of Science, Department of Physics, Cameroon.

E-mail addresses: ndemanoupeggy@gmail.com, b.ndemanou@uy1.uninet.cm (B.P. Ndemanou), nananbandjo@yahoo.com (B.R. Nana Nbandjo), Uwe.dorka@uni-kassel.de (U. Dorka).

hazard mitigation. The authors found that the coupled building control using MR damper is very effective for seismic response reduction of both buildings. The effectiveness of that control device for seismic hazard mitigation of a plan asymmetric building studied in Ref. [11]. They explained MR damper-based control systems are effective in reducing the seismic response reduction varies with the characteristics of the earthquake ground motion.

All aforementioned studies on reduction of vibration of buildings only considered the approach of single or multi-degree of freedoms and other adopt the simple-flexure or shear deformations in neglecting the combination of both rotary inertia and shear effects to model the engineering structures. In additional way of these studies, the approach displays multi-modes by taking into account the neglected mentioned effects is adopted in this paper to model the mechanical structures. Afterwards of that, each building is considered as an equivalent continuum structure [22,29] which also takes into account the flexural deformation. The well-known model that combine the influence of these cited effects is the Timoshenko beam theory, which is employed in this case to model the buildings interconnected by a MR device. Based on the experimental data from this latter, Spencer et al. [27] proposed the phenomenological model that was numerically tractable and effectively portrays the behaviour of a MR damper. The authors used a least-squares optimization method to determine appropriate parameters for the analytical model. The illustrated work of this paper is based on a theoretical study, as it is difficult to have a MR damper with the obtained parameters experimentally, that will lead to the minimization of excessive vibration of mechanical structures. To avoid this drawback, Erkus et al. [17] proposed the suitable control parameters therefore the objective was to have the values leading to the efficiency of the control. This procedure is used in this paper in order to have an optimization control of buildings under the repeated non-stationary random loads. The mathematical model of this excitation in the case of this study has been presented by Abbas and Takewakib [4]. These authors mentioned ground acceleration of multiplied sequences could result in more damage to the structure than a single ordinary event. In this work, the considered earthquake loads acting on both buildings is unidirectional.

The objective of this work is to suppress the vibration mode induced by earthquake excitation on two interconnected buildings using a magneto-rheological shock absorber.

The organization of the paper will be detailed as follows. Firstly the mathematical model describing the dynamics behavior of the structural system equipped of a magneto-rheological under the repeated seismic load is presented. The nonstationary stochastic approach is used to characterize the nature of a real earthquake excitation. Secondly modal equations and the form of the state space of the mechanical system equipped of the control device are obtained. Thirdly, using Lyapunov function approach, the control law is define and used to guider the voltage, with the aims to attenuate the vibration is also presented. All these is illustrated through the numerical approach. Finally, the conclusion is presented.

2. Description of the system

The structural system is constituted of two cantilever beams (Bg_1) and (Bg_2). These ones are subjected to the same disturbance force denoted seismic load. At a located point of each tall building, is connected a semi-active controller dubbed MR damper, as illustrated in Fig. 1. This shock absorber generates the variable forces acting on the mechanical structures to safeguard them against undesirable vibrations. The control device is equipped of a moving piston head, which is fixed on the structure (Bg_2), another extremity of this device is embedded on the second structure (Bg_1), which

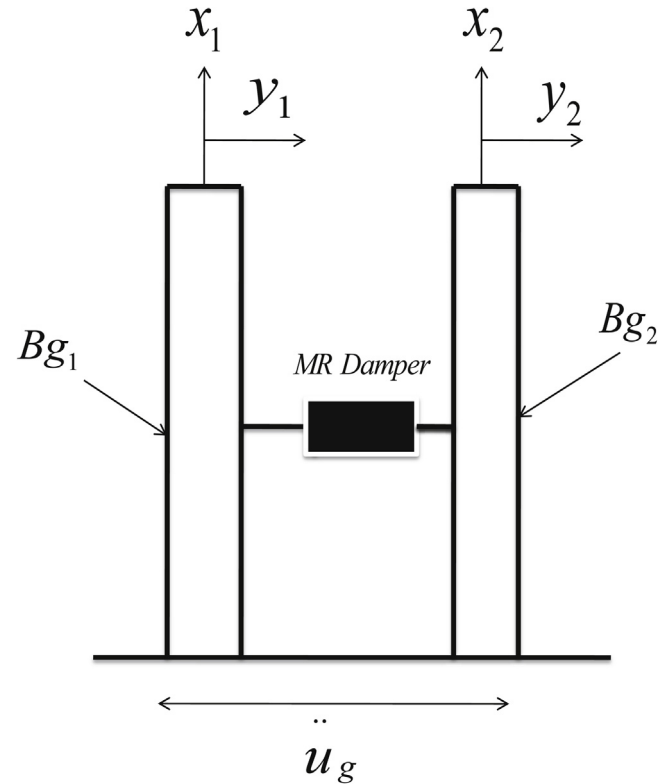


Fig. 1. Simplified model.

not only is subjected to earthquake excitation and at the same time play the role of support of the controller.

2.1. The mathematical modelling

Both buildings under investigation are modelled each like an continuum cantilever Timoshenko beam, where I_1 and I_2 are the moments of inertia of the cross-section; G_1 and G_2 are the shear modulus of elasticity, E_1 and E_2 are the Young's modulus; the mass per unit length are $m_1 = \rho_1 A_1$ and $m_2 = \rho_2 A_2$; k_s is the shear coefficient depending on the shape of the cross section of each beam and function of Young's modulus; $r_1 = (I_1/A_1)^2$ and $r_2 = (I_2/A_2)^2$ are the radius of gyration; $\delta(\cdot)$ denotes the Dirac function; c_a and c_b are the mechanical damping coefficients. f_d is the MR damper force which depend of the relative displacements and velocities of the structure. The subscript 1 and 2 denoted the beams Bg_1 and Bg_2 , respectively. Moreover the vibration amplitude of the structural system are described by $y_1 = y(x_1, t)$ and $y_2 = y(x_2, t)$, which depend on axial coordinate x_1 and x_2 and time, namely the relative traverse displacements.

In considering the Timoshenko model, which is governing by the differential partial equation. This implies that the equations of motion for both interconnected buildings by the magneto rheological damper under the earthquake excitation are given [6]

$$m_1 \frac{\partial^2 y_1}{\partial t^2} + c_a \frac{\partial y_1}{\partial t} + E_1 I_1 \frac{\partial^4 y_1}{\partial x_1^4} - m_1 r_1^2 \left(1 + \frac{E}{k_s G_1}\right) \times \frac{\partial^4 y_1}{\partial x_1^2 \partial t^2} = -m_1 \ddot{u}_g(t) + f_d(t) \delta(x_1 - x_3) \quad (1a)$$

$$m_2 \frac{\partial^2 y_2}{\partial t^2} + c_b \frac{\partial y_2}{\partial t} + E_2 I_2 \frac{\partial^4 y_2}{\partial x_2^4} - m_2 r_2^2 \left(1 + \frac{E_2}{k_s G_2}\right) \times \frac{\partial^4 y_2}{\partial x_2^2 \partial t^2} = -m_2 \ddot{u}_g(t) - f_d(t) \delta(x_2 - x_3) \quad (1b)$$

x_3 represents the located point of the MR device on Bg_1 and Bg_2 .

The nonstationary ground acceleration \ddot{u}_g adopted here, is the form of n sequences [4]. This random function is assumed to take the form of a filtered Gaussian stationary white noise modulated by a deterministic envelope function. This mentioned form describes the real earthquake that has the time-variation of both the intensity and frequency content. Expression of this term is defined as follows

$$\ddot{u}_g(t) = \begin{cases} e_1(t)\ddot{w}_1(t) & 0 \leq t \leq T_1 \\ 0 & T_1 \leq t \leq \sum_{i=1}^2 T_i \\ e_2 \left(t - \sum_{i=1}^2 T_i \right) \ddot{w}_2(t) & \sum_{i=1}^2 T_i \leq t \leq \sum_{i=1}^3 T_i \\ 0 & \sum_{i=1}^3 T_i \leq t \leq \sum_{i=1}^4 T_i \\ \dots & \dots \\ e_n \left(t - \sum_{i=1}^{n-1} T_i \right) \ddot{w}_n(t) & \sum_{i=1}^{n-1} T_i \leq t \leq \sum_{i=1}^n T_i \end{cases} \quad (2)$$

where $e_1(t)$, $e_2(t)$, ..., $e_n(t)$ are the envelope function associated with the acceleration sequences 1, 2, ..., n , $\ddot{w}_1(t)$, $\ddot{w}_2(t)$, ..., $\ddot{w}_n(t)$ are stationary random processes and T_1, T_2, \dots, T_{n+2} are the time durations of the acceleration sequences and T_2, T_4, \dots, T_{n+1} are the time intervals separating these sequences.

The envelope function for the i th sequence is expressed as

$$e_i(t) = e_{0i} \left(t - \sum_{i=1}^n T_i \right) \exp \left[-\alpha_i \left(t - \sum_{i=1}^n T_i \right) \right]; \quad (3)$$

$$\sum_{i=1}^{n+1} T_i \leq t \leq \sum_{i=1}^{n+2} T_i$$

where e_{0i} and α_i are $2n$ positive constants that control the intensity and the non-stationarity trend of the i th acceleration sequence. The taken spectral density of each sequence is defined by the Kanai Tajimi model given by

$$S_{\ddot{w}_i}(\omega) = s_0 \frac{\omega_g^4 + (2\zeta_g \omega_g \omega)^2}{(\omega_g^2 - \omega^2)^2 + (2\zeta_g \omega_g \omega)^2} \quad (4)$$

where s_0 is the intensity of the white noise process at the rock level, ω_g is the dominant frequency of the soil site and ζ_g is the associated damping ratio of the soil layer.

The equations governing the force f_d generated by the MR damper at the located point x_3 is expressed as follows

$$f_d = c_1(\dot{y} - \dot{y}_1(x_3, t)) + k_1 [(y_2(x_3, t) - y_1(x_3, t)) - y_0] \quad (5)$$

y is an internal displacement, governed by

$$\dot{y} = \frac{1}{c_0 + c_1} [\alpha z + c_0 \dot{y}_2(x_3, t) + c_1 \dot{y}_1(x_3, t) + k_0 (y_2(x_3, t) - y)] \quad (6)$$

$$\dot{z} = -\gamma |\dot{y}_2(x_3, t) - \dot{y}| |z|^{n-1} - \beta (\dot{y}_2(x_3, t) - \dot{y}) \times |z|^n + \delta_a (\dot{y}_2(x_3, t) - \dot{y}) \quad (7)$$

where c_0 and c_1 are the viscous damping at larger velocities and low velocities respectively; k_1 is the accumulator stiffness; k_0 represents the stiffness at large velocity; γ , β and δ_a are the shape parameters of the hysteresis loops.

In Eq. (6), some parameters depend on the command voltage u are given by

$$c_0 = c_{0a} + c_{0b}u, \quad c_1 = c_{1a} + c_{1b}u \quad \text{and} \quad \alpha = \alpha_a + \alpha_b u \quad (8)$$

where the command voltage u is accounted for through the first order filter

$$\dot{u} = \eta_p(u - v_c) \quad (9)$$

v_c is the voltage applied to current driver.

Introducing the dimensionless variables, these lead to following expressions.

$$Y_1 = \frac{y_1}{L}, \quad Y_2 = \frac{y_2}{L}, \quad Z = z, \quad Y = \frac{y}{L}, \quad \tau = \frac{t}{T}, \quad \kappa_1 = \frac{c_a T}{m_1},$$

$$\kappa_2 = \frac{c_b T}{m_2}, \quad a_1 = \frac{E_1 I_1 T^2}{L^4 m_1}, \quad a_2 = \frac{E_2 I_2 T^2}{L^4 m_2}, \quad a_3 = \frac{r_1^2}{L^2},$$

$$a_5 = \frac{E_1}{k_s G_1}, \quad a_4 = \frac{r_2^2}{L^2}, \quad a_6 = \frac{E_2}{k_s G_2}, \quad \ddot{y}_g(\tau) = \frac{\ddot{u}_g(t) T^2}{L}$$

$$F_d = \frac{f_d(t) T^2}{m_1 L^2}, \quad \mu = \frac{m_1}{m_2}, \quad \alpha_b = \frac{\alpha T}{(c_0 + c_1)}, \quad C_0 = \frac{c_0}{c_0 + c_1},$$

$$C_1 = \frac{c_1}{c_0 + c_1}, \quad K_0 = \frac{k_0 T}{c_0 + c_1}, \quad c_l = \frac{c_l T}{m_1 L}, \quad K_1 = \frac{k_1 T^2}{m_1 L},$$

$$\gamma_l = \gamma L^2, \quad \delta_l = \delta_a, \quad \beta_l = \beta L^2, \quad s_{01} = \frac{s_0}{S_0}, \quad \Omega = \omega T,$$

$$\Omega_g = \omega_g T, \quad T = L \sqrt{\frac{\rho}{k_s G_1}}, \quad \eta_T = \eta T, \quad U = \frac{u}{V_1}, \quad V_c = \frac{v_c}{V_1}$$

From the relation between variables and dimensionless parameters, the resulting relationships lead us to the below equations, which are illustrated as follows

$$\frac{\partial^2 Y_1}{\partial \tau^2} + \kappa_1 \frac{\partial Y_1}{\partial \tau} + a_1 \frac{\partial^4 Y_1}{\partial X_1^4} - a_3 (1 + a_5) \frac{\partial^4 Y_1}{\partial X_1^2 \partial \tau^2} = -\ddot{y}_g(\tau) + F_d(\tau) \delta(X_1 - X_3) \quad (10a)$$

$$\frac{\partial^2 Y_2}{\partial \tau^2} + \kappa_2 \frac{\partial Y_2}{\partial \tau} + a_2 \frac{\partial^4 Y_2}{\partial X_2^4} - a_4 (1 + a_6) \frac{\partial^4 Y_2}{\partial X_2^2 \partial \tau^2} = -\ddot{y}_g(\tau) - \mu F_d(\tau) \delta(X_2 - X_3) \quad (10b)$$

The dimensionless form of the magneto rheological damper force is given by

$$F_d(\tau) = c_l (\dot{Y} - \dot{Y}_1(X_3, \tau)) + K_1 (Y_2(X_3, \tau)) - K_1 (Y_1(X_3, \tau) + Y_0) \quad (11)$$

Y and Z are governed by the below equations

$$\dot{Y}(\tau) = \alpha_b Z + C_0 \dot{Y}_2(X_3, \tau) + C_1 \dot{Y}_1(X_3, \tau) + K_0 (Y_2(X_3, \tau) - Y) \quad (12)$$

$$\dot{Z}(\tau) = -\gamma_l |\dot{Y}_2(X_3, \tau) - \dot{Y}| |Z|^{n-1} - \beta_l \dot{Y}_2(X_3, \tau) + \beta_l \dot{Y} \times |Z|^n + \delta_l (\dot{Y}_2(X_3, \tau) - \dot{Y}) \quad (13)$$

The set of equations (10)–(13) is the dimensionless mathematical model which describe the dynamics behaviour of the structural system linked by a controller.

2.2. Modal equations

To reduce the partial differential equation to an set of ordinary differential equations. The general solutions of Y_1 and Y_2 can be written as separation variables of $\xi(\tau)$ and $\chi(\tau)$, which are the time dependent functions by the shape functions $\Phi_1(X_1)$ and $\Phi_2(X_2)$, respectively.

$$Y_1 = \sum_{i=1}^{n_m} \xi_i(\tau) \Phi_1^i(X_1), \quad Y_2 = \sum_{i=1}^{n_m} \chi_i(\tau) \Phi_2^i(X_2) \quad (14)$$

n_m is the total number of modes. The shape functions are written as

$$\begin{aligned} \Phi_1^i(X_1) &= (d_1^i \sin(\delta_1^i X_1) + \cos(\delta_1^i X_1) - d_3^i \sinh(\epsilon_1^i X_1) - \cosh(\epsilon_1^i X_1)); \\ \Phi_2^i(X_2) &= (d_{11}^i \sin(\delta_2^i X_2) + \cos(\delta_2^i X_2) - d_{33}^i \sinh(\epsilon_2^i X_2) - \cosh(\epsilon_2^i X_2)) \end{aligned} \quad (15)$$

the coefficients d_1^i, d_3^i, d_{11}^i and d_{33}^i are obtained by using the boundary conditions of the cantilever Timoshenko beam.

The eigenvalues $\delta_1^i, \delta_2^i, \epsilon_1^i$ and ϵ_2^i have the miscellaneous values at different modes of vibration. These parameters are obtained through an appropriate algorithm, for more details see [23].

In what follows, substituting the mode decomposition of equations (14) into (10), multiplying by the different spatial expression and integrating from 0 to 1, one obtain the modal forms of above equations, that are defined as follows

$$\ddot{\xi}_i(\tau) + \zeta_1^i \dot{\xi}_i(\tau) + \zeta_1^i \xi_i(\tau) = -\sigma_1^i \ddot{y}_g(\tau) + \epsilon_1^i F_d(\tau) \quad (16a)$$

$$\ddot{\chi}_i(\tau) + \zeta_2^i \dot{\chi}_i(\tau) + \zeta_2^i \chi_i(\tau) = -\sigma_2^i \ddot{y}_g(\tau) - \epsilon_2^i F_d(\tau) \quad (16b)$$

The dimensionless voltage U is given as

$$\dot{U} = -\eta_T(U - V_c) \quad (17)$$

Introducing the new variable, this leads us to yield the set of equations that are now be written as

$$\ddot{z}_1(\tau) + \zeta_1^i \dot{z}_1(\tau) + \zeta_1^i z_1(\tau) = -\sigma_1^i \ddot{y}_g(\tau) + \epsilon_1^i F_d(\tau) \quad (18a)$$

$$\ddot{z}_2(\tau) + \zeta_2^i \dot{z}_2(\tau) + \zeta_2^i z_2(\tau) = -\sigma_2^i \ddot{y}_g(\tau) - \epsilon_2^i F_d(\tau) \quad (18b)$$

with

$$F_d(\tau) = c_l(\dot{z}_2 - \dot{Y}_h - \dot{z}_1) + K_l(z_2 - z_1 - Y_0) \quad (19)$$

where Y

$$\dot{Y}_h(\tau) = -\alpha_b Z + (1 - C_0)\dot{z}_2 - C_1 \dot{z}_1 - K_0 Y_h \quad (20)$$

and Z is governed by

$$\dot{Z}(\tau) = \dot{Y}_h [\delta_a - |Z|^n (\beta_l + \gamma_l \text{sgn}(\dot{Y}_h) \text{sgn}(Z))] \quad (21)$$

This made transformation allows us now to rewrite the set of equations (16) under the form of the state space equation, therefore expression is given as

$$\dot{\mathbf{W}}(\tau) = \Sigma \mathbf{W}(\tau) + \mathbf{B} \ddot{y}_g + \mathbf{B}_1 F_d(\tau) \quad (22)$$

$$\mathbf{W} = \begin{bmatrix} z_1 \\ z_2 \\ \dot{z}_1 \\ \dot{z}_2 \end{bmatrix}, \quad \Sigma = \begin{bmatrix} 0 & 0 & 1 & 0 \\ 0 & 0 & 0 & 1 \\ -\zeta_1^i & 0 & -\zeta_1^i & 0 \\ 0 & -\zeta_2^i & 0 & -\zeta_2^i \end{bmatrix}$$

$$\mathbf{B} = \begin{bmatrix} 0 \\ 0 \\ -\sigma_1^i \\ -\sigma_2^i \end{bmatrix}, \quad \mathbf{B}_1 = \begin{bmatrix} 0 \\ 0 \\ \epsilon_1^i \\ -\epsilon_2^i \end{bmatrix}$$

It is observed on these equations, an independence of different modes exhibit by the mechanical structures. The dimensionless nonstationary acceleration ground can be expressed as Fig. 2 shows Kanai Tajimi filter with variation of the shape. This filter allows to have the stationary acceleration by passing white noise with the intensities $s_{01} = 0.02$ in Fig. 2(a) and 0.015 in Fig. 2(b), for that the reference intensity is $S_0 = 1 \text{ m}^2/\text{s}^3$. The used parameters are those of a medium soil site with $\eta_g = 0.04, \Omega_g = 0.09\pi$ and the number of acceleration sequences $n = 2$.

The dimensionless nonstationary ground acceleration for two sequences with the separating time interval both of them, is shown in Fig. 3. The associated frequency contents are (0–0.3) and (0–0.24), respectively. The parameters of the envelope function are taken as $\alpha_{11} = 0.009, \alpha_{12} = 0.0105, e_{11} = 0.0245$ and $e_{12} = 0.0285$. The geometric and material properties of beams Bg1 and Bg2 are

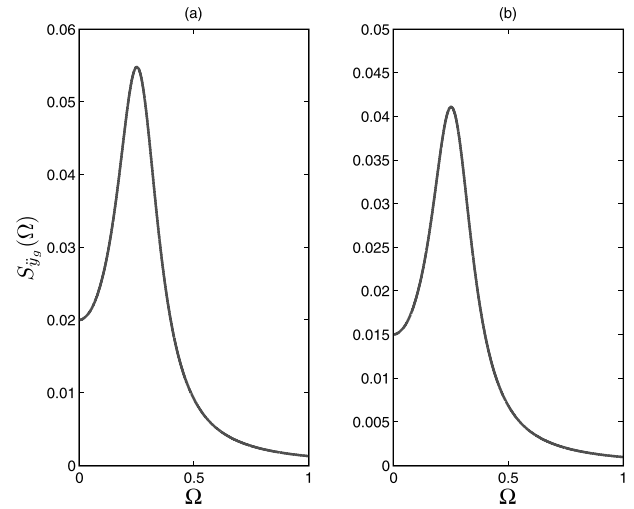


Fig. 2. Power spectral density: (a) 0.02 and (b) 0.15.

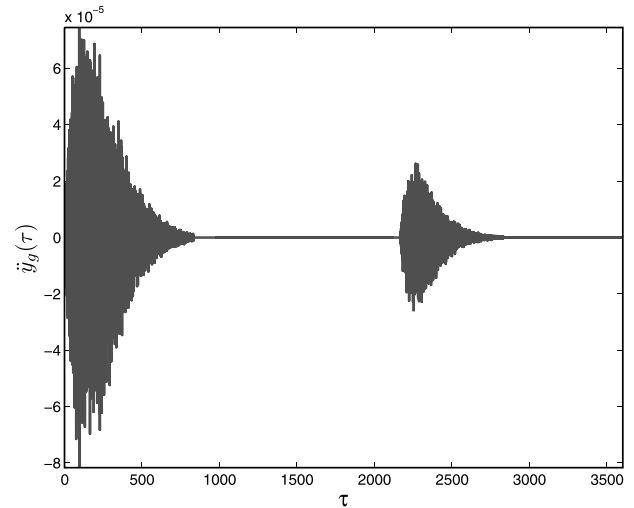


Fig. 3. Dimensionless ground acceleration earthquake.

$E_1 = E_2 = 2.1 \times 10^{11} \text{ N/m}^2; A_1 = 25 \times 20 \text{ m}^2; A_2 = 15 \times 10 \text{ m}^2; L = 80 \text{ m}; I_1 = 16666.7 \text{ m}^4; I_2 = 1250 \text{ m}^4; \rho_1 = \rho_2 = 7850 \text{ kg/m}^3; \nu = 0.3$ and these lead to the dimensionless values

$$\delta_2 = 1.872345984225808; \quad \delta_1 = 1.864590299469015;$$

$$\epsilon_2^1 = 1.855233725311230; \quad \epsilon_1^1 = 1.799611769800091$$

$$\zeta_1^1 = 0.1794505064; \quad \zeta_2^1 = 0.04807614922;$$

$$T = 0.03 \quad \epsilon_1^1 = -0.2925535449; \quad \epsilon_2^1 = -1.004587910;$$

$$X_3 = 0.3 \quad \sigma_2^1 = -0.7604937075; \quad \sigma_1^1 = -0.7823279832$$

Second mode

$$\delta_2^2 = 4.634055034532558; \quad \epsilon_1^2 = 3.761593512952180;$$

$$\delta_2^2 = 4.493412592175132; \quad \epsilon_2^2 = 4.391485181266631;$$

$$\sigma_1^2 = -0.2915422860; \quad \sigma_2^2 = -0.2283758422;$$

$$\epsilon_1^2 = -0.7120277150; \quad \epsilon_2^2 = -3.188313916$$

$$\zeta_1^2 = 5.597669667; \quad \zeta_2^2 = 2.028598833;$$

Third mode

$$\delta_1^3 = 7.506566286307134; \quad \epsilon_1^3 = 5.070688617236388;$$

Table 1
Model parameters of the MR damper.

$\delta_a = 301$	$n_1 = 2$
$\gamma \text{ (m}^{-2}\text{)} = 363$	$\eta_p \text{ (s}^{-1}\text{)} = 190$
$\beta \text{ (m}^{-2}\text{)} = 363$	$k_1 \text{ (N/m)} = 617.31 \text{ MF}$
$k_0 \text{ (N/m)} = 46.90 \text{ MF}$	$y_0 \text{ (m)} = 0.0$
$\alpha_a \text{ (N/m)} = 14,000 \text{ MF}$	$\alpha_b \text{ (N/mV)} = 69,500 \text{ MF}$
$c_{0a} \text{ (Ns/m)} = 2100 \text{ MF}$	$c_{0b} \text{ (Ns/mV)} = 350 \text{ MF}$
$c_{1a} \text{ (Ns/m)} = 28,300 \text{ MF}$	$c_{1b} \text{ (Ns/mV)} = 295,000 \text{ MF}$

$$\begin{aligned} \delta_2^3 &= 7.721052093237568; \epsilon_2^3 = 6.732692537780257 \\ \zeta_1^3 &= 28.38752152; \zeta_2^3 = 13.23675353; \\ \sigma_1^3 &= -0.08394819892; \sigma_2^3 = -0.05571034952 \\ \epsilon_1^3 &= -0.4449994270; \epsilon_2^3 = -3.447827322 \end{aligned}$$

The parameter values, which are listed in Table 1 are those used in Ref.[23]. It is observed these parameters depend on the coefficient MF. This one allows to modify the properties of the damper, in order to have the parameter values for a large scale MR damper, enable to control the mechanical structure in the optimal condition.

3. Numerical results of the controlled mechanical system

With a view to obtain the optimal input voltage corresponding to the desired damper force, the control algorithm used in semi-active control based on the Lyapunov stability theory [20] is employed. The Lyapunov function, denoted $L_y(\mathbf{W})$ must be a positive function of the state of the system, \mathbf{W} . According to the Lyapunov stability theory, if the rate of change of lyapunov function, $\dot{L}_y(\mathbf{W})$, is negative semi-definite, the origin is stable. Lyapunov function is chosen of the form

$$L_y = \frac{1}{2} \|\mathbf{W}\|_p^2 \tag{23}$$

where $\|\Sigma\|_p = P$ -norm of the states defined by

$$\|\Sigma\|_p = [\Sigma^T \mathbf{P}_L \Sigma]^{1/2} \tag{24}$$

where \mathbf{P}_L is real, symmetric, positive definite matrix. \mathbf{P}_L is found using Lyapunov equation.

$$\Sigma^T \mathbf{P}_L + \mathbf{P}_L \Sigma = -\mathbf{Q}_p \tag{25}$$

\mathbf{Q}_p is a positive definite matrix. The derivative of the Lyapunov function for a solution of the state-space equation is

$$\dot{L}_y = -\frac{1}{2} \mathbf{W}^T \mathbf{Q}_p \mathbf{W} + \mathbf{W}^T \mathbf{P}_L \mathbf{B}_1 F_d + \mathbf{W}^T \mathbf{P}_L \mathbf{B}_2 \ddot{y}_g \tag{26}$$

the control law which minimize \dot{L}_y

$$V_c = V_{max} H(-\mathbf{W}^T \mathbf{P}_L \mathbf{B}_1 F_d) \tag{27}$$

where V_{max} is the maximum voltage and $H(\cdot)$ is Heaviside step function. When this function is greater than zero, the voltage (V_c) applied to the damper should be maximum (V_{max}), otherwise, the command voltage is set to zero.

By considering all defined parameter in the dimensionless form of mechanical structures, with those of controller, which are associated with an appropriated algorithm to display Figs. 4–6, therefore each one expresses at a specified mode. In what follows, these figures show a considerable reduction of vibration of the amplitude of buildings (Bg1) and (Bg2) at a interconnected point $X_3 = 0.25$ of the MR device. These lead us to conclude the MR damper it is a element that reduces the excessive energy bring by the external disturbances. To observe the efficiency of MR damper on the structures. Root mean square displacement of each building is presented. Figs. 7–9 display root mean square of Bg1 and Bg2 controlled and uncontrolled at different mode of vibration and different located points of the MR device, in order to have the optimal location. In Fig. 7 the good located points where the controller can offer

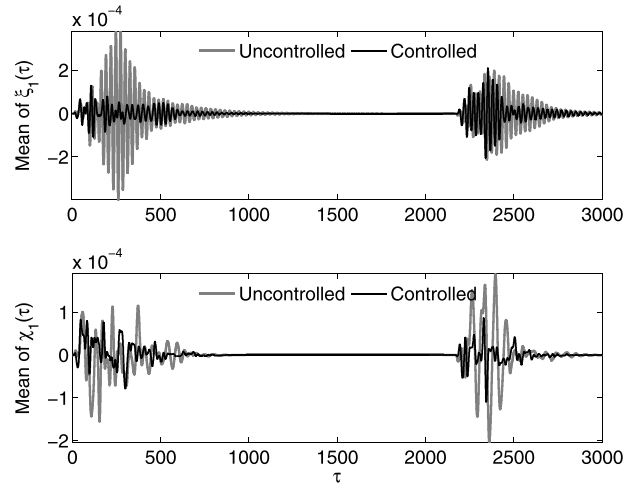


Fig. 4. Time history of buildings Bg1 and Bg2 (first mode), $V_{max} = 2.0$, $MF = 12090$, $X_3 = 0.25$.

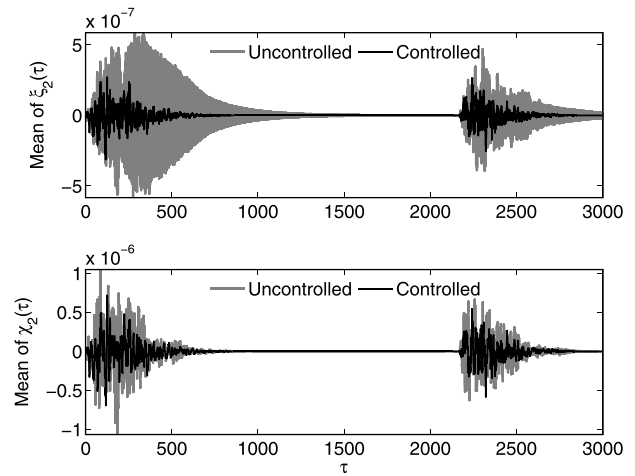


Fig. 5. Time history of buildings Bg1 and Bg2 (second mode), $V_{max} = 2.0$, $MF = 12090$, $X_3 = 0.25$.

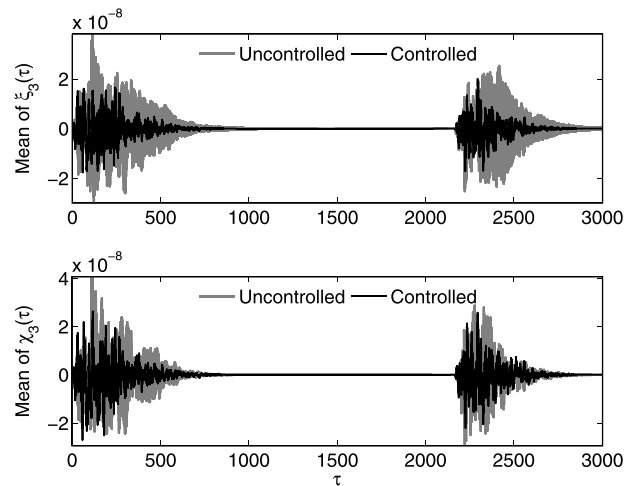


Fig. 6. Time history of buildings Bg1 and Bg2 (third mode), $V_{max} = 2.0$, $MF = 12090$, $X_3 = 0.25$.

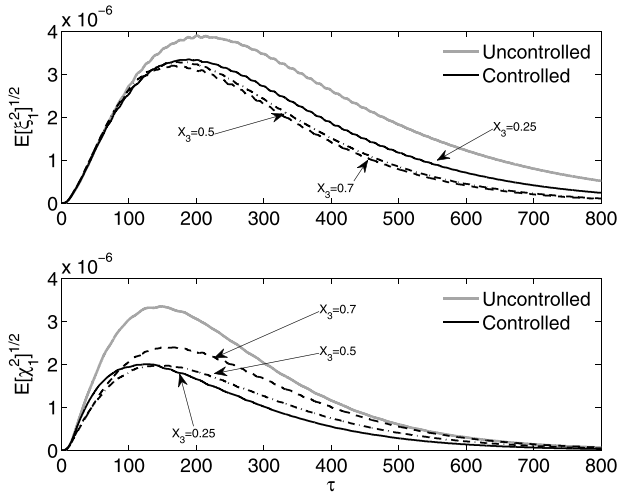


Fig. 7. Root square response Bg1 and Bg2 (first mode), $V_{max}=2.0$, $MF=12090$.

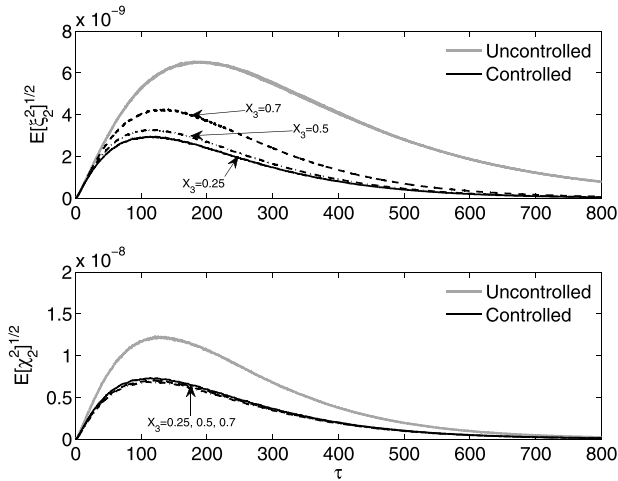


Fig. 8. Root square response Bg1 and Bg2 (second mode), $V_{max}=2.0$, $MF=12090$.

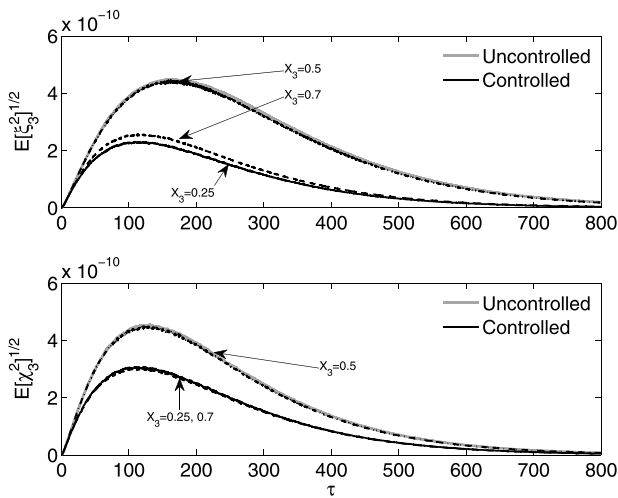


Fig. 9. Root square response Bg1 and Bg2 (third mode), $V_{max}=2.0$, $MF=12090$.

a best performance are $X_p=0.7$ and $X_p=0.25$ for Bg1 and Bg2, respectively. It is observed that at the located point $X_3=0.25$, the controller reduce even better the vibration than the points $X_3=0.5$ and $X_3=0.75$ in Fig. 8. As regards in Fig. 9, at the located point

$X_p=0.5$ it is seen that there is no exist a difference between controlled and uncontrolled cases. This proves that the controller is not able to reduce the excessive vibrations on the two buildings. While the located points $X_p=0.25$ and $X_p=0.7$, one observe that the shock absorber performs a considerable effort to attenuate the vibration.

One clearly see in these figures, illustrating the root mean square for all the modes show that the optimal position of the dynamic controller on the buildings is the point $X_p=0.25$. It is observed in this location, the MR device reduce better the excessive vibrations. By resuming all the mentioned details, one can note that the MR device is a good candidate that has the capacity to minimize disturbances. As further information that one can have from these figures, the time that the controller will launch to act on the structures, which can be computed through the following expression given by

$$\epsilon_{1i} = \frac{E[\xi_i^2]_{uncontrolled}^{1/2} - E[\xi_i^2]_{controlled}^{1/2}}{\max \left(E[\xi_i^2]_{uncontrolled}^{1/2} - E[\xi_i^2]_{controlled}^{1/2} \right)} \quad (28)$$

$$\epsilon_{2i} = \frac{E[\chi_i^2]_{uncontrolled}^{1/2} - E[\chi_i^2]_{controlled}^{1/2}}{\max \left(E[\chi_i^2]_{uncontrolled}^{1/2} - E[\chi_i^2]_{controlled}^{1/2} \right)}$$

The time where the controller begin to attenuate the vibration on buildings Bg1 and Bg2 is got if $\epsilon_{1i} < h_1$ and $\epsilon_{2i} < h_1$, respectively.

For instance at a fixed position $X_3=0.25$ and the chosen precision is $h_1=10^{-2}$, the time that the MR damper launch to reduce the excessive vibration is, at the first mode $\tau=45.42$ for Bg1 and $\tau=18.48$ for Bg2, at the second mode $\tau=13.59$ for Bg1 and $\tau=4.2$ for Bg2, at the third mode $\tau=11.49$ for Bg1 and $\tau=7.05$ for Bg2.

It should be noted that the employed root mean square displacement approach also allows to assess the percentage reduction of excessive vibrations from the external loads by the controller.

4. Conclusion

The dynamics response of two building excited by the earthquake loads has been investigated. The filtered random modulated by a deterministic enveloping function is considered to describe the nonstationary stochastic ground motion. Timoshenko Model which takes into account the shear and rotational effects has been adopted to model each building. Lyapunov stability theory based on semi active control has been used to select the suitable voltage that operate MR damper. The mean square value has been employed to observe better the contribution of this controller at the varied location. It is shown the controller is not efficient at all located position on the mechanical structures. It is observed that the analytical investigation of other modes is really necessary to obtain the optimal position. In addition to that, the time where the MR damper start to act on each building is pointed out through the numerical simulations.

Acknowledgements

Part of this work was completed during a research visit of Pr. Nana Nbandjo at the University of Kassel in Germany. He is grateful to the Alexander von Humboldt Foundation for financial support within the Georg Forster Fellowship.

Appendix A. Supplementary data

Supplementary data associated with this article can be found, in the online version, at <http://dx.doi.org/10.1016/j.mechrescom.2016.10.001>.

References

- [1] U.E. Dorka, V. Bayer, Distribution of seismic links in Hysteretic Device Systems, in: Proc. 12th World Conf. Earthq. Eng., Auckland, New Zealand, 2000.
- [2] S.J. Dyke, B.F. Spencer, M.K. Sain, J.D. Carlson, Modeling and control of magnetorheological dampers for seismic response reduction, *Smart Mater. Struct.* 5 (1996) 565.
- [3] H.J. Pradlwarter, G.I. Schuëller, U.E. Dorka, Reliability of MDOF-systems with hysteretic devices, *Eng. Struct.* 20 (1998) 685–691.
- [4] M. Abbas, I. Takewakib, Response of nonlinear single-degree-of-freedom structures to random acceleration sequences, *Eng. Struct.* 33 (2011) 1251–1258.
- [6] H.H. Abramovich, I. Elishakoff, Application of the Krein's method for determination of natural frequencies of periodically supported beam based on simplified Bresse–Timoshenko equations, *Acta Mech.* 66 (1987) 39–59.
- [8] H. Zhu, Y. Wen, H. Iemura, A study on interaction control for seismic response of parallel structures, *Comput. Struct.* 79 (2001) 231–242.
- [9] M. Basili, M. Angelis, Optimal passive control of adjacent structures interconnected with nonlinear hysteretic devices, *J. Sound Vib.* 301 (2007) 106–125.
- [10] S.D. Bharti, S.M. Dumne, M.K. Shrimali, Seismic response analysis of adjacent buildings connected with MR dampers, *Eng. Struct.* 32 (2010) 2122–2133.
- [11] S.D. Bharti, S.M. Dumne, M.K. Shrimali, Earthquake response of asymmetric building with MR damper, *Earthq. Eng. Vib.* 13 (2014) 305–316.
- [12] A. Bhaskararao, R. Jangid, Seismic analysis of structures connected with friction dampers, *Eng. Struct.* 28 (2006) 690–703.
- [14] E.R. Christenson, B.F. Spencer, E.A. Johnson, K. Seto, Coupled building control considering the effects of building/connector configuration, *J. Struct. Eng.* 132 (2006) 853–863.
- [15] E.R. Christenson, B.F. Spencer, E.A. Johnson, Semiactive connected control method for adjacent multidegree-of-freedom buildings, *J. Struct. Mech.* 133 (2007) 290–298.
- [16] O. Cundumi, Numerical investigation of a variable damping semiactive device for the mitigation of the seismic response of adjacent structures, *Comput. Aided Civil Infrastruct. Eng.* 23 (2008) 291–308.
- [17] B. Erkus, M. Abe, Y. Fujino, Investigation of semi-active control for seismic protection of elevated highway bridges, *Eng. Struct.* 24 (2002) 281–293.
- [20] M. Laura, S.J. Dyke, Semiactive control strategies for MR dampers: comparative study, *J. Eng. Mech.* 126 (2000) 795–803.
- [21] E.U. Mehmet, N.S. Muhammad, Optimal design of semi active control for adjacent buildings connected by MR damper based on integrated fuzzy logic and multi-objective genetic algorithm, *Eng. Struct.* 69 (2014) 135–148.
- [22] E. Miranda, Approximate seismic lateral deformation demands in multistory buildings, *J. Struct. Eng.* 125 (1999) 417–425.
- [23] B.P. Ndemanou, J. Metsebo, N.B.R. Nana, P. Wofo, Dynamics and magneto-rheological control of vibration of cantilever Timoshenko beam under earthquake loads, *Nonlinear Dyn.* 78 (2014) 163–171.
- [25] A. Richardson, K.K. Walsh, M.M. Abdullab, Closed-form equations for coupling linear structures using stiffness and damping elements, *Struct. Control Health Monit.* 20 (2011) 259–281.
- [26] B. Samali, L.S. Djajakesukma, H. Nguyen, S. Li, An experimental study of a five storey steel frame using semi-active control system, in: Proceedings 10th Asia-Pacific Vibration Conference Cold Coast, 2003, pp. 604–609.
- [27] B.F. Spencer, S.J. Dyke, M.K. Sain, J.D. Carlson, Phenomenological model for magnetorheological, *J. Eng. Mech.* 123 (1997) 230–238.
- [28] E. Tubaldi, Dynamic behavior of adjacent buildings connected by linear viscous/viscoelastic dampers, *Struct. Control Health Monit.* 22 (2015) 1086–1102.
- [29] A.P. Wang, R.F. Fung, S.C. Huang, Dynamic analysis of a tall building with a tuned-mass-damper device subjected to earthquake excitations, *J. Sound Vib.* 244 (2001) 123–136.
- [31] Z.D. Yang, S.S. Eddie, Dynamic responses of two buildings connected by viscoelastic dampers under bidirectional earthquake excitations, *Earthq. Eng. Vib.* 13 (2014) 137–150.
- [32] W.S. Zhang, Y.L. Xu, Vibration analysis of two buildings linked by Maxwell model-defined fluid damper, *J. Sound Vib.* 233 (2000) 775–796.

RESEARCH ARTICLE

Reduction of vibration on a cantilever Timoshenko beam subjected to repeated sequence of excitation with magnetorheological outriggers

Buris Peggy Ndemanou¹  | Eliane Raïssa Fankem¹ | Blaise Romeo Nana Nbandjo^{1,2}

¹Laboratory Modeling and Simulation in Engineering, Biomimetism and Prototypes, Department of physics, Faculty of science, University of Yaounde I, Yaounde, Cameroon
²Steel and Composite structures, University of Kassel, Germany

Correspondence

Buris Peggy Ndemanou, Laboratory of Modeling and Simulation in Engineering, Biomimetism and Prototypes, Department of physics, Faculty of science, University of Yaounde I, P. Box 812, Yaounde, Cameroon.
Email: ndemanoupeggy@gmail.com

Funding information

Alexander von Humboldt Foundation

Summary

This paper deals with the statistical effects of an outrigger system on a cantilever beam under seismic excitation. The nonstationary random approach is employed to simulate seismic events. The Timoshenko beam approach is used to model the frame-core tube linked at a point of its length by the damped outriggers, therefore are connected vertically two magnetorheological damper devices. The peak root-mean-square values of displacement responses is employed as a best measure effective to specify the optimal locations of outriggers according to different vibration modes. To evaluate the performance of the control system, the control algorithm based on Lyapunov stability theory is adopted to seek the input voltage leading to the reduction of vibration.

KEYWORDS

Lyapunov stability, MR dampers, nonstationary random, outriggers, peak RMS, Timoshenko beam

1 | INTRODUCTION

Since several decades, researchers and engineers do not cease to multiply the intensive research efforts, in view of reinforcing the degree of energy dissipation of tall buildings to further resist to the energy from the external disturbances. Due to the vulnerability of those structures to environmental dynamic loads, various alternatives in this sense carried out, with a view to increase structural safety in minimizing the damage effects that could lead to a premature collapse. The configuration of these ones is done such as the dynamic forces are transferred upon one another in such manner that they work as a group.^[1] As the further element, the passive, active, and semiactive devices are inserted into those structures to enhance control performance by providing energy dissipation. In the same view, another designed way to improve efficiency of tall buildings such as the outrigger system, which is consisted of a core wall, external columns, and outriggers, was developed and implemented. Smith and Willford^[2] described that structural system like a new concept for the structural design of high-rise buildings. The authors mentioned that the performance of this type of system depends on the flexural and shear stiffness of various core or wall and also of the axial stiffness of the perimeter columns and their distance from the core. In this regard, Tan et al.^[3] presented the experimental work on the outrigger damping system. They showed that the damped outrigger system can achieve a better performance than the outrigger structure in reducing the seismic response of the structure. Asai et al.^[4] defined that new structural concept like a novel energy dissipation system, which can mostly be used to protect high rise and tall buildings against the hazard loads, such as severe earthquakes and strong winds. Chang et al.^[5] has indicated that outrigger system provides additional damping that can reduce structural response, and that the bending deformation of the building is transformed into shear deformation across dampers placed between the outrigger and the perimeter column. Park et al.^[6] studied an optimal design method for minimizing the volume of the primary structural members. According to authors, the flexural rigidity of the core wall and the axial rigidity of the external column vary linearly with respect to height. Some investigations about outrigger damping systems employing the magnetorheological (MR) dampers, which are inserted vertically between the outriggers, and the perimeter columns studied by previous studies.^[5,7,8] The particularities of MR devices are due to its semiactive nature, inherent stability, mechanical simplicity, large temperature operating range, and require a low voltage to achieve high control performance.^[9] In the present paper, outrigger system will be constituted of a core and outriggers equipped of the two MR dampers installed vertically at the ends, This signifies, in other words, that the influence of the perimeter columns is neglected. All these illustrated assumptions lead us to have the signifies model.^[10,11]

To investigate the dynamic responses, the different approaches were employed by the authors to model the outrigger system such as the elastic flexural deformation beam,^[4, 10–12] known on the name of the Euler–Bernoulli beam, the shear-flexural cantilever.^[13] Thus, it is important to mention that up to now, there is a lack of research work in the literature that takes into account the combination of shear-type deformation and rotary inertia effects in the dynamic behaviours in investigating transverse vibration of the structure. As a result, the core tube adopted here is a cantilever beam in which the influence of the shear deformation and rotary inertia is taken into account in the modelling. Timoshenko^[14] was the first to demonstrate the importance of shear deformation and rotational inertia effect in the dynamics of elastic beams. That model is a mathematical expansion of the Euler–Bernoulli theory associated with the quoted effects.

In this work, the frame-core tube is considered as a continuum cantilever Timoshenko beam theory characterized by a set of partial differential equations. As damped element, two MR dampers are installed vertically at the ends of each outrigger, which are fixed at one point of the mentioned core structure. The whole structure is adopted to mitigate the earthquake sequence response. The main objective is to find the suitable location of outriggers at the first three modes by varying the distance of these ones from the core, in order to evaluate the effective response of the structural system. These results are obtained through the passive-on strategy. It is important to note that the employed optimisation principle is very necessary to minimize the earthquake-induced structural vibration.

2 | DESCRIPTION OF PHYSICAL SYSTEM

The physical model represented in Figure 1 is a structural system that is constituted of an uniform cantilever beam and one outrigger truss. The set of the system is subjected to the same environmental dynamic force in the horizontal direction denoted ground excitation, which is considered to

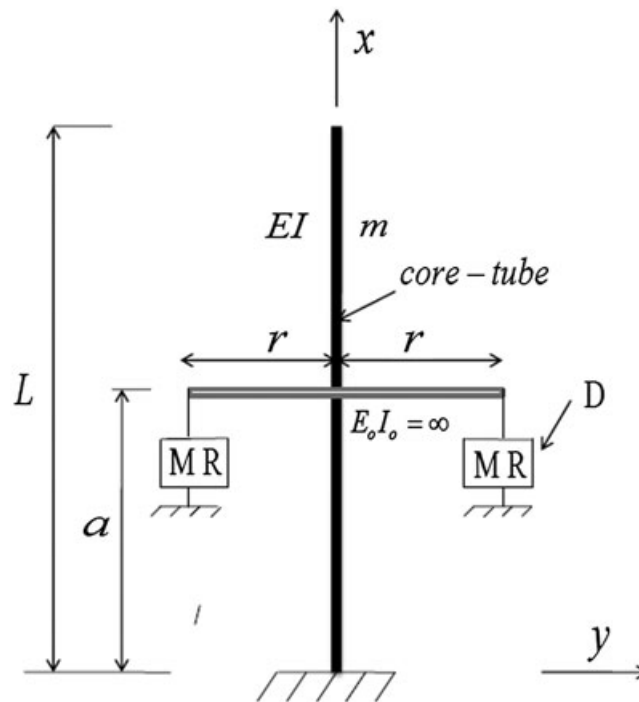


FIGURE 1 Cantilever beam with magnetorheological (MR) outriggers

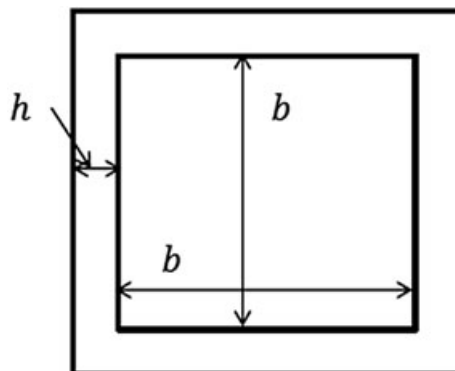


FIGURE 2 Cross-section of the core tube

simulate a seismic motion. The outriggers and the exterior columns have commonly a high stiffness. In this context, they are assumed to be infinitely rigid. As a result, the outrigger behaves as a rigid body and is located at a point a from the end of the core tube. In view of increasing the capacity of the dynamic response of the structural system to resist of the better way against the nonstationary excitation, two semiactive devices dubbed MR dampers (D) are installed vertically and symmetrically; therefore, the generated forces are applied to the core tube through the outriggers.

2.1 | Dynamic model formulation

The mass per unit length is m_1 ; I is the moment of inertia of the cross-section about the neutral axis, E is the Young's modulus; G is the shear modulus of elasticity; r_a is the radius of gyration. These geometrical characteristics are assumed constant. Thus, the lateral displacement is defined by $y(x, t) = y$, which varies with the coordinate along the beam x and with time t . The control device f_d is generated by a MR damper. The influence of the perimeter columns on the dynamics of the core is not taken into consideration. As a result, the governing equations describing the dynamics of the cantilever Timoshenko beam with one damped outrigger under the earthquake loadings can be written as

$$m_1 \frac{\partial^2 y}{\partial t^2} + EI \frac{\partial^4 y}{\partial x^4} - m_1 r_a^2 \left(1 + \frac{E}{k_s G} \right) \frac{\partial^4 y}{\partial x^2 \partial t^2} = -m_1 \ddot{x}_g(t) + \frac{\partial M_a}{\partial x}, \quad (1)$$

where the distributed moment generated by the MR dampers is

$$M_a = 2\delta(x - a) r f_d(t), \quad (2)$$

in which $\delta(x - a)$ denotes the Dirac function. This one indicates that the point a is the place where the damped outriggers is installed. The distance from the control devices to the centre of the core is denoted r . The dimensionless quantity k_s is the shear coefficient depending on the geometric of the cross section of the beam and depend on as well as of the Poisson's ratio. It is assumed in this paper that the dimensional ratio of the width on the area to the thickness is very small, reason why the core tube is considered like a beam being the cross section at the small thickness. This analysis leads us to adopt that, the expression of this mentioned coefficient associated with the cross-section of the core tube is given by Cowper^[15]:

$$k_s = \frac{20(1 + \nu)}{48 + 39\nu}. \quad (3)$$

ν is the Poisson's ratio coefficient, it is clearly seen that k_s is connected with that coefficient, which its value depends solely on the material property. In what follows, the moment of inertia and area of the cross-section can be formulated as (Figure 2)

$$A = (b + 2h)^2 - b^2; \quad I = \frac{(b + 2h)^4}{12} - \frac{b^4}{12}.$$

In this formulation in Equation 1, the first two terms correspond to the classical Bernoulli–Euler beam model. The third term represents the correction for rotary inertia, and the fourth term represents the shear deformation effect.^[16] For convenience in the present study, the joint action of rotary inertia and shear deformation effects is neglected. Thereafter, the bending stiffness for the outriggers is assumed to be infinite.^[10]

The mathematical model of the nonstationary ground acceleration $\ddot{x}_g(t)$ of n sequences proposed by Abbas and Takewakib^[17] is adopted in this paper. According to the authors, ground acceleration of multiplied sequences could result in more damage to the structure than a single ordinary event. This is because the structure gets damaged in the first sequence, and additional damage accumulates from secondary sequence before any repair is possible. As a result, this random function is assumed to take the form of a filtered Gaussian stationary white noise modulated by a deterministic envelope function under the sequence form. Expression of this term is defined in Equation 4 as follows:

$$\ddot{u}_g(t) = \begin{cases} e_1(t) \ddot{w}_1(t) & 0 \leq t \leq T_1 \\ 0 & T_1 \leq t \leq \sum_{i=1}^2 T_i \\ e_2(t - \sum_{i=1}^2 T_i) \ddot{w}_2(t) & \sum_{i=1}^2 T_i \leq t \leq \sum_{i=1}^3 T_i \\ 0 & \sum_{i=1}^3 T_i \leq t \leq \sum_{i=1}^4 T_i \\ \dots & \dots \\ e_n \left(t - \sum_{i=1}^{n-1} T_i \right) \ddot{w}_n(t) & \sum_{i=1}^{n-1} T_i \leq t \leq \sum_{i=1}^{n+2} T_i \end{cases}, \quad (4)$$

where $e_1(t), e_2(t), \dots, e_n(t)$ are the envelope functions associated with the acceleration sequences 1, 2, ..., n , $\ddot{w}_1(t), \ddot{w}_2(t), \dots, \ddot{w}_n(t)$ are stationary random processes, T_1, T_3, \dots, T_{n+2} are the time durations of the acceleration sequences, and T_2, T_4, \dots, T_{n+1} are the time intervals separating these sequences. Thus, the envelope function for the i th sequence is expressed as

$$e_i(t) = e_{0i} \left(t - \sum_{i=1}^n T_i \right) \exp \left[-\alpha_i \left(t - \sum_{i=1}^n T_i \right) \right]; \quad \sum_{i=1}^{n+1} T_i \leq t \leq \sum_{i=1}^{n+2} T_i, \quad (5)$$

where e_{0i} and α_i are $2n$ positive constants that control the intensity and the nonstationarity trend of the i th acceleration sequence.

The phenomenological model, which is based on Bouc-Wen modified version, proposed by Spencer et al.^[18] is adopted here to describe the dynamic of the control device in order to predict its response. This model can exhibit a wide variety of hysteretic behaviours. To valid their mathematical model, authors have done a comparative approach between these analytical data and those obtained experimental results. The analysis of that study on the basis of their results have pointed out the approach numerically tractable and effectively portrays the behaviour of the MR damper. In other words, the proposed mathematical model describes the dynamic behaviour of the MR damper very well. As a result, the equation governing force f_d generated by the control device:

$$f_d(t) = c_1 \dot{y}_1 + k_1(y(a, t) - y_0). \quad (6)$$

The internal displacement y_1 is illustrated:

$$\dot{y}_1 = \frac{1}{(c_0 + c_1)} (\alpha z + c_0 \dot{y}(a, t) + k_0(y(a, t) - y_1)), \quad (7)$$

and z is an evolutionary variable given by

$$\dot{z} = -\gamma |\dot{y}(a, t) - \dot{y}_1| |z|^{n-1} + (\delta_1 - \beta |z|^n)(\dot{y}(a, t) - \dot{y}_1), \quad (8)$$

where c_0 and c_1 are the viscous damping at larger and low velocities, respectively; k_1 is the accumulator stiffness; k_0 represents the stiffness at large velocity; γ , δ_1 and β are the shape parameters of the hysteresis loops. Moreover some of these parameters depend on the command voltage u_1 , which are given by

$$c_0 = c_{0a} + c_{0b}u_1, \quad c_1 = c_{1a} + c_{1b}u_1, \quad \alpha = \alpha_a + \alpha_b u_1, \quad (9)$$

where the command voltage u_1 is accounted for through the first order filter:

$$\dot{u}_1 = \eta_p(u_1 - v_c). \quad (10)$$

v_c is the maximum applied voltage that is associated with the saturation of the magnetic field in the MR damper, and η_p is a positive number that reflects the delay time of the MR damper.

Introducing the new parameters, one has the expressions defined as follows:

$$Y = \frac{y}{L}, \quad \tau = \frac{t}{T}, \quad \delta_a = \delta_1 L, \quad \gamma_L = \gamma L, \quad \zeta_a = \frac{2r}{L}, \quad \ddot{y}_g(\tau) = \frac{T^2}{L} \ddot{x}_g(t); \quad a_1 = \frac{EIT^2}{mL^4}, \quad a_2 = \frac{r_a^2}{L^2} \left(1 + \frac{E}{k_s G}\right),$$

$$C_0 = \frac{c_0}{c_0 + c_1}, \quad K_0 = \frac{k_0 T}{c_0 + c_1}, \quad \alpha_b = \frac{\alpha T}{(c_0 + c_1)L}, \quad C_1 = \frac{c_1 T}{mL}, \quad K_1 = \frac{k_1 T^2}{mL}, \quad T = L \sqrt{\frac{\rho}{k_s G}}, \quad Y_0 = \frac{y_0}{L}.$$

The relationship between the parameters leads to new reformulation, which is described by the below equation:

$$\frac{\partial^2 Y}{\partial \tau^2} + a_1 \frac{\partial^4 Y}{\partial X^4} + a_2 \frac{\partial^4 Y}{\partial X^2 \partial \tau^2} = -\ddot{y}_g(\tau) + \zeta_a F_d(\tau) \frac{\partial}{\partial X} \delta(X - X_0). \quad (11)$$

The dimensionless equation of the MR damper force is rewritten as

$$F_d(\tau) = C_1 \dot{Y}_1 + K_1(Y(X_0, \tau) - Y_0). \quad (12)$$

Y_1 and Z are governed by the below equations:

$$\dot{Y}_1 = \alpha_b Z + C_0 \dot{Y}(X_0, \tau) + K_0(Y(X_0, \tau) - Y_1), \quad (13)$$

$$\dot{z} = -\gamma_L |\dot{Y}(X_0, \tau) - \dot{Y}_1| |Z|^{n-1} + (\delta_1 - \beta |Z|^n)(\dot{Y}(X_0, \tau) - \dot{Y}_1), \quad (14)$$

where X_0 is the location of the damped outriggers. By observing closely the Equations 12, 13, and 14, one can notice that these depend on the quoted location point. This shows that the outrigger position is an important issue in terms of ensuring the efficiency of lateral displacement control.^[6] For the sake of simplicity, it is necessary to assess the dynamic responses of the structural system through the modal properties.

2.2 | Modal equations

To reduce the partial differential equations to a set of ordinary differential equations, in order to assess the dynamic behaviour response of the structural system. Thus, the general solution of the Equation 11 can be written as separation variables of $\chi(\tau)$, which is the time dependent function and the shape function $\Phi(X)$:

$$Y = \sum_{j=1}^{n_m} \Phi_j(X) \chi_j(\tau). \quad (15)$$

n_m is the total of modes with

$$\Phi(X) = \left(d_1^j \sin(\delta_1^j X) + \cos(\delta_1^j X) - d_3^j \sinh(\epsilon_1^j X) - \cosh(\epsilon_1^j X) \right). \quad (16)$$

The spatial function is obtained from Equation 11 without the right member. The superscript j represents the j th mode.

The coefficients d_1^j and d_3^j are obtained by using the boundary conditions of the cantilever Timoshenko beam^[19,20]:

$$d_1^j = \frac{\cos(\delta_1^j) + \frac{(\epsilon_1^{j2} + \mu_1 \delta_1^{j2})}{(\delta_1^{j2} + \mu_1 \epsilon_1^{j2})} \cosh(\epsilon_1^j)}{-\left(\sin(\delta_1^j) + \frac{\delta_1^j}{\epsilon_1^j} \sinh(\epsilon_1^j) \right)}, \quad d_3^j = -\left(\frac{\delta_1^j + \mu_1 \frac{\epsilon_1^{j2}}{\delta_1^j}}{\epsilon_1^j + \mu_1 \frac{\delta_1^{j2}}{\epsilon_1^j}} \right) d_1^j.$$

In which δ_1^j and ϵ_1^j are eigenvalues defined at the j^{th} mode of the vibration. Impossible to adopt an analytical consideration, these quoted eigenvalues are obtained from Equation 17, by using an numerical appropriate algorithm:

$$\begin{cases} \left[\left(\delta_1^{j2} + \Gamma_1 \epsilon_1^{j2} \right)^2 + \left(\epsilon_1^{j2} + \Gamma_1 \delta_1^{j2} \right)^2 \right] \cos(\delta_1^j) \cosh(\epsilon_1^j) - \left(\delta_1^{j2} + \Gamma_1 \epsilon_1^{j2} \right) \left(\epsilon_1^{j2} + \Gamma_1 \delta_1^{j2} \right) \times \\ \left(-2 + \frac{(\delta_1^{j2} - \epsilon_1^{j2})}{\delta_1^j \epsilon_1^j} \sin(\delta_1^j) \sinh(\epsilon_1^j) \right) = 0 \\ \left(\delta_1^{j2} - \epsilon_1^{j2} \right) \Gamma_2 - \left(1 + \frac{1}{\Gamma_1} \right) \delta_1^{j2} \epsilon_1^{j2} = 0, \end{cases} \quad (17)$$

with $\Gamma_1 = \frac{E}{k_s G}$, $\Gamma_2 = L \frac{k_s GA}{EI}$.

In what follows, by using the mode decomposition of the illustrated expression in Equation 15 and substituting them into Equation 11, multiplying by the different spatial expression and performing the integration from 0 to 1, by adding the damping coefficient. One gets the modal forms of above equations that can be expressed as follows:

$$\ddot{\chi}_j(\tau) + \zeta_j \dot{\chi}_j(\tau) + \varsigma_j \chi_j(\tau) = -\sigma_j \ddot{y}_g(\tau) - \zeta_a \eta_j F_d(\tau). \quad (18)$$

The dimensionless equation of the force generated by the MR device is satisfied by the illustrated expressions as follows:

$$F_d(\tau) = C_1 \dot{Y}_1 + K_1 (\chi_j(\tau) \Phi_j(X_0) - Y_0), \quad (19)$$

where Y_h and Z can be rewritten as

$$\dot{Y}_1 = \alpha_6 Z + C_0 \dot{\chi}_j(\tau) \Phi_j(X_0) + K_0 (\chi_j(\tau) \Phi_j(X_0) - Y_1), \quad (20)$$

$$\dot{z} = -\gamma_L |\dot{\chi}_j(\tau) \Phi_j(X_0) - \dot{Y}_1| Z |Z|^{n-1} + (\delta_L - \beta_L |Z|^n) (\dot{\chi}_j(\tau) \Phi_j(X_0) - \dot{Y}_1). \quad (21)$$

The applied voltage to the control device is defined by the dimensionless expression which is given by

$$U = \eta_T (U - Vc), \quad (22)$$

with

$$\varsigma_j = \frac{a_1 b_3}{b_1 + a_2 b_2}, \quad \eta_j = \frac{\Phi_j'(X_0)}{b_1 + a_2 b_2}, \quad \sigma_j = \frac{b_4}{b_1 + a_2 b_2},$$

in which

$$b_1 = \int_0^1 \Phi_j(X)^2 dX, \quad b_2 = \int_0^1 \Phi_j''(X) \Phi_j(X) dX, \quad b_3 = \int_0^1 \Phi_j''''(X) \Phi_j(X) dX, \quad b_4 = \int_0^1 \Phi_j(X) dX.$$

Equations 18- 22 describe the time evolution of the concrete core tube which is fixed at the point X_0 by the damped outriggers. It is useful to observe that the parameter of the Equation 18 varied at each vibration mode and that the force generated by MR device depends on the attachment point of the damped outriggers on core tube. All these results indicate that outrigger locations could modify the structural response at the different vibration mode and can provide a better understanding of the outrigger design.

2.3 | Semiactive controller

With a view to obtain the optimal input voltage corresponding to the desired damper force and to assess the performance of control system, the control algorithm as an effective mean used in semiactive control based on the Lyapunov stability theory^[9] is employed. Because the control device is not directly controllable and that only applied voltage can be adjusted. Also the mentioned control algorithm is developed for characterizing adequately the damper's intrinsic nonlinear behaviour.^[18] Thus, the Lyapunov function denoted $L_v(\mathbf{W})$ must be a positive function of the state of the system, \mathbf{W} . According to the Lyapunov stability theory, if the rate of change of lyapunov function, $\dot{L}_v(\mathbf{W})$, is negative semidefinite, the origin is stable.

Lyapunov function is chosen of the form

$$L_y = \frac{1}{2} \|\mathbf{W}\|_p^2, \quad (23)$$

where $\|\Sigma\|_p$ = p -norm of the states defined by

$$\|\Sigma\|_p = [\Sigma' \mathbf{P}_L \Sigma]^{1/2}, \quad (24)$$

where \mathbf{P}_L is real, symmetric, positive definite matrix. \mathbf{P}_L is found using Lyapunov equation.

$$\Sigma' \mathbf{P}_L + \mathbf{P}_L \Sigma = -\mathbf{Q}_p \quad (25)$$

\mathbf{Q}_p is a positive definite matrix. The derivative of the Lyapunov function for a solution of the state-space equation is

$$\dot{L}_y = -\frac{1}{2} \mathbf{W}' \mathbf{Q}_p \mathbf{W} + \mathbf{W}' \mathbf{P}_L \mathbf{B}_1 F_d + \mathbf{W}' \mathbf{P}_L \mathbf{B}_2 \ddot{y}_g, \quad (26)$$

The above parameters are defined as follows:

$$\mathbf{W} = \begin{bmatrix} \dot{x}_j \\ \dot{x}_j \end{bmatrix}, \Sigma = \begin{bmatrix} 0 & 1 \\ -\zeta_j & -\zeta_j \end{bmatrix}, \mathbf{B} = \begin{bmatrix} 0 \\ -\sigma_j \end{bmatrix}, \mathbf{B}_1 = \begin{bmatrix} 0 \\ -\zeta_a \eta_j \end{bmatrix}.$$

The control law which will minimize \dot{L}_y

$$V_c = V_{max} H(-\mathbf{W}' \mathbf{P}_L \mathbf{B}_1 F_d), \quad (27)$$

where V_{max} is the maximum voltage and $H(\cdot)$ is Heaviside step function. When this function is greater than zero, the voltage (V_c) applied to the damper should be maximum (V_{max}), otherwise, the command voltage is set to zero.

3 | RESULTS AND DISCUSSIONS

To investigate efficiency of the simplified model, the concrete core is assumed to be $12m \times 12m$ with a $0.5m$ thickness, and with the height of $210m$.^[5] The mass per unit length is $m_1 = 62500K_g/m$. The eigenvalues are obtained from Equation 17 through the Newton–Raphson numerical. These results obtained through this method are illustrated in Table 1.

The listed parameter values in Table 2 when MF= 1.0 are those obtained from the analysis of experimental data and theoretical results by Jung et al.^[21] As it is difficult to have an MR damper with the obtained parameters experimentally that will lead to the optimal minimization of excessive vibration of mechanical structures. To avoid this drawback, it is observed from this Table 2 that some parameters depend on MF, named, the modification factor that allows of multiplying the damping; stiffness and hysteretic constants of the model magnify the damper force. In this regard, the objective here is to modify the properties of the damper, in view of having the parameter values for a large scale MR damper, enable to control the mechanical structure.^[22]

TABLE 1 Parameters of the structural system

Parameter	First	Second	Third
δ_1^j	1.873	4.649	7.752
ϵ_1^j	1.860	4.465	6.979
d_1^j	-0.743	-1.127	-1.283
d_3^j	-0.731	-1.023	-0.998
ζ_1^j	0.039	1.579	13.918

TABLE 2 Model parameters of the magnetorheological damper

Parameter	Value	Parameter	Value
δ_a	1107.2	n_1	2
$\gamma(m^{-2})$	164.0×10^4	$\eta_p(s^{-1})$	190
$\beta(m^{-2})$	164.0×10^4	$k_1(N/m)$	9.7 MF
$k_0(N/m)$	2 MF	$Y_0(m)$	0.0
$\alpha_a(N/m)$	46.2×10^3 MF	$\alpha_b(N/mV)$	41.2×10^3 MF
$c_{0a}(Ns/m)$	11×10^4 MF	$c_{0b}(Ns/mV)$	114.3×10^3 MF
$c_{1a}(Ns/m)$	8359.2×10^3 MF	$c_{1b}(Ns/mV)$	7482.9×10^3 MF

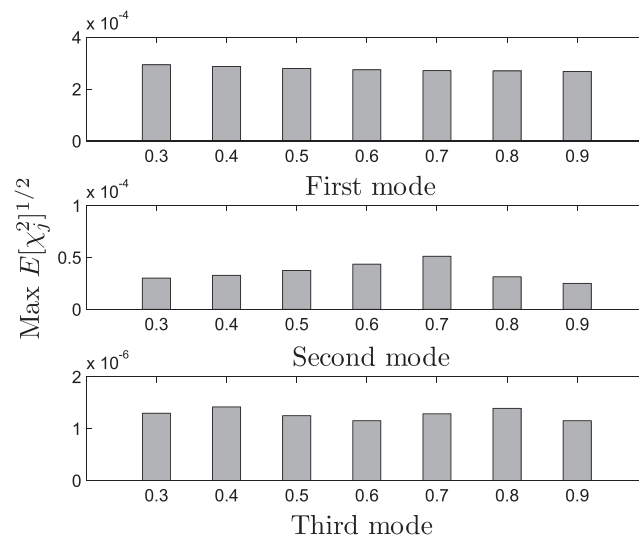


FIGURE 3 Optimal position of damped outriggers, $\zeta_a = 0.762$ and MF=1.0

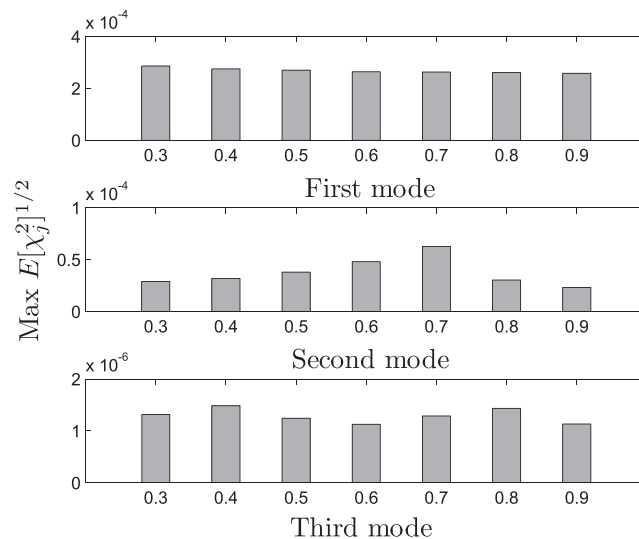


FIGURE 4 Optimal position of damped outriggers, $\zeta_a = 0.095$ and MF=1.0

To assess the optimal position of outriggers on the core tube, the passive-on strategy of the controller is employed. Thus, Figures 3 and 4 display the peak RMS versus locations of outriggers on the structure.

Figure 3 presents at the first mode, a slight variation between the amplitude at the different position of outriggers on the core tube. For that, one can realize that the positions 0.7, 0.8, and 0.9 at this quoted mode are the location points of damped outriggers where the displacement of the structural system is reduced slightly in relation to other positions. The second mode exhibits only one best position of outriggers on the core tube which is 0.9. It is well-seen that at this point the vibration amplitude is reduced dramatically. As regards the third mode, the optimal positions are 0.6 and 0.9. In these points, the peak amplitude of the structure are reduced than other positions. The global analysis of different observations from Figure 3 leads us to mention that the optimal attachment point of outriggers benefits for the three vibration modes is 0.9.

The same observation from Figure 3 is illustrated in Figure 4, that is to say that the point 0.9 stays only the best position of outriggers on the frame core tube. Analysing these figures, as can be seen, the point 0.9 is better attachment point of damped outriggers on the frame-core tube favourable for the three first vibration mode. Moreover, the variation of the length of each outrigger does not affect the value of its optimal attachment point on the beam.

As mentioned before, it is difficult to have the best parameters from experimental results of the MR damper, which incorporated into the structure leading to efficient control. For that, Figure 5 displays the peak RMS versus the scale coefficient MF at the first three vibration modes. It is observed from this figure that the increasing of this quoted coefficient affects the performance of damped outrigger in reducing the seismic response of the structure. It is important to note that the choice of MF is done such as the control device cannot increase the mechanical energy in the structural system. In other words, the control device should reinforce the stability of the structure in order to avoid their premature destruction.

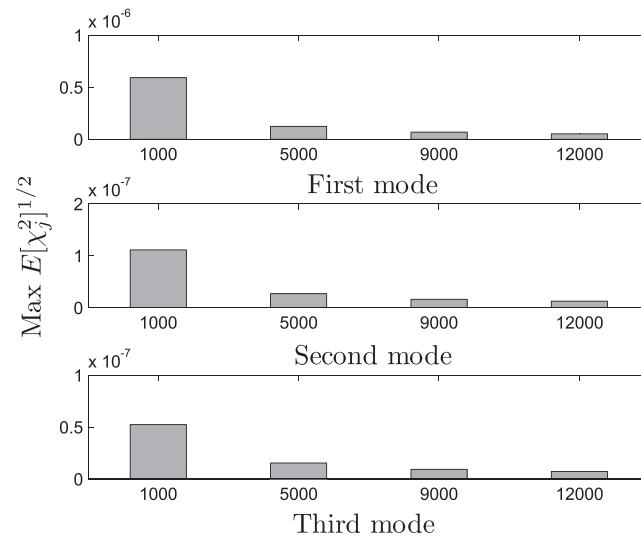
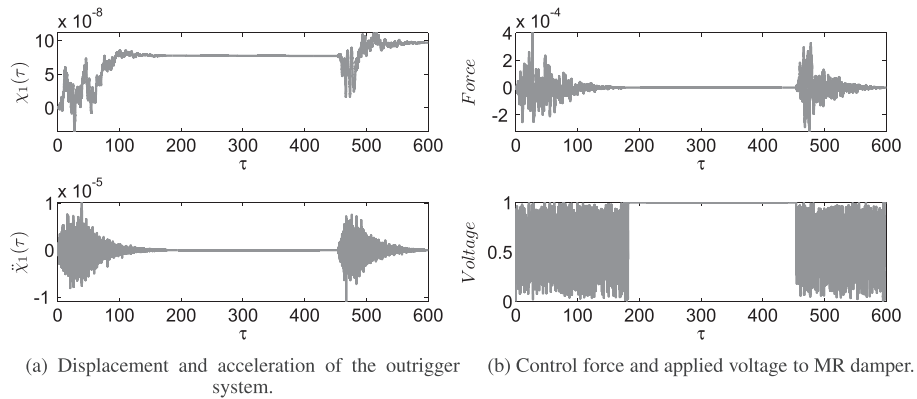
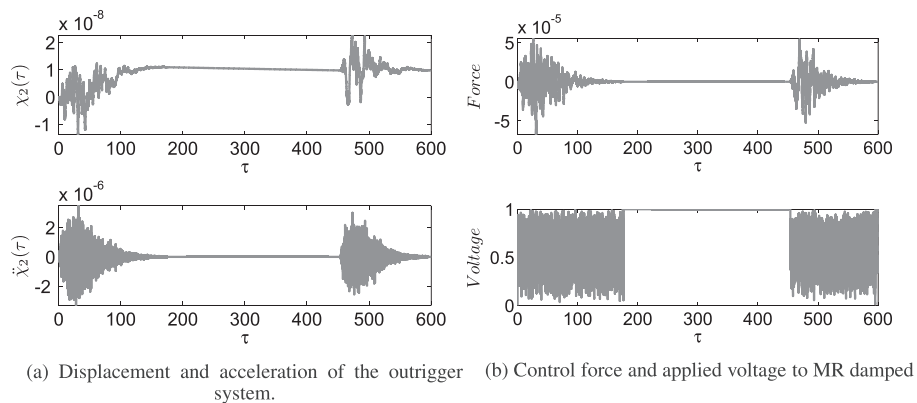


FIGURE 5 Optimal scale coefficient MF



(a) Displacement and acceleration of the outrigger system. (b) Control force and applied voltage to MR damper.

FIGURE 6 Time histories at the first vibration mode



(a) Displacement and acceleration of the outrigger system. (b) Control force and applied voltage to MR damped system.

FIGURE 7 Time histories at the second vibration mode

By taking into account of optimal position of damped outriggers and scale coefficient, one displays in Figures 6, 7, and 8, the time histories of traversal displacement, acceleration, control force, and applied voltage to MR damper at the first, second, and third vibration modes for MF= 9,000. The structural response of the outrigger system at the three first vibration modes is shows in Figures 6(a), 7(a) and 8(a). One can see the structural response show two sequences of the vibration.

The command signal V_c is selected through the control algorithm based on Lyapunov stability illustrated in Equation 27. The numerical result of this adopted strategy allows of having Figures 6b, 7b, and 8b at the first, second, and third vibration modes. The observed separating time interval between $\tau = 170$ and $\tau = 460$ indicates that the controller is in passive-off mode. Since in this relaxation time, the structure did not receive the

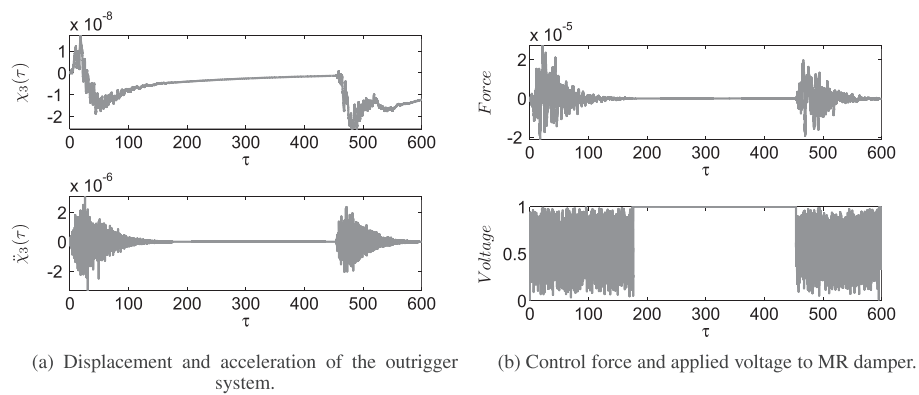


FIGURE 8 Time histories at the third vibration mode

input produced by earthquake, as a result, the system cease to exhibit the vibration. All the same, this explains the dynamic behaviour of the control device because this is depended on the structural response.

4 | CONCLUSION

In this present paper, the dynamic response of the outrigger system under the two sequences of the nonstationary stochastic ground motion has been investigated. The adopted outrigger system is constituted of a core-tube and outriggers employing the MR dampers, which are inserted vertically. Timoshenko beam theory, which takes into account the combination of shear type deformation and rotary inertia effects, has been considered to model the dynamic behaviours of the outrigger system. The statistical analysis through the peak root mean square displacement of the structural system has been employed, to evaluate the influence of optimal attachment points of outriggers on the core tube. The obtained results show that the analytical investigation of other modes is really necessary to seek the optimal position of outriggers. By taking into account of this strategy, it is observed all position of outriggers can not lead to optimal minimization of the seismic vibration of the structural system. On top of that, the best scale coefficient MF of the parameter of the MR device leading to the maximum force by maintaining the efficient control has been determined. Lyapunov stability theory based on semiactive control has been used to select the suitable voltage that operate MR damper. The repeated sequence of the input voltage response reveals that this strategy has been adequated for the control devices.

ACKNOWLEDGEMENTS

BP Ndeமானou. He is grateful to ICTP for invitation and for financial support. Part of this work was completed during a research visit of Pr Nana Nbenjo at the University of Kassel in Germany. He is grateful to the Alexander von Humboldt Foundation for financial support within the Georg Forster Fellowship.

REFERENCES

- [1] M. E. Sandoval, L. B. Ugarte, B. F. Spencer, in Proceeding of the 15th WCEE, Lisbon, Portugal **2012**, 1–10.
- [2] R. J. Smith, M. R. Willford. *The Struct. Design Tall Spec. Build.* **2007**, *16*, 501–517.
- [3] P. Tan, C. J. Fang, W. R. Tu, F. L. Zhou, Y. Wang, M. Jiang, in Proceeding of the 15th WCEE, Lisbon, Portugal **2012**, 1–7.
- [4] T. Asai, C. M. Chang, B. M. Phillips, B. F. Spencer. *Eng. Struct.* **2013**, *57*, 177–188.
- [5] C. M. Chang, Z. Wang, B. F. Spencer, Z. Chen. *Smart Struct. Syst.* **2013**, *11*, 435–451.
- [6] H. S. Park, S. Lee, S. W. Choi, B. Kwan oh, T. Cho, Y. Kim. *Eng. Struct.* **2016**, *117*, 496–505.
- [7] C. M. Chang, T. Asai, Z. Wang, B. F. Spencer, Z. Chen, in Proceedings of the 15th WCEE, Lisbon, Portugal **2012**, 1–10.
- [8] Z. Wanga, C. M. Chia-Ming Chang, B. F. Spencer, Z. Chen. *Proc. SPIE* **2010**, 7647[[SPI-AQ6]].
- [9] M. Laura, S. J. Dyke. *J. Eng. Mech.* **2000**, *126*, 795–803.
- [10] Y. Chen, D. M. McFarland, Wang Z., B. F. Spencer, L. A. Bergman. *J. Struct. Eng.* **2010**, *136*, 1435–1443.
- [11] K. Deng, P. Pan, A. Lam, Y. Xue, in *The Structural Design of tall and Special Buildings* **2013**, 1158–1170.
- [12] T. Ping, F. Chuangjie, Z. Fulin. *Earthquake Eng. Eng. Vibr.* **2014**, *13*, 293–304.
- [13] J. Lee, M. Bang, J. Y. Kim. *The Struct. Design Tall Spec. Build.* **2008**, *17*, 839–851.
- [14] S. P. Timoshenko. *Philos. Mag.* **1921**, *41*, 744–746.
- [15] Cowper. *J. Appl. Mech.* **1966**, *33*, 335–340.
- [16] A. F. Mosaad. *Comput. Struct.* **1999**, *71*, 663–670.
- [17] M. Abbas, I. Takewakib. *Eng. Struct.* **2011**, *33*, 1251–1258.

- [18] B. F. Spencer, S. J. Dyke, M. K. Sain, J. D. Carlson. *J. Eng. Mech.* **1997**, 123, 230–238.
- [19] J. Xie, Z. Wen, in *Proceeding of the 14th WCEE*, Beijing **2008**, 1–13.
- [20] B. P. Ndeமானou, J. Metsebo, B. R. Nana Ndeமானou, P. Woafo. *Nonlinear Dyn.* **2014**, 78, 163–171.
- [21] H. J. Jung, B. F. Spencer, I. W. Lee. *J. Struct. Eng.* **2003**, 129, 873–883.
- [22] B. Erkus, M. Abe, Y. Fujino. *Eng. Struct.* **2002**, 24, 281–291.

Buris Peggy Ndeமானou obtained his MS degree in 2012 at University of Yaoundé I, Cameroon. He got his bachelor degree in 2010 at University of Yaoundé I. Currently, he is a Ph.D. candidate at University of Yaoundé I and his research interests include modelling and simulation of non-linear mechanical systems, adaptive control.

Eliane Raïssa Fankem got her MS degree at University of Yaoundé I, Cameroon. She got his bachelor degree at University of Douala, Cameroon. Currently, she is a Ph.D. candidate at University of Yaoundé I and her research interests include structural health monitoring using dynamic's evaluation particularly on cantilever beam.

Blaise Romeo Nana Ndeமானou Received is PhD in Nonlinear Mechanics in 2004 at University of Yaoundé I, Cameroon. He is currently an Associate Professor at the same University. His research interests include Nonlinear Dynamics and control.

How to cite this article: Ndeமானou BP, Fankem ER, Nana Ndeமானou BR. Reduction of vibration on a cantilever Timoshenko beam subjected to repeated sequence of excitation with magnetorheological outriggers. *Struct Design Tall Spec Build.* 2017;26:e1393. <https://doi.org/10.1002/tal.1393>